

Wind Conditions Around High-rise Buildings

A Method for Evaluating Wind
Conditions by Computational
Fluid Dynamics

Jonatan Hjul
Inge-Mette Kjemtrup
Thomas Bank Lauridsen



Sohngårdsholmsvej 57
DK-9000 Aalborg
+45 96 35 80 80
<http://www.bsn.aau.dk>

Title:

Wind Conditions Around
High-rise Buildings

Subtitle:

A Method for Evaluating Wind
Conditions by Computational
Fluid Dynamics

Dansk titel:

Vindforhold omkring Høje
Bygninger

Dansk undertitel:

En Metode til Evaluering af
Vindforhold med
Computerstøttet Fluid Dynamik

Project:

Master Thesis
Master of Science in Structural
and Civil Engineering

Participants:

Jonatan Hjul
Inge-Mette Kjemtrup
Thomas Bank Lauridsen

Supervisor:

Michael R. Rasmussen

Editions: 5

Number of pages: 152

Completed: 4th June 2010

Synopsis:

This project is conducted in order to investigate the possibilities of analysing wind conditions at pedestrian level by use of Computational Fluid Dynamics (CFD). The purpose is to establish an operational procedure for evaluating wind conditions by coupling CFD, wind statistics, and evaluation criteria.

The project consists of three parts:

Part I deals with the problem of formulating evaluation criteria based on mean wind speed and turbulence. Based on the literature criteria are established for comfort and danger, along with limits of how often the criteria should be allowed to be exceeded.

Part II presents the mathematical model used to evaluate the flow field. This includes treatment of the wind statistics, modelling boundary conditions, selection of turbulence model, and comparison of the CFD model with field measurement in order to evaluate the proposed model.

It is showed that the SST $k-\omega$ model by [Menter \(1994\)](#) with parameters suggested by [Yang et al. \(2009\)](#) is best for modelling the turbulence. A method for transformation of wind statistics from meteorological sites to the location of interest is applied based on the work of [Verkaik et al. \(2005\)](#) and [Wieringa \(1986\)](#).

The overall procedure of evaluating wind conditions is presented, and in Part III two case studies are conducted. One from Høje Brygge, Nørresundby, where also the field measurements are conducted. Here the residents suffer under severe wind conditions. The other case study, from Viborgvej/Bredskiftevej in Århus, is for a proposed group of high-rise buildings.

In both cases the comfort and danger are evaluated and a number of solutions are suggested in order to reduce the wind speed at ground level. The directional discretisation is investigated and considerations on how to choose an adequate discretisation is presented.

Jonatan Hjul

Inge-Mette Kjemtrup

Thomas Bank Lauridsen

Denne rapport er skrevet som afrapporteringen af afgangsprojektet “Vindforhold omkring høje bygninger”, der er gennemført på kandidatuddannelsen til Civilingeniør i Bygge- og Anlægskonstruktion ved Aalborg Universitet.

Projektet omhandler evaluering af vindforhold i bymiljøet ved anvendelse af en numerisk metode kaldet Computerstøttet Fluid Dynamik (CFD), der anvendes som en virtuel vindtunnel. Formålet er at opstille et redskab til undersøgelse af vindforhold omkring eksisterende og planlagte bebyggelser.

I Danmark er den største del af bebyggelserne lave bygninger, men i en del nyere lokalplaner er det foreslået at konstruere højere bygninger. Høje bygninger kan give problemer med vindforholdene på jordniveau i bygningens umiddelbare nærhed, da bygninger der er højere end den omkringliggende bygningsmasse forstyrrer en større del af den atmosfæriske strømning.

Det er derfor i projektet søgt at opstille en anvendelig procedure til evaluering af vindforholdene. Denne procedure er opstillet på baggrund af den tilgængelige litteratur kombineret med egne studier. Evaluering af vindforhold kan evalueres på baggrund af kendskab til vinds påvirkning på mennesker, statistik på vindens hastighed og retning, samt vindens aktuelle strømning omkring bygningerne på lokaliteten.

Evalueringsskriterier, der fastsætter grænser for hvornår vinden bliver ukomfortabel og hvornår den bliver farlig, er fastsat på baggrund af forsøg i en vindtunnel gennemført af [Hunt, Poulton og Mumford \(1976\)](#). Der findes intet dansk normgrundlag for, hvor hyppigt farlige og ukomfortable vinde må forekomme, men SBI-anvisning 128 angiver disse grænser. Det er i projektet vist, at disse grænser er for høje, og at grænserne i den hollandske vindkomfortnorm NEN 8100 giver et mere fornuftigt billede af vindforholdene.

Der er opstillet en metode til transformering af vindstatistikker fra meteorologiske målestationer til randen af de aktuelle evalueringsdomæner, hvori CFD-beregningerne er udført. Metoden baserer sig på arbejde af [Verkaik et al. \(2005\)](#) og [Wieringa \(1986\)](#).

Strømningsberegningerne omkring bygningerne på lokaliteten, bestemt ved CFD, er valideret med feltmålinger foretaget ved Høje Brygge i Nørresundby. Det er vist at anvendelse af $k-\omega$ SST-modellen af [Menter \(1994\)](#) med parametre foreslået af [Yang et al. \(2009\)](#), er bedst til at modellere både middelhastigheden og turbulensen i strømmingen.

Den overordnede procedure opstillet til evaluering af vindforhold er anvendt til to case-studier. I den ene case, ved et eksisterende byggeri ved Høje Brygge i Nørresundby, er beboerne udsat for kraftige vinde, der påvirker brugsværdien af området. Den opstillede beregningsmodel bekræfter de forhold, beboerne oplever. Der er foretaget undersøgelser af forskellige muligheder til forbedring af vindforholdene.

Den anden case er fra et projekt under udvikling i Århus ved Viborgvej/Bredskiftevej. Beregningerne viser, at der er problemer med vindforholdene med den originale bygningsgeometri. Det er vist, at en mindre ændring kan forbedre vindforholdene, dog ikke tilstrækkeligt til at overholde angivelserne i NEN 8100.

Growing interest for construction of high-rise buildings has raised new engineering problems, which are not necessarily covered by existing codes of practice. These issues arise in connection with determination of wind loads and changed wind conditions at pedestrian level. The problems of evaluating wind conditions are addressed in this master thesis.

The field of Computational Wind Engineering (CWE) is growing rapidly, and is replacing simulations made in wind tunnels. In Denmark there is no code of practice for evaluation of wind conditions at pedestrian level. The present project is an attempt to establish basis and conventions for the evaluation of wind conditions in Denmark and other non-mountainous regions.

This report is a result of a master project at the M.Sc. in Structural and Civil Engineering at Aalborg University. The report is divided into three parts: (I) The Importance of Proper Wind Conditions, (II) Development of Mathematical Model, and (III) Evaluation of Wind Comfort in Practice.

Part I introduce why evaluation of wind comfort around high-rise buildings is important and establishes limits used for the critical wind speed and the probability of exceedance.

Part II covers the theoretical background for evaluation of wind conditions. This is divided into a chapter on the use of Computational Fluid Dynamics (CFD) for atmospheric flow, an evaluation of turbulence models, a chapter on the treatment of the wind statistics, an evaluation of the calculations compared with field measurements, and finally an overview of the procedure of evaluation of wind conditions.

Part III includes two case studies where wind conditions are evaluated in practice. One case from Høje Brygge in Nørresundby, Denmark where the wind conditions around an existing building is evaluated, and one case from Viborgvej/Bredskiftevej in Århus, Denmark where a proposed hotel and congress centre is evaluated for wind conditions at pedestrian level before construction.

On the enclosed CD vector plots are provided of the models presented in the report.

Table of Contents

| | |
|--|------------|
| Dansk resumé | iii |
| Preface | v |
| Nomenclature | xi |
| | |
| I The Importance of Proper Wind Conditions | 1 |
| 1 Introduction | 3 |
| 1.1 Evaluation of Wind Conditions | 4 |
| 1.2 Problem Statement for the Thesis | 5 |
| 1.3 Outline of Project | 5 |
| 2 Criteria for Evaluation of Wind Conditions | 7 |
| 2.1 The Scope of the Problem | 7 |
| 2.2 Definition of Criteria | 8 |
| 2.2.1 Pedestrian Activities to Consider | 8 |
| 2.2.2 Criteria for Pedestrian Activities | 9 |
| 2.3 Limits for Acceptable Wind Climate | 9 |
| 2.4 Conclusion on Criteria | 10 |
| | |
| II Development of Mathematical Model | 11 |
| | |
| 3 CFD simulations of Atmospheric Flow | 13 |
| 3.1 Mathematical Basis for Description of Atmospheric Flow | 13 |
| 3.2 Description of Boundaries | 15 |
| 3.2.1 Inlet Boundary Condition | 15 |
| 3.2.2 Outlet Boundary Condition | 16 |
| 3.2.3 Ground Surface Boundary Condition | 16 |
| 3.2.4 Building Surface Boundary Condition | 17 |
| 3.2.5 Free Stream Conditions | 17 |
| 3.3 Obtaining a Stable Atmospheric Boundary Layer | 18 |
| 4 Choice of Turbulence Model for Urban Flow | 21 |
| 4.1 The problem of Turbulence Modelling | 21 |
| 4.2 Literature Studies on Performance of Turbulence Models | 21 |
| 4.3 Performed Studies on Turbulence Models | 22 |
| 4.3.1 Experimental Data | 22 |
| 4.3.2 Computational Domain | 24 |
| 4.3.3 Boundary Conditions | 24 |
| 4.4 Analysis of Computed Results and Experimental Data | 26 |
| 4.5 Discussion and Perspectives of the Turbulence Models | 28 |
| 4.6 Conclusion on Turbulence Modelling | 29 |
| 5 Treatment of Wind Statistics | 31 |
| 5.1 The Atmospheric Boundary Layer | 31 |

Table of Contents

| | | |
|------------|--|-----------|
| 5.1.1 | Use of Similarity Theory | 32 |
| 5.1.2 | The Geostrophic Relations of Rossby Similarity Theory | 33 |
| 5.2 | Applied Atmospheric Model | 34 |
| 5.2.1 | Choosing the Roughness Heights | 35 |
| 5.3 | Implementation Issues | 36 |
| 5.4 | Verification and Validation of Transformation Procedure | 38 |
| 5.5 | Conclusion and Perspectives on Statistical Treatment | 39 |
| 5.6 | Linearity with Respect to the Velocity | 39 |
| 5.6.1 | Study on a 4×4×1 Cube | 39 |
| 5.6.2 | Study on a Cylinder | 40 |
| 5.7 | Coupling between Wind Statistics and CFD Calculations | 41 |
| 6 | Validation of CFD Model | 43 |
| 6.1 | Calibration of anemometers | 43 |
| 6.1.1 | Uncertainties in Calibration | 44 |
| 6.2 | Preparation of Equipment | 45 |
| 6.3 | Choosing Time-Averaging Period | 45 |
| 6.4 | Measurements at Høje Brygge | 46 |
| 6.5 | Comparison of Mean Wind Speed and Direction | 48 |
| 6.5.1 | Evaluation of Wind from North-east | 48 |
| 6.5.2 | Evaluation of Wind from West | 50 |
| 6.6 | Measurements of Turbulence | 51 |
| 6.7 | Conclusions on Comparison Between CFD and Measurements | 54 |
| 7 | Procedure for Evaluating Wind Conditions based on CFD | 57 |
| 7.1 | Outline of Procedure | 57 |
| 7.2 | Method for Automate the Calculation Procedure | 62 |
| 7.3 | Sensibility of Parameters in Evaluation Procedure | 63 |
| 7.3.1 | Uncertainties in the Mathematical Submodels | 63 |
| 7.3.2 | Assessment of Uncertainties in Evaluation of the Flow | 64 |
| III | Evaluation of Wind Comfort in Practice | 65 |
| 8 | Evaluation of Wind Conditions at Høje Brygge | 67 |
| 8.1 | Stories From Residents | 68 |
| 8.2 | Surrounding Areas | 69 |
| 8.3 | Build-up of Model for Høje Brygge | 70 |
| 8.4 | Geometrical Model and Spatial Discretisation | 70 |
| 8.5 | Wind Phenomena at Høje Brygge | 73 |
| 8.5.1 | Venturi Effect | 73 |
| 8.5.2 | Flow Around Cylinders | 73 |
| 8.5.3 | High Building Behind Low Building | 74 |
| 8.5.4 | Corner Streams | 76 |
| 8.6 | Level of Comfort and Safety | 78 |
| 8.7 | Suggested Solutions for Høje Brygge | 80 |
| 8.7.1 | Changing Location of Entrance | 80 |
| 8.7.2 | Minimising the Wind Speed | 80 |
| 8.7.3 | Pent Roof | 81 |

| | | |
|-----------|---|------------|
| 8.7.4 | Application of Windbreak | 84 |
| 8.7.5 | Combination of Pent Roof and Windbreaks | 85 |
| 8.7.6 | Other Solutions | 87 |
| 8.8 | Conclusions on Wind Evaluation at Høje Brygge | 87 |
| 9 | Evaluation of Wind Conditions at Viborgvej | 89 |
| 9.1 | Surrounding Areas | 90 |
| 9.2 | Build-up of Model for Viborgvej | 91 |
| 9.3 | Geometrical model and Spatial Discretisation | 92 |
| 9.3.1 | Convergence Analysis | 93 |
| 9.4 | Wind Phenomena at Viborgvej | 94 |
| 9.5 | Level of Comfort and Safety | 94 |
| 9.5.1 | Comfort Criterion | 94 |
| 9.5.2 | Danger Criterion | 96 |
| 9.5.3 | Evaluation after SBI-direction | 97 |
| 9.6 | Sensibility of the Roughness length | 97 |
| 9.7 | Suggested Solutions for Viborgvej | 98 |
| 9.7.1 | Modelling of Solution | 99 |
| 9.8 | Conclusions on Wind Evaluation at Viborgvej/Bredskiftevej | 100 |
| 10 | Investigation of Directional Discretisation | 101 |
| 10.1 | Computed realisations for Høje Brygge | 101 |
| 10.2 | Computed realisations for Viborgvej/Bredskiftevej | 105 |
| 10.3 | Analysis of Directional Discretisation | 108 |
| 10.3.1 | Influence Roses for the Directional Discretisation | 108 |
| 10.3.2 | New Approach to the Directional Discretisation | 109 |
| 10.4 | Conclusion on Directional Discretisation | 111 |
| | Conclusion | 113 |
| 10.5 | Further Studies | 114 |
| | Bibliography | 115 |
| | List of Figures | 119 |
| | List of Tables | 123 |
| IV | Appendices | 125 |
| A | Closure Coefficients for the Turbulence Models | 127 |
| B | Model With Larger Origin Shift | 129 |
| C | Measurements | 131 |
| C.1 | Calibration of 2D Anemometers | 131 |
| C.2 | Calibration of 3D Anemometer | 132 |
| C.3 | Sources of Error | 133 |
| C.4 | List of Equipment for Measurements | 133 |
| C.4.1 | Least Square for Positioning of Anemometers | 134 |

Nomenclature

| | |
|----------------------|---|
| ABL | Atmospheric Boundary Layer |
| CFD | Computational Fluid Dynamics |
| CWE | Computational Wind Engineering |
| DES | Detached Eddy Simulation |
| GPS | Global Positioning System |
| LES | Large Eddy Simulation |
| RANS | Reynolds Averaged Navier-Stokes |
| Re | Reynolds number |
| RSM | Reynolds Stress Model |
| SST | Shear Stress Transport |
| URANS | Unsteady Reynolds Averaged Navier-Stokes |
| β_* | Closure coefficient [-] |
| δ | Height of ABL [m/s] |
| ε | Turbulent dissipation rate [J/(kg·s)] |
| κ | von Karman's Constant [-] |
| ν | Kinematic viscosity [m ² /s] |
| ω | Specific dissipation rate [1/s] |
| ρ | Density [kg/m ³] |
| σ | Standard deviation |
| σ_k | Closure coefficient [-] |
| σ_ε | Closure coefficient [-] |
| A | Constant in the geostrophic relations [-] |
| A | Weibull scale parameter [m/s] |
| a | Relation between \sqrt{k} and σ [-] |
| B | Constant in the geostrophic relations [-] |
| c | Constant in determination of height of ABL [-] |
| C_1 | Constant in turbulence inlet profiles [-] |
| C_2 | Constant in turbulence inlet profiles [-] |
| C_s | Constant which takes the type of roughness into account ($C_s = 0.254$ in Star-CCM+) [-] |
| $C_{1\varepsilon}$ | Closure coefficient [-] |
| $C_{2\varepsilon}$ | Closure coefficient [-] |
| C_μ | Closure coefficient [-] |
| D | Foot print length scale [m] |
| d | Origin shift [m] |
| E | Constant in the wall function ($E = 9$ in Star-CCM+) [-] |
| f | Coriolis parameter [1/s] |
| G | Geostrophic wind speed [m/s] |
| k | Turbulent kinetic energy [J/kg] |
| k | Weibull shape parameter [-] |
| k_s | Sand-grain roughness [m] |

Nomenclature

| | |
|------------------|--|
| n_θ | Resolution of sectors [-] |
| P | Probability [-] |
| p | Pressure [Pa] |
| p_k | Peak factor [-] |
| R^2 | Regression coefficient [-] |
| R_+ | Roughness parameter [-] |
| S_{err} | Standard error |
| t | Time [m] |
| U, V, W | Mean wind speed components [m/s] |
| U_* | Friction velocity [m/s] |
| U_{eq} | Equivalent mean wind speed [m/s] |
| U_{max} | Threshold for equivalent mean wind speed [m/s] |
| U_{ref} | Reference mean wind speed [m/s] |
| U_i | Mean velocity vector [m/s] |
| u_i | Instantaneous velocity vector [m/s] |
| u'_i | Fluctuation velocity vector [m/s] |
| x_i | Position vector [m] |
| z | Height above ground level [m] |
| z_0 | Roughness height [m] |

Part I

The Importance of Proper Wind Conditions

1 Introduction

Wind influences human life and activities in several different ways. Wind has positive effects, e.g. removal of air pollutants, but several wind effects can be treated as negative, e.g. cooling of the human body, loads on constructions, and discomfort and danger for pedestrians, as illustrated in [Figure 1.1](#) and [1.2](#).



Figure 1.1 Woman exposed to wind. **Figure 1.2** Bike pushed over by the wind ([Maryland Weather 2010](#))

The wind conditions are however not solely a nature phenomena, but is affected by mankind through changes of the ground surface through time. Historically a much larger part of the earth was covered with forest, but the need for farming land has resulted in a significant forest cutting.

Along with the increased level of high-rise development in urban communities, it has leaved the pedestrian level much more exposed to wind. An increasing need for the evaluation of wind conditions at pedestrian level, as a part of urban planning is therefore needed. In [Figure 1.3](#) it is seen how the wind affects people in areas around a high-rise building in Nørresundby.

Evaluation of pedestrian wind conditions has developed as a sub branch of Computational Wind Engineering (CWE), which covers loads on constructions, simulating boundary conditions for indoor climate problems and building heat losses, ventilation of urban spaces, driving rain, and snow distribution, among others.

The evaluation of pedestrian wind conditions as a tool for urban planning is scattered by the broad range of other parameters influencing the quality of the urban spaces. In general urban spaces should be designed as a compromise between all these parameters,



Figure 1.3 Wind conditions affected by high-rise building in Nørresundby.

but the task of taking all parameters into account is still too comprehensive. Fortunately the main microclimatic issue in Denmark is shelter due to the wind.

In Denmark some local authorities have required the evaluation of danger for pedestrians for new high-rise buildings as a part of the process for obtaining a building permission by including the evaluation in the environmental impact assessment. This has led to an increased interest in the evaluation of wind conditions.

1.1 Evaluation of Wind Conditions

The wind conditions at a location is given by statistics on the wind velocity and the direction over a large number of years. Such data are only available at meteorological stations typically located at Airports. Therefore some models has to be applied in order to couple the wind statistics at meteorological stations and the location of interest.

Actual evaluation of wind conditions at a given location became available with the construction of boundary layer wind tunnels in the sixties. Thereby it became possible to construct a model of the buildings and then measure the flow around the buildings in the model. In a wind tunnel the model is placed on a turntable so different directions can be investigated.

Since Computational Fluid Dynamics (CFD) has become available, and the first evaluations of wind conditions by CFD were reported in the mid eighties ([a broad range of studies are listed by Blocken and Carmeliet 2004](#)). The CFD calculations are in principle a virtual wind tunnel.

At the meteorological stations time series of the wind has been registered over a range of years. In principle the time series of the wind could be simulated in a wind tunnel or by CFD, but a number of points make this procedure less feasible:

- It would take very long time in a wind tunnel or by CFD, which demand a very high amount of computer power not available for the time being.
- The meteorological station and the location of interest are often separated by a distance which does not allow for simulation in the same domain.

Therefore another approach has to be followed, based on the frequency that a given wind is approaching with a given direction, and assuming stationary conditions, at least for some averaging period. In the present thesis it is investigated how this can be determined by CFD.

Therefore a process including the following steps is applied.

- Obtaining and processing directional wind statistics.
- Evaluating the flow by use of CFD.
- Establishing criteria for human comfort and danger when exposed to wind.

The overall wind conditions can be determined by the synthesis of all three parts into maps of the comfort and danger levels, evaluated at pedestrian level.

1.2 Problem Statement for the Thesis

The intention of the present thesis is:

To analyse and investigate the overall procedure for evaluation of wind conditions by CFD, in order to set up an operational procedure for evaluation of wind conditions at routine basis.

While the project has a general focus, the procedure is applied for two different cases in Denmark, at Høje Brygge, Nørresundby and Viborgvej, Århus.

1.3 Outline of Project

In the present thesis the aim is to evaluate wind conditions by CFD. In order to establish an overall method for applying CFD a number of investigations is executed, which is demonstrated by [Figure 1.4](#).

Three general outcomes are sought, that is establishing a valid CFD model, to be able to asses wind climate at a given location, and propose improvements at a given location.

The validation of the CFD model is executed through field measurements. A geometrical model of a given area combined with CFD calculations is applied to identify flow phenomena, which can be counteracted by remedial measures. By application of evaluation criteria of how people is affected by wind gives the overall wind conditions in a given area.

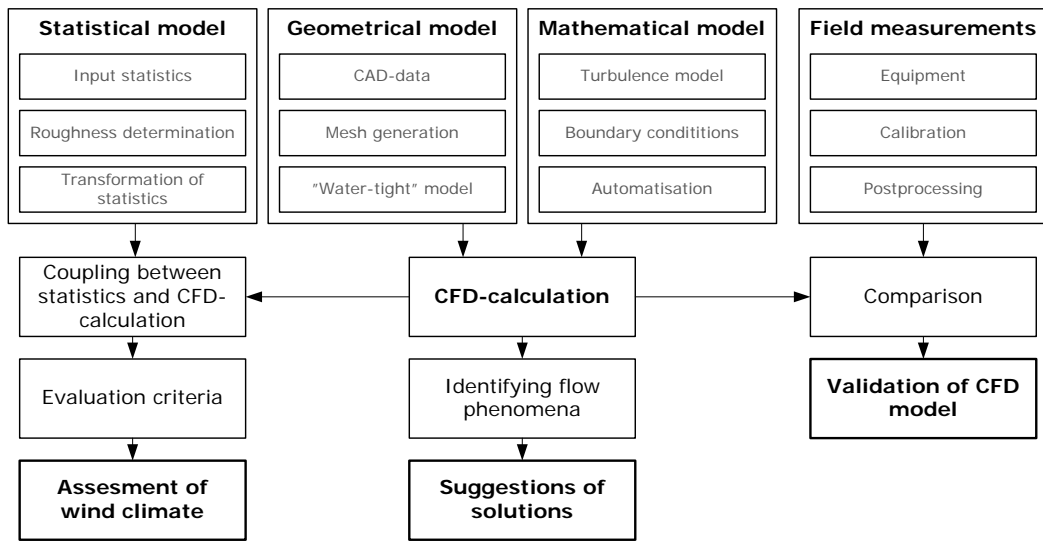


Figure 1.4 Outline of project.

2 Criteria for Evaluation of Wind Conditions

In order to evaluate the wind conditions, at a given location, information is required on what good or bad conditions are. Therefore criteria whereby wind conditions can be evaluated by are required. Typically criteria have been defined for a given activity by a threshold and a limit for how often the threshold is allowed to be exceeded, without halting the intended use of the area.

There is no code of practice in Denmark for “acceptable” wind conditions, but there is published a SBI-direction (no. 128, Bjerregaard and Nielsen 1981). The criteria given in the SBI-direction is based on the work of Davenport (1976).

The criteria in SBI-direction 128 are solely based on the probability that the mean velocity exceeds 5 m/s and does not take wind gusts into account. Such a criterion might be convenient, but it seems unacceptable to evaluate all activities by a 5 m/s-criterion, especially the “resistance against falling”.

In the following more realistic evaluation criteria is therefore suggested, based on a review of the literature. The proposed evaluation criteria are a result of two things: First of all the intention is to evaluate the wind conditions by CFD, while the traditional approach is wind tunnel evaluation, and secondly important results have been published since 1981.

2.1 The Scope of the Problem

People’s feeling of comfort or lack of safety is in nature not objective phenomena. The problem of defining evaluation criteria is scattered by people’s individual preferences and can at best be characterised by demographic parameters such as age and sex, personal parameters such as clothing and activity, and physical parameters such as time of the day or temperature. However individual preferences remain even after such characterisation.

Unfortunately most of these parameters cannot be determined for a given urban space, unless for some special cases such as retirement homes. Therefore criteria for a given activity can at best be defined for an average person.

Ideally microclimatic considerations of urban spaces should involve solar exposure and temperature along with the wind climate. While it is possible to take these parameters into account separately it is much more complicated to evaluate their coherent effect. Stathopoulos (2006) have listed some of the initial considerations in such an approach. In the following only the mechanical effect of wind is therefore considered.

2.2 Definition of Criteria

Almost all criteria in the literature are defined by an expression of the form:

$$U_{\text{eq}} = U + p_k \sigma_U \geq U_{\text{max}} \quad (2.1)$$

$$P(U_e > U_{\text{max}}) \quad (2.2)$$

Where:

| | |
|------------------|--|
| U_{eq} | Equivalent mean wind speed [m/s] |
| U | Mean wind speed [m/s] |
| σ_U | Standard deviation of the wind speed [m/s] |
| p_k | Peak factor [-] |
| P | Probability [-] |
| U_{max} | Threshold for equivalent mean wind speed [m/s] |

This is interpreted as, for a given activity a certain combination of U and σ_U above a given threshold U_{max} is unacceptable. How often this threshold is exceeded designates the quality of executing the activity in a given area.

However the literature is very inconclusive on the value of p_k , U_{max} and acceptable limits for P . As a given criterion is two-dimensional, that is, it consists of a statement of both U_{max} and P even when p_k is determined, different criteria are hard to compare.

[Sanz-Andres and Cuerva \(2006\)](#) have offered a method for comparing criteria if the velocity is assumed Weibull distributed and [Ratcliff and Peterka \(1990\)](#) and [Koss \(2006\)](#) have compared most of the available criteria, but none of these comparisons end up concluding that one criterion is better than another, they just point out the differences.

So where does it leave the effort of establishing criteria? First of all the following assumption can be stated: For a given activity there is a certain limit where the execution of the activity is affected. This statement might seem obvious, but strangely there are a lot of examples of control of walking evaluated by 5 m/s.

As [Bottema \(2000\)](#) puts it, this might be correct for one wind climate, as the limit for acceptable exceedance can just be set very high, but it cannot be correct for all wind climates, as changes in the probability of occurrence of a given wind can yield very unsatisfactory results.

2.2.1 Pedestrian Activities to Consider

Two main focuses are the aim of the evaluation, which is whether pedestrian feel comfortable, and whether buildings induce dangerous winds at a higher rate than expected. Whether the wind is dangerous can be defined by the activity of maintaining balance.

Comfort however cannot be directly coupled to an activity, as pedestrians perform different activities. It can be expected that a person playing sports would find more wind acceptable than a person sitting still, but the wind might affect the activity before it affect the actors (e.g. the ball in football or badminton).

2.2.2 Criteria for Pedestrian Activities

While there might be differences in the threshold for acceptable wind to feel comfortable, proper investigation of different activities are scarce in the literature. [Bottema \(2000\)](#) have investigated the available literature and suggests the following criterion for comfort:

$$U_{eq,c} = U + \sigma_U \geq 6 \text{ m/s} \quad (2.3)$$

This criterion is a result of two things: The threshold value of 6 m/s in turbulent wind is reported in most studies. In the most thorough investigation in the literature, [Hunt, Poulton and Mumford \(1976\)](#) determined this threshold by experiments in a large scale wind tunnel.

About the peak factor there is more debate. The value of 1 suggested by [Bottema \(2000\)](#) is a result of a reanalysis of the data of [Hunt, Poulton and Mumford \(1976\)](#) and [Jackson \(1978\)](#).

For the danger criterion [Hunt, Poulton and Mumford \(1976\)](#) conducted investigations of people's ability to walk. This resulted in the following criterion:

$$U_{eq,d} = U + 3\sigma_U \geq 20 \text{ m/s} \quad (2.4)$$

The peak factor of 3 is determined by investigating people's performance in uniform wind and turbulent wind, and compare these to see which winds yields the same performance. The value of 3 corresponds to a gust with duration of 3 s if the mean wind is averaged on an hourly basis and Gaussian turbulence is assumed ([Bottema 2000](#)).

2.3 Limits for Acceptable Wind Climate

Hereby criteria are stated for which winds that are unacceptable. The remaining question is how often it should be tolerated. In principle this is a question for local authorities, but some guidance is proper.

In the Netherlands a code of practice NEN 8100 is recently published ([Willemsen and Wisse 2007](#)). This code is based on the exceedance of a 5 m/s criterion for the mean wind. In the development of the code [Willemsen and Wisse \(2007\)](#) state that taking turbulence into account is important, but the Dutch wind tunnels do not measure it on a routine basis. In the present application the wind conditions are evaluated by CFD, and thereby there is no reason for limit the evaluation to the mean wind.

The philosophy behind the comfort criterion given by the Dutch code is that the different activities, traversing, strolling, and sitting are affected above the same threshold, but the tolerance of the wind is different. Therefore different classes of comfort are proposed by the limits given in [Table 2.1](#). Some of the values given correspond well to those stated in SBI-direction 128, but there are significant differences for some of the figures.

For the danger criterion, NEN 8100 is based on the exceedance of 15 m/s uniform wind, but the same reason for excluding turbulence as for the comfort criterion apply. Three different levels of danger in [Table 2.2](#) are defined.

Table 2.1 Levels of comfort divided after probability of exceedance (%) in the Dutch code of practice for NEN 8100 (after Willemssen and Wisse 2007).

| Exc. prop. | Designation | Traversing | Strolling | Sitting |
|------------|-------------|------------|-----------|----------|
| <2.5 | A | Good | Good | Good |
| 2.5-5.0 | B | Good | Good | Moderate |
| 5.0-10.0 | C | Good | Moderate | Poor |
| 10-20 | D | Moderate | Poor | Poor |
| >20 | E | Poor | Poor | Poor |

Table 2.2 Levels of danger divided after probability of exceedance (%) in the Dutch code of practice NEN 8100 (after Willemssen and Wisse 2007).

| Exc. prop. | Designation | Level |
|------------|-------------|--------------|
| <0.05 | A | Safe |
| 0.05 – 0.3 | B | Limited risk |
| >0.3 | C | Dangerous |

2.4 Conclusion on Criteria

It is suggested to use the criteria given by Equation 2.3 and 2.4 in combination with the comfort classes given by Table 2.1 and the levels of danger given by Table 2.2.

It can be argued that the different classes of comfort are based on another threshold value, but on the other hand turbulence is included in the wind assessment. The two criteria $U + 3\sigma_U \geq 20$ m/s and $U \geq 15$ m/s are equal if the turbulence intensity is 11 %. Petersen et al. (1998) reports turbulence intensities from 8 % above sea and 20 % or more for complex terrain. The criterion is therefore slightly more restrictive for most wind climates, than the criterion in NEN 8100.

The actual quality of the evaluation criteria can only be investigated by empirical evaluation in different cases. Thereby it can be investigated whether the criteria yield an unacceptable wind climate in areas where the wind climate is known to be unacceptable and vice versa. Some evidence of this is presented in Chapter 8.

There is no doubt that this area calls for further studies, but the methods applicable are somewhat outside engineering, that is, methods used in psychology or sociology would be more proper.

Part II

Development of Mathematical Model

3 CFD simulations of Atmospheric Flow

CFD has evolved as a tool for problems in Computational Wind Engineering. In the following the mathematical basis for simulating CFD calculations are reviewed in order to establish a mathematical basis applicable for evaluating atmospheric flows.

In this chapter, statement of the governing equation, the problem of obtaining a stable atmospheric boundary layer and proper descriptions of the boundary conditions are performed.

Central for solving the problem introduced in this thesis is the mathematical model, which should be applied in a given case where wind conditions are of interest.

The following demands for the mathematical model are stated:

- **Reliability:** The model should describe the mean flow and the fluctuations satisfactory enough to evaluate the overall comfort.
- **Computational speed:** The computational cost is prioritised above accuracy, but should still be able to resolve the overall flow characteristics.
- **Flexibility:** The mathematical description should be applicable for different urban geometries.

The second criterion is a requirement if the technique has to be practically applicable. The mathematical model of the physics involved is chosen to accommodate these criteria, and therefore certain compromises has to be made between accuracy in resolving the flow field and the computational cost.

3.1 Mathematical Basis for Description of Atmospheric Flow

The mathematical basis for describing fluid flow is given by the Navier-Stokes (NS) equations. For low Mach number flows (< 0.3), air can be treated as incompressible (Kundu and Cohen 2002). For an incompressible Newtonian fluid the Navier-Stokes equations are stated as:

$$\frac{\partial u_j}{\partial x_j} = 0 \quad (3.1)$$

$$\frac{\partial u_i}{\partial t} + \frac{\partial u_i u_j}{\partial x_j} = -\frac{1}{\rho} \frac{\partial p}{\partial x_j} + \nu \frac{\partial}{\partial x_j} \left(\frac{\partial u_i}{\partial x_j} + \frac{\partial u_j}{\partial x_i} \right) \quad (3.2)$$

Where:

- u_i Instantaneous velocity vector [m/s]
- x_i Position vector [m]
- t Time [s]
- ρ Density [kg/m³]
- p Pressure [Pa]
- ν Kinematic viscosity [m²/s]

Direct numerical solution of the NS-equations is still too computational expensive for engineering problems, and other solution techniques therefore have to be considered.

These techniques fall into two categories. The first is the mean flow solution of the Reynolds Averaged Navier-Stokes equations (RANS), where the interactions between the time depended eddies are considered by a turbulence model.

The second category includes techniques, which by nature are transient. These techniques resolve the large scale flow and models the small scale eddies. In Large Eddy Simulation (LES) a sub grid model is applied to the eddies smaller than the grid. Detached Eddy Simulation (DES) is a combination of a LES and a RANS model, where the RANS model is used near walls and the LES model resolves the free stream flow.

As the intention is to evaluate the mean flow, RANS is the natural approach, if the results of this technique are adequate. The RANS equations which are obtained from Equation 3.1 and 3.2 by time averaging are stated as:

$$\frac{\partial U_i}{\partial x_i} = 0 \quad (3.3)$$

$$\frac{\partial U_i}{\partial t} + \frac{\partial U_i U_j}{\partial x_j} = -\frac{1}{\rho} \frac{\partial \bar{p}}{\partial x_j} + \nu \frac{\partial}{\partial x_j} \left(\frac{\partial U_i}{\partial x_j} + \frac{\partial U_j}{\partial x_i} \right) - \frac{\partial \overline{u'_i u'_j}}{\partial x_j} \quad (3.4)$$

Where:

- U_i Mean velocity vector [m/s]
- u'_i Fluctuation velocity vector [m/s]

The new last term introduces in principle six new unknowns, which have to be treated by a turbulence model in order to close the equation set. The most popular turbulence models are based on the Boussinesq approximation where the turbulence is treated as an addition to the viscosity.

The program used to evaluate the mathematical models is Star-CCM+ by CD-adapco, which is a commercial CFD code.

3.2 Description of Boundaries

The flow in a given domain is governed by the conditions at the boundaries. In the following the options available are surveyed in order to appoint proper conditions to the models.

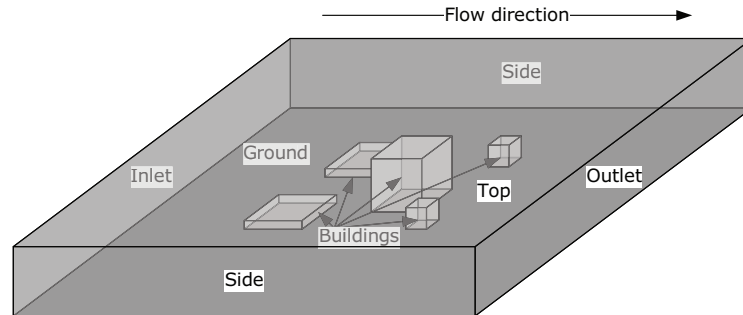


Figure 3.1 General definition of boundaries.

3.2.1 Inlet Boundary Condition

The most important boundary condition is the inlet condition. Above a uniform plane terrain the wind profile is logarithmic (von Karman 1931). Above rough walls the origin of the velocity profile is not the same as the ground level. It is therefore chosen to describe the inlet by an origin shifted log-law:

$$U(z) = \frac{U_*}{\kappa} \ln \left(\frac{z-d}{z_0} \right) \quad (3.5)$$

Where:

- U_* Friction velocity [m/s]
- κ von Karman's constant [-]
- z Height above ground level [m]
- d Origin shift [m]
- z_0 Roughness height [m]

The parameter d is the origin shift and is of the magnitude 70 % to 80 % of the highest obstacles upstream (Garratt 1992). Velocities lower than the origin of the log profile is set to zero. In the actual calculations d is set to three times z_0 , which yields satisfactory values. If the inlet is a distance away from the region of interest the actual value of d is of minor importance, as showed in Appendix B.

The traditional approach for describing the inlet turbulence profiles is given by Richards and Hoxey (1993). Yang et al. (2009) has however introduced the viewpoint that the profiles should be derived from the turbulence model itself. These profiles results in very small horizontal flow gradients when applied for a simulation of a stable atmospheric boundary layer, as showed in Section 3.3.

This has resulted in the turbulence profiles derived for a stable atmospheric boundary layer. For the k - ω Shear Stress Transport (SST) model by Menter (1994), the profile of the turbulent kinetic energy and specific dissipation rate are given by Yang et al. (2008):

$$k(z) = \frac{U_*^3}{\sqrt{C_\mu}} \sqrt{C_1 \ln\left(\frac{z+z_0}{z_0}\right) + C_2} \quad (3.6)$$

$$\omega(z) = \frac{U_*^3}{\kappa \sqrt{C_\mu}} \frac{1}{z+z_0} \quad (3.7)$$

Where:

C_1, C_2 Constants [-]

For the k - ε models Yang et al. (2009) states for the turbulent dissipation rate:

$$\varepsilon = \frac{U_*^3}{\kappa (z+z_0)} \sqrt{C_1 \ln\left(\frac{z+z_0}{z_0}\right) + C_2} \quad (3.8)$$

In order to comply with the origin shifted velocity distribution $z+z_0$ is changed to $z-d$. The part of the profiles that lies below $z=z_0+d$ is given the values at $z=z_0+d$. When the k - and ε -profiles reaches zero at the top where $z > z_0 \exp\left(\frac{-C_2}{C_1}\right) + d$ the value is set to zero.

The log-law only applies to the nearest 150 m of the atmosphere (Garratt 1992). At higher levels the wind changes direction due to the Coriolis force. If very high buildings are evaluated this might influence the conditions at ground level, especially if one of these very high buildings lies in the wake of another.

3.2.2 Outlet Boundary Condition

At the outlet the typical approach is no gradients of all flow variables in the stream wise direction.

3.2.3 Ground Surface Boundary Condition

The ground surface in urban environment is typically rough. Furthermore a number of obstacles as cars and signposts etc. are complicated to model explicitly. Therefore these objects are better treated implicitly as a part of a ground roughness field. Unfortunately application of rough walls is not straightforward in CWE problems.

Richards and Hoxey (1993) suggested to apply the so-called z_0 -type boundary condition given by:

$$U_w = \frac{U_*}{\kappa} \ln\left(\frac{z_w}{z_0}\right) \quad (3.9)$$

Where:

w Denotes centre of wall adjacent cell

This type of boundary condition is the correct boundary condition to apply in atmospheric flows, as it follows directly from the law of the wall. However commercial CFD solvers do not support this type of boundary. Instead k_s -type boundary conditions are available for rough walls. This type is implemented in the form:

$$\frac{U_w}{U_*} = \frac{1}{\kappa} \ln \left(\frac{E z_w}{C_s k_s} \right) \quad (3.10)$$

Where:

- E Constant in the wall function ($E=9$ in Star-CCM+)
- k_s Sand-grain roughness [m]
- C_s Constant which takes the type of roughness into account ($C_s=0.254$ in Star-CCM+)

These two types of boundary conditions are equal if $k_s = \frac{E}{C_s} z_0$ which corresponds to $k_s = 35.4 z_0$ with the standard values given in Star-CCM+. This result has [Blocken, Stathopoulos and Carmeliet \(2007\)](#) and [Hargreaves and Wright \(2007\)](#) stated in longer reviews of the problems with the wall functions.

However Star-CCM+ and other commercial CFD codes limit the value of k_s to the value of y_w . Therefore a high roughness cannot be used on a fine grid. The actual roughness is given by the product $C_s k_s$, and in Star-CCM+ there is no limit on the value of C_s , in opposition to Fluent and CFX.

Therefore the ground roughness is modelled by a value of k_s which is a factor of 10 or 100 too low, and a value of C_s which is a corresponding factor higher, depending on the applied mesh. [Blocken, Stathopoulos and Carmeliet \(2007\)](#) have argued that from a numerical point of view, there should be no problems with introducing roughness higher than z_w .

In practice Star-CCM+ have solved all cases with a factor of 10 change in roughness, and most with a factor of 100. Star-CCM+ complains for higher changes, depending on the state of the solution.

In order to implement the change in roughness properly, the limits for for $R_{+,smooth}$ and $R_{+,rough}$, where R_+ is given by $\frac{k_s U_*}{\nu}$, should be changed in the same way as k_s .

3.2.4 Building Surface Boundary Condition

Buildings can be modelled both smooth and rough depending on how detailed the buildings explicitly are modelled.

The resolution of the flow near building surfaces is not so important, so the problems encountered with the ground surface are not required for the building surfaces. The same procedures can however be implemented.

3.2.5 Free Stream Conditions

At the side boundaries symmetry is the obvious choice. For the top boundary [Richards and Hoxey \(1993\)](#) suggest applying a shear stress corresponding to the velocity profile at the inlet or describing the velocity directly.

In Star-CCM+ neither of these options is available. Instead symmetry is applied on this boundary as well. This is chosen as the least worse of the available options, as symmetry leads to a velocity profile without any slope at the top, which does not comply with the log-law.

3.3 Obtaining a Stable Atmospheric Boundary Layer

Several authors (e.g. Hargreaves and Wright 2007; Yang et al. 2009) have pointed out that obtaining a stable Atmospheric Boundary Layer (ABL) above a uniform flat terrain is a prerequisite for evaluating problems in CWE. If the ABL is not stable then the mathematical model itself induces changes in the streamwise direction, along with geometry of the obstacles in the domain examined.

The stability of the ABL can be examined in an empty domain by comparing the inlet and outlet profiles. Theoretically the profile above a non-slip wall is logarithmic for high Re numbers, and the shape depends only on the roughness of the wall.

Yang et al. (2009) has investigated the problem by making a CFD model and compared the profiles of the velocity U , the turbulent kinetic energy k , and the turbulent dissipation rate ε , for the k - ε model in a wind tunnel without any obstacles.

The inlet profiles are in principle independent on closure coefficients, but Yang et al. (2009) showed that the closure coefficients of the standard k - ε model are not the most suitable to maintain the derived inlet profile through an empty domain.

Based on measurements in atmospheric boundary layers, Yang et al. (2009) suggest to change the closure coefficients of the standard k - ε model by Launder and Spalding (1974) to the values given in Table 3.1.

Table 3.1 New parameters in the k - ε turbulence model suggested by Yang et al. (2009).

| Parameter | Launder and Spalding (1974) | Yang et al. (2009) |
|----------------------|-----------------------------|--------------------|
| C_μ | 0.09 | 0.028 |
| $C_{1\varepsilon}$ | 1.44 | 1.50 |
| $C_{2\varepsilon}$ | 1.92 | 1.92 |
| σ_k | 1.00 | 1.67 |
| σ_ε | 1.30 | 2.51 |

The difference between the two sets of closure coefficients is illustrated by inlet and outlet profiles of U , k , and ε showed in Figure 3.2 and 3.3, based on calculations in an empty domain with dimensions $1.8 \text{ m} \times 1.8 \text{ m} \times 12 \text{ m}$.

As seen in Figure 3.3 the atmospheric boundary layer is more stable with the changed parameters given by Yang et al. (2009). With the original parameters k decreases to almost half the inlet value at the bottom. The same is the case for ε .

Although the velocity profile does not seem to change much in either of the models, the profile still keeps its shape a little better with the changed parameters. Figure 3.4 shows the change in percent from the inlet value for both models.

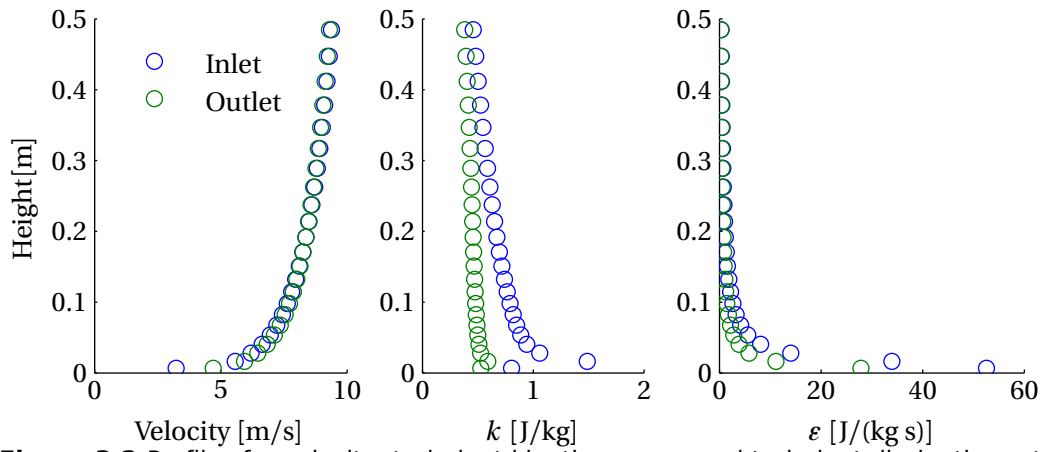


Figure 3.2 Profiles for velocity, turbulent kinetic energy, and turbulent dissipation rate with parameters by [Launder and Spalding \(1974\)](#).

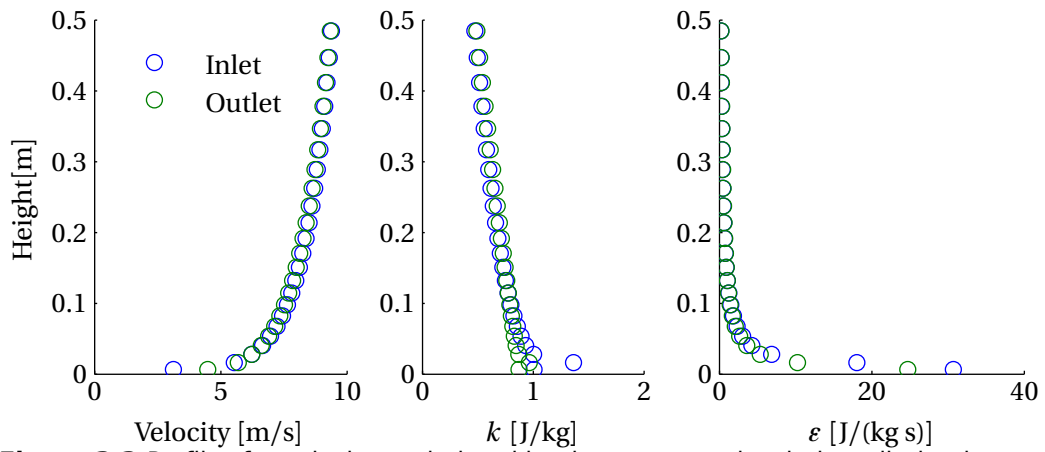


Figure 3.3 Profiles for velocity, turbulent kinetic energy, and turbulent dissipation rate with parameters from [Yang et al. \(2009\)](#).

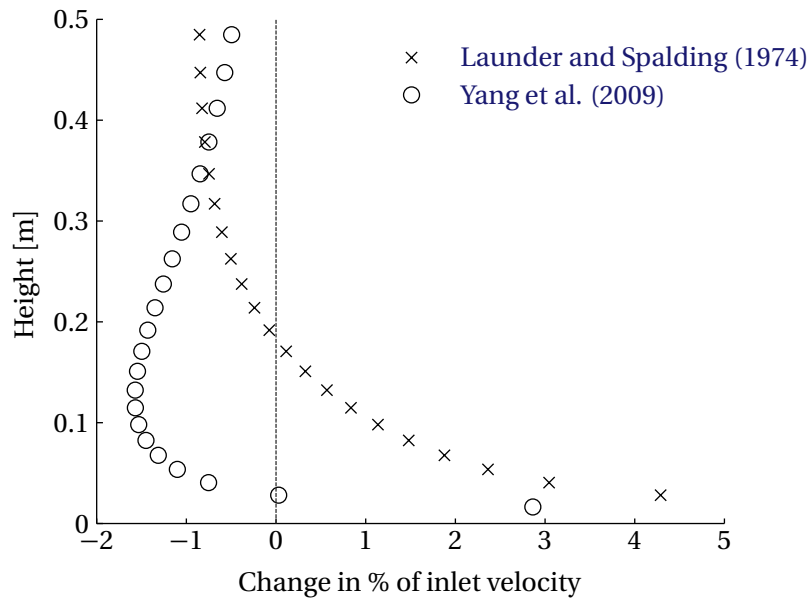


Figure 3.4 Relative change in velocity between inlet and outlet for parameters by [Launder and Spalding \(1974\)](#) and [Yang et al. \(2009\)](#).

The turbulence model with the changed parameters clearly demonstrates a better equilibrium boundary layer, but the question is whether these coefficients also describe the turbulent flow around obstacles better? This question is examined in [Chapter 4](#).

4 Choice of Turbulence Model for Urban Flow

In the present chapter the problems of selecting a proper turbulence model and the applicability of the RANS equations for modelling atmospheric flow are addressed.

Through comparison with measurements conducted by Shirasawa et al. (2003) it is argued that for computational wind engineering problems involving atmospheric flows the SST k - ω model by Menter (1994), with parameters suggested by Yang et al. (2009) should be selected.

In general the RANS approach is found adequate for computational wind engineering problems at the time being, at least for the Re numbers of interest.

4.1 The problem of Turbulence Modelling

Several techniques exist for modelling fluid flow, whereof the most popular approach is the RANS approach. To evaluate the RANS equations for turbulent flow, a turbulence model is required. Since different turbulence models are available, the question arises “which turbulence model describes atmospheric flow the best?”.

To compromise between accuracy and computational cost, the results computed by the different models available are investigated. These are variations of the k - ε model and the SST k - ω model.

4.2 Literature Studies on Performance of Turbulence Models

Several studies have been conducted in order to investigate bluff body flows. Mochida et al. (2002) compared six different k - ε models and a Reynolds Stress Model (RSM), concluding that “the standard k - ε model could not reproduce the back flow on the roof”, in opposition to the revisited k - ε models. No recommendations are stated though.

The recommendations by Franke et al. (2004) state that “the standard k - ε model should not be used in the simulation of wind engineering problems”, and recommend revisited k - ε models or the SST-model by Menter (1994).

Furthermore Franke et al. (2004) cite a range of studies which indicate that non-linear models, which are able to account for anisotropy predicts the flow field better than the linear eddy viscosity models. Unfortunately none of these models are available in Star-CCM+. The only RANS approach in Star-CCM+ which is able to account for anisotropy is an RSM-model.

4.3 Performed Studies on Turbulence Models

Because no recommendations on choice of turbulence models are given, a study based on some of the available turbulence models given in Star-CCM+ is conducted.

In order to choose a turbulence model, simulations are conducted with different turbulence models on a $4 \times 4 \times 1$ cube. The turbulence models applied are listed in Table 4.1.

In all of the models closure has been applied by certain model constants. Yang et al. (2008); Yang et al. (2009) has proposed another set of closure coefficients for both $k-\epsilon$ models and the $k-\omega$ SST model, which models an equilibrium atmospheric boundary layer better, as showed in Section 3.3.

The models have been applied both with the original set of closure coefficients by Launder and Spalding (1974) and those provided by Yang et al. (2009). The applied closure coefficients for the different models are given in Appendix A

Table 4.1 Different turbulence models applied on a $4 \times 4 \times 1$ cube.

| Model name | Reference |
|-----------------------------------|--|
| Standard $k-\epsilon$ | (Launder and Spalding 1974) |
| Standard $k-\epsilon$ Two-layer | (Launder and Spalding 1974; Rodi 1991) |
| Realisable $k-\epsilon$ | (Shih et al. 1995) |
| Realisable $k-\epsilon$ Two-layer | (Rodi 1991; Shih et al. 1995) |
| $k-\omega$ Shear Stress Transport | (Menter 1994) |

4.3.1 Experimental Data

In addition to the computed results, measurements focused on pedestrian level wind speeds are available, from an experiment made in a boundary layer wind tunnel by Shirasawa et al. (2003) (described in English by Tominaga et al. 2004).

The experiment is conducted using hotwire anemometers in a $1.6 \text{ m} \times 1.6 \text{ m}$ wind tunnel. The computational domain showed in Figure 4.1 is chosen to accommodate the dimensions of the wind tunnel, in which the measurements are conducted, but with a vertical plane of symmetry.

The anemometers are located in the positions given by Figure 4.2 and 4.3. In Figure 4.4 and 4.5 contour plots of the U velocity component are given based on the experimental data.

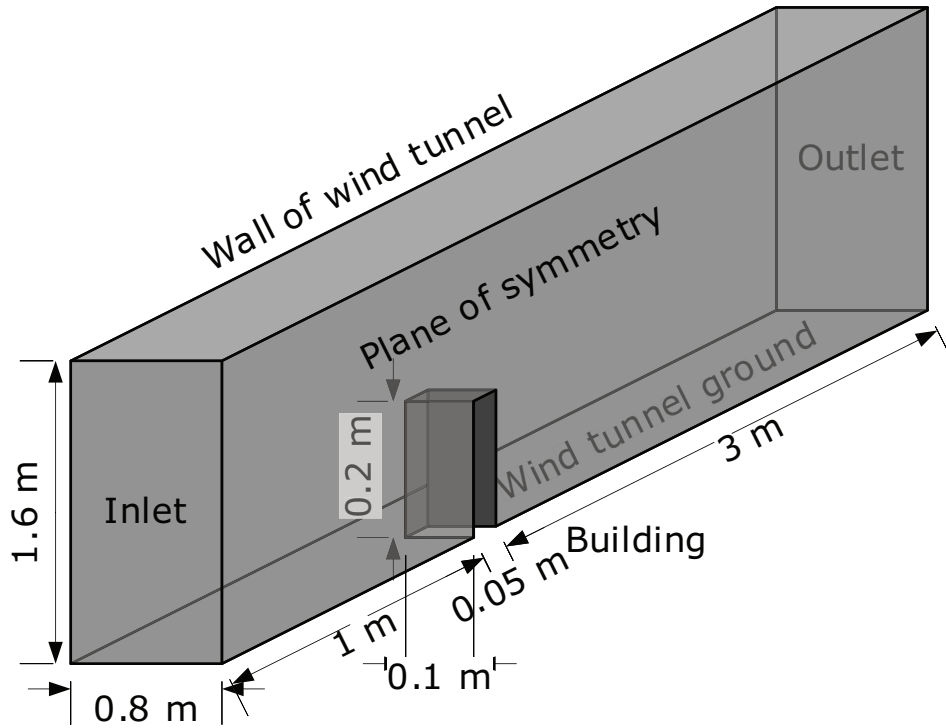


Figure 4.1 Computational Domain for $4 \times 4 \times 1$ cube.

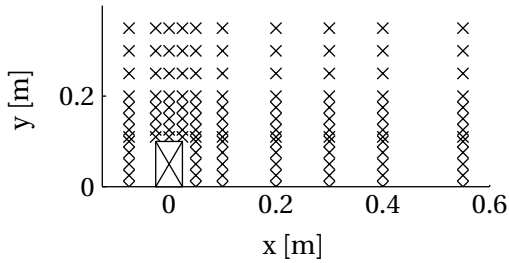


Figure 4.2 Measuring points, horizontal section, $z = 12.5$ mm.

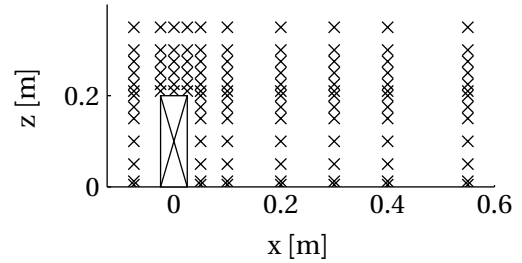


Figure 4.3 Measuring points, vertical section $y = 0$ mm.

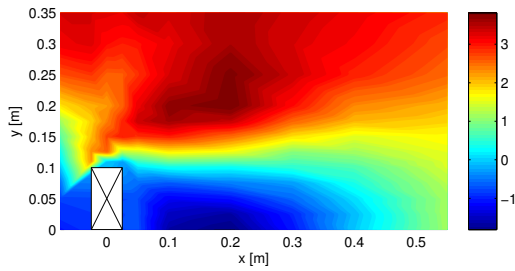


Figure 4.4 Contour plot of measured U , horizontal section.

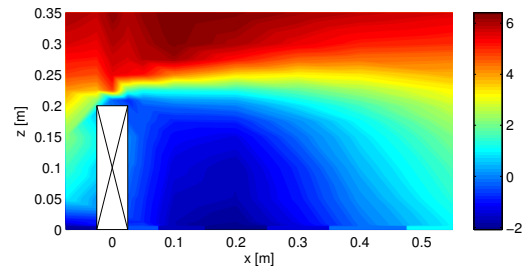


Figure 4.5 Contour plot of measured U , vertical section.

4.3.2 Computational Domain

The domain is discretised into a mesh of 826 000 cells, which is applied for all turbulence models. The mesh is showed in Figure 4.6.

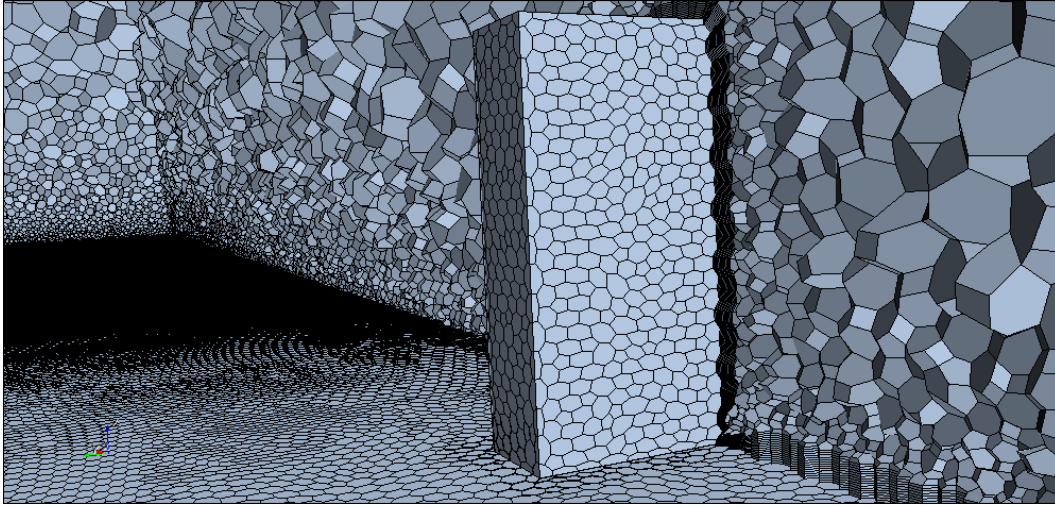


Figure 4.6 Mesh applied for analysis of turbulence models.

Another mesh with 2290000 cells is generated in order to show that the discretisation is adequate. The flow with the $k-\omega$ SST model with Yang et al. (2009) parameters are computed on this finer mesh showing that the discretisation is adequate. In Figure 4.7 the finer mesh is compared to the standard mesh.

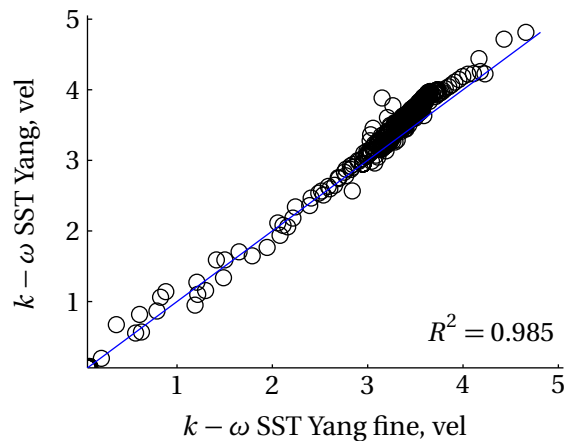


Figure 4.7 Comparison of wind speed computed on fine and standard grid.

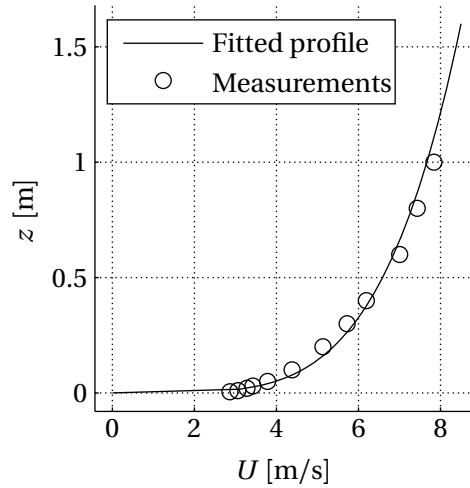
4.3.3 Boundary Conditions

The intended boundary conditions are stated in Table 4.2, but some remedial measures have been applied in order to apply these boundary conditions.

Inlet At the inlet, measurements of the velocity and k are available. A power law is fitted to the velocity measurements, and tabulated values of k are applied directly to the inlet by mean of linear interpolation.

Table 4.2 Boundary conditions for analysis on $4 \times 4 \times 1$ cube.

| Condition | Velocity |
|-----------|--|
| Inlet | Measured, given by Figure 4.8 and 4.9. |
| Outlet | Zero gradient in the stream wise direction for all flow variables. |
| Ground | Rough wall, $z_0 = 9.6 \times 10^{-5}$ m converted to sand grain roughness k_s . |
| Symmetry | Symmetry. |
| Walls | Smooth wall. |
| Building | Smooth wall. |

**Figure 4.8** Inlet velocity profile for analysis on $4 \times 4 \times 1$ cube.

The inlet conditions are only given up to 1 m. For the velocity a power law is fitted and used in the full height. For k the values above the kink in the profile, near the ground, are used for extrapolation above 1 m, as seen in Figure 4.9.

Applying the extrapolation to the full height would lead to a negative k which is not physically meaningful. Therefore zero is set as the lower limit of k . The ε profile is obtained by the following relation given by Yang et al. (2009) for local equilibrium conditions ($P_k = \rho \varepsilon$):

$$\varepsilon = \sqrt{C_\mu} k \frac{\partial U}{\partial z} \quad (4.1)$$

The ω profile is obtained by the following identity:

$$\omega = \frac{\varepsilon}{\beta_* k} \quad (4.2)$$

Where:

$$\beta_* \quad \text{Constant [-]}$$

Ground At the ground a rough wall is applied. The roughness height is converted to an equivalent sand-grain roughness. It is a well known problem with commercial CFD codes that the roughness is limited to the half of the height of the wall adjacent cell (Blocken, Stathopoulos and Carmeliet 2007; Hargreaves and Wright 2007). A remedial measure has been applied in order to introduce the intended roughness. The details of the remedial procedure are given in Section 3.2.3.

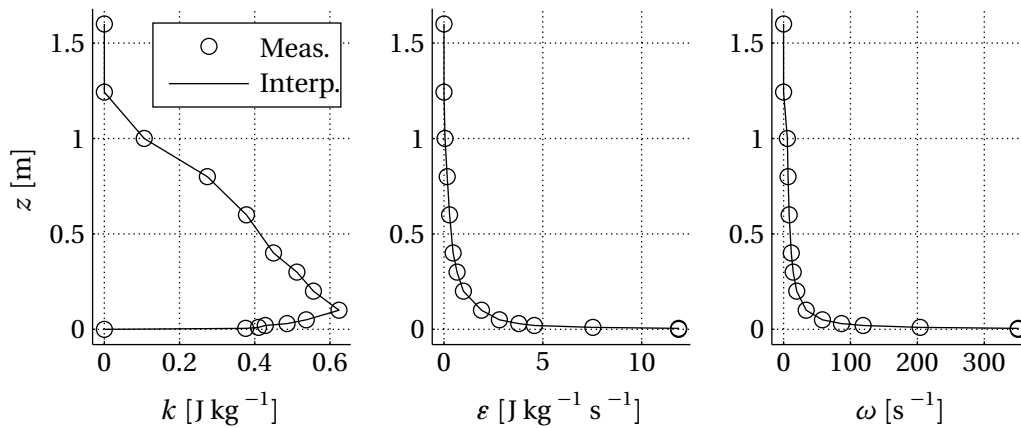


Figure 4.9 Inlet turbulence profiles for analysis on the $4 \times 4 \times 1$ cube.

4.4 Analysis of Computed Results and Experimental Data

The intention of using CFD calculations to evaluate wind conditions, implies that the turbulence models should be evaluated by the comfort and danger criteria. As stated in [Chapter 2](#) two parameters are combined to describe comfort and danger, namely the horizontal velocity $|U_H|$ and the standard deviation thereof. Hence these two parameters are central for this investigation.

In addition to the evaluation criteria, the overall flow should be modelled properly, therefore other flow parameters than the U and V , composing the horizontal velocity, is interesting. The standard deviation of the velocity is modelled through the turbulent kinetic energy k .

In [Table 4.3](#) regression coefficients are given between the measurements and the CFD results, for the different parameters. The regression coefficient is evaluated in the measurement points as given by [Figure 4.2](#).

Table 4.3 Horizontal section. R^2 for the different models and parameters.

| Model | U | V | W | $ U_H $ | $ U_i $ | k |
|--|-------|-------|-------|---------|---------|--------|
| k - ω SST | 0.860 | 0.823 | 0.633 | 0.675 | 0.680 | 0.013 |
| k - ω SST Yang et al. (2009) | 0.900 | 0.864 | 0.561 | 0.808 | 0.810 | 0.023 |
| Realisable k - ϵ | 0.835 | 0.843 | 0.449 | 0.728 | 0.726 | 0.0075 |
| Realisable k - ϵ Yang et al. (2009) | 0.854 | 0.858 | 0.441 | 0.837 | 0.833 | 0.0092 |
| Realisable k - ϵ Two Layer | 0.776 | 0.836 | 0.390 | 0.674 | 0.668 | 0.028 |
| Realisable k - ϵ Two Layer Yang et al. (2009) | 0.804 | 0.859 | 0.381 | 0.811 | 0.807 | 0.095 |
| Standard k - ϵ | 0.859 | 0.875 | 0.422 | 0.825 | 0.822 | 0.027 |
| Standard k - ϵ Yang et al. (2009) | 0.827 | 0.813 | 0.570 | 0.577 | 0.580 | 0.0057 |
| Standard k - ϵ Two Layer | 0.818 | 0.870 | 0.381 | 0.782 | 0.777 | 0.045 |
| Standard k - ϵ Two Layer Yang et al. (2009) | 0.815 | 0.817 | 0.573 | 0.541 | 0.544 | 0.0032 |

It appears that the k - ω model with Yang parameters performs best for describing the individual velocity component, while the realisable k - ϵ with Yang parameters is best for describing the overall wind speed. This is attributed to that determining the wind speed

is not a linear operation, and while the realisable $k-\varepsilon$ model get the wind speed right, the $k-\omega$ model gets the direction right.

For all the tested models, except the standard $k-\varepsilon$, the parameters given by Yang et al. (2009) performs significantly better than the models with the standard parameters. This supports the precondition stated in Section 3.3, that a correct modelling of the atmospheric boundary layer is important.

Results computed for the vertical section are given in Table 4.4. The V -component and the wind speeds are not given, as the vertical section is a plane of symmetry.

Also for the vertical section the $k-\omega$ SST with Yang parameters performs best. Even the turbulent kinetic energy is modelled by the $k-\omega$ SST to some extent.

Table 4.4 Vertical section. R^2 for the different models and parameters.

| Model | U | W | k |
|---|-------|-------|-------|
| $k-\omega$ SST | 0.941 | 0.810 | 0.514 |
| $k-\omega$ SST Yang et al. (2009) | 0.954 | 0.838 | 0.606 |
| Realisable $k-\varepsilon$ | 0.933 | 0.827 | 0.054 |
| Realisable $k-\varepsilon$ Yang et al. (2009) | 0.931 | 0.839 | 0.103 |
| Realisable $k-\varepsilon$ Two Layer | 0.918 | 0.804 | 0.021 |
| Realisable $k-\varepsilon$ Two Layer Yang et al. (2009) | 0.920 | 0.817 | 0.067 |
| Standard $k-\varepsilon$ | 0.929 | 0.823 | 0.048 |
| Standard $k-\varepsilon$ Yang et al. (2009) | 0.926 | 0.806 | 0.177 |
| Standard $k-\varepsilon$ Two Layer | 0.924 | 0.809 | 0.028 |
| Standard $k-\varepsilon$ Two Layer Yang et al. (2009) | 0.924 | 0.802 | 0.168 |

The turbulent kinetic energy is either not measured right or modelled right. The first is properly the case, as problems with measuring turbulence with hotwire anemometers are reported for high turbulence intensities (Bottema, Leene and Wisse 1992).

In Figure 4.10 the turbulence intensity is plotted with a threshold of 0.45 % as Bottema, Leene and Wisse (1992) showed as the limit for hotwire anemometers to measure the fluctuations correctly.

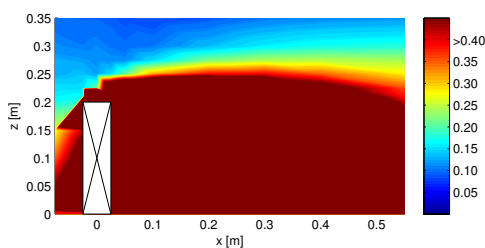


Figure 4.10 Plot of turbulence intensity exceedance for hotwire anemometers.

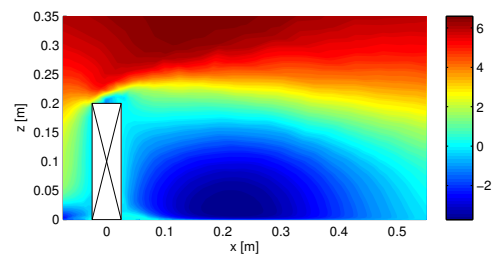


Figure 4.11 Contour plot of U with $k-\omega$ model, vertical section.

If a regression analysis for k is conducted only with anemometers located outside the zone with too high turbulence intensity, R^2 is 0.824 for the vertical section with the SST $k-\omega$ model with the parameters suggested by Yang et al. (2009). Contour plots of U , and regression plots of the measured and computed values with the $k-\omega$ SST model are given in Figure 4.11 and 4.12, for a vertical section.

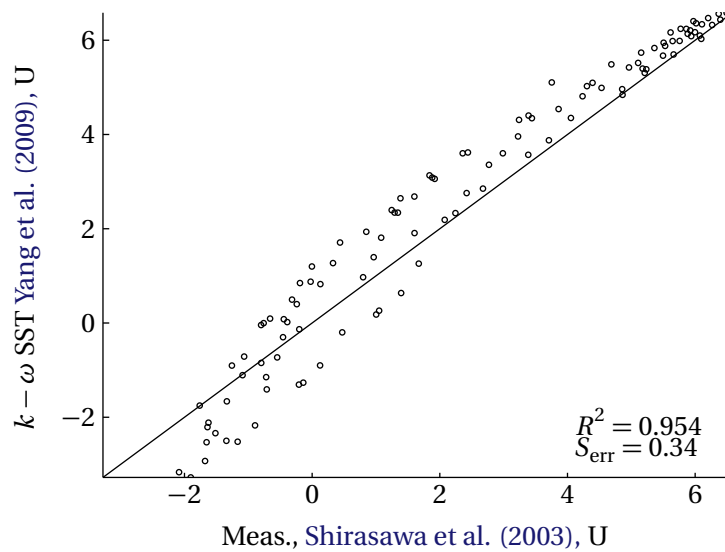


Figure 4.12 Regression plot of U with $k-\omega$ model, vertical section.

The $k-\omega$ SST model performs best overall, and is therefore recommended as turbulence model for computational wind engineering applications. At least some of the components in the flow field is remarkable well modelled by this model, and leaves no basis for using transient techniques for the time being.

The computational cost of the models is almost the same, as all of the applied models require two extra differential equations solved, along with the RANS equations.

4.5 Discussion and Perspectives of the Turbulence Models

The $4 \times 4 \times 1$ cube is selected as experimental data is available and it is relatively simple case. Urban geometry is typically characterised by the sharp edges of the buildings. Some cases is however composed of cylindrical elements, for instance the case at Høje Brygge, Nørresundby, presented in Chapter 8.

For rectangular geometry the flows separation points are located at the corners. The specific location of the separation points for cylindrical geometries on the other hand are not known and more severe differences between the different turbulence models are to be expected.

It would therefore be interesting to evaluate the models against experimental data for cylinders. Fortunately cylindrical geometries are rare in urban environments, and there is no reason to expect that the best models for rectangular geometries should be the worst for cylindrical geometries.

A number of studies report on the inaccuracies of RANS models for cylindrical geometries, and evaluate the possibilities in more refined techniques as LES, DES and URANS (Catalano et al. 2003; Spalart 2009).

Although better results are achieved with these refinements, the computational cost of transient solutions still makes these techniques inapplicable for computational wind engineering problems. Even though a large amount of extra information is obtained in transient analyses, nothing more than the mean flow and its standard deviation is the goal of the simulations.

4.6 Conclusion on Turbulence Modelling

In the present chapter comparison of various turbulence models with the data obtained by Shirasawa et al. (2003) is conducted. The models are evaluated on basis of their applicability to computational wind engineering problems, especially problems of pedestrian wind comfort.

Two sets of model constants are evaluated; the original suggested by Launder and Spalding (1974) for the standard k - ϵ model, and a modified set suggested by Yang et al. (2009), in order to model a neutral atmospheric boundary layer.

The SST k - ω model, the standard k - ϵ model, and the realisable k - ϵ model are evaluated and the models performs better with the parameters suggested by Yang et al. (2009), for all evaluated variables except W for the k - ϵ models.

The SST k - ω model performs better on all the individual velocity components while the realisable k - ϵ model performs best on the overall velocity magnitude. This is attributed to the fact that the errors in the individual velocity components equal each other out.

It is argued that the fluctuations are not measured correctly in large parts of the domain, due to large turbulence intensities. A cautious statement is that the k - ω model computes the turbulent kinetic energy best.

For computational wind engineering problems involving atmospheric flow the SST k - ω model by Menter (1994) is recommended with the parameters suggested by Yang et al. (2009).

5 Treatment of Wind Statistics

In the following chapter statistical basis for evaluating wind conditions is considered through the transformation of wind statistics.

A two-layer model for the atmospheric boundary layer, based on the studies by Wieringa (1986) and Verkaik et al. (2005), have been applied in order to transform the statistics from the meteorological site to the location.

The model shows good agreement in comparison with the more thorough model applied by Troen (1989). Further improvements are suggested if wind conditions are to be evaluated on a routine basis.

The basis for evaluating problems in computational wind engineering is on one hand an evaluation of the flow, either by wind tunnel testing or by CFD, and on the other hand statistical data on the occurrence of the modelled flow phenomena.

The topic of interest in the following is this second part, the treatment of the wind statistics. If the surroundings of the meteorological site and the evaluation site are different, at least the change in ground friction should be considered.

Wind statistics are readily available for a number of locations (in Europe covered by Troen (1989) for instance). These wind statistics are based on point measurements typically 10 m above ground level.

The question is, “how should the wind statistics of the considered location be linked to the wind statistics of the meteorological site?” And since the distance between these two locations are often of an order which does not allow for modelling both locations in the same domain, at least by full CFD models, some statistical treatment based on atmospheric models have to be considered.

5.1 The Atmospheric Boundary Layer

As stated by Rossby and Montgomery (1935), the atmospheric boundary layer is divided into two layers, a surface layer, and an Ekman layer, as seen in Figure 5.1.

In the surface layer the direction of the wind is determined by the force balance between the ground friction, pressure difference, and the Coriolis force. In the Ekman layer, the effect of the ground friction vanishes and the wind is turning to reach the geostrophic wind at the top of the ABL.

The angle between the surface wind and the geostrophic wind depend on the roughness. Therefore a change in roughness not only implies a change in the friction velocity, but also in the direction in which the surface wind approaches.

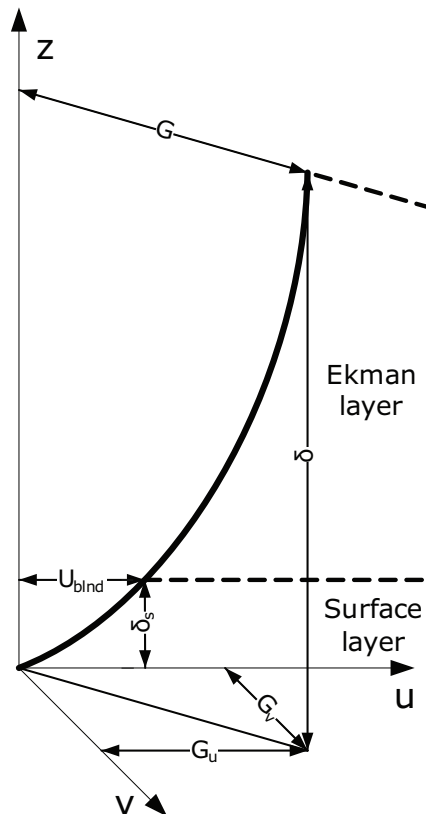


Figure 5.1 Two-layer model of the atmospheric boundary layer. In the surface layer no turning occurs, but in the Ekman layer the wind has a components in both the u and the v direction.

5.1.1 Use of Similarity Theory

The flow in the ABL is a function of geostrophic wind, surface roughness, latitude and the heat flux from the ground, which in turns is a function of time and cloud cover.

The so-called similarity theory attributed to [Rossby \(1932\)](#) describes the relation between the surface wind and the geostrophic wind in the case of a horizontal homogeneous, neutral atmosphere. That being without any heat flux from the ground, whereby the generation of turbulence is purely mechanic.

The similarity theory by [Monin and Obukhov \(1954\)](#) takes the heat flux into account, but it is only valid in the surface layer. [Deardorff \(1972\)](#) combined these two theories into a common similarity theory for the full ABL.

This theory of the full ABL can in principle be applied for the wind statistics, but for the following reasons only Rossby similarity theory will be applied, and the heat flux from the ground is neglected:

- In strong wind, which contributes most to the exceedance probability of the evaluation criteria, the flow is solely driven by pressure differences as the sky typically is clouded, whereby buoyancy can be neglected.
- Taking the heat flux into account requires statistics on the cloud cover, and its correlation with the wind velocities.

- Monin-Obukhov theory is derived for horizontal homogeneous terrain with constant heat flux, which is almost never the case in reality.
- Recent investigations have raised concerns over the general validity of Monin-Obukhov theory, and in comparison with measurements a large amount of scatter remains (Foken 2006; Johansson et al. 2001; Khanna and Brasseur 1998; McNaughton 2009).
- Wieringa (1986) argues that transformation error upward from the surface wind to the geostrophic wind using Rossby similarity theory counterbalances the transformation error downward from the geostrophic wind to the surface wind.

The last point is important, since it implies that, although the wind statistics transformed to geostrophic level is not correct, the wind statistics determined when transformed down at another location is still correct, at least to the precision of the typical anemometers used to obtain the wind statistics, and the uncertainty in determining the roughness height.

5.1.2 The Geostrophic Relations of Rossby Similarity Theory

The geostrophic relations of Rossby similarity theory are as follows (derived in the present form by Csanady (1967) and Blackadar and Tennekes (1968)):

$$G_u = \frac{U_*}{\kappa} \left(\ln \frac{\delta}{z_0} - A \right) \quad (5.1a)$$

$$G_v = -\frac{U_* B}{\kappa} \quad (5.1b)$$

Where:

- G_u, G_v Geostrophic wind parallel and perpendicular to the surface wind respectively [m/s]
 δ Height of ABL [m]
 A, B Constants for neutral ABL [-]

These equations form a relation between the surface wind and the geostrophic wind. The angle between the surface wind and the geostrophic wind is given by:

$$\tan \theta = \frac{G_v}{G_u} = \frac{B}{\ln \frac{\delta}{z_0} - A} \quad (5.2)$$

The height of the ABL is determined by:

$$\delta = c \frac{U_*}{f} \quad (5.3)$$

Where:

- c Constant [-]
 f Coriolis parameter [1/s]

The constant c is usually set to approximately 0.3 (Blackadar and Tennekes 1968). The Coriolis parameter f is dependent on the longitude of the location. In a recent survey on the constants A and B Hess and Garratt (2002) suggested the values 1.3 and 4.4 respectively.

A more simple relation is suggested by Simiu and Scanlan (1978), which relates the difference in roughness directly to the change in friction velocity:

$$\frac{U_{*,1}}{U_{*,2}} = \left(\frac{z_{0,1}}{z_{0,2}} \right)^{0.0706} \quad (5.4)$$

Bottema (1992) reported the accuracy of the formulation to better than 5 % compared to using the full relations given by Equation 5.1. This relation does however not take any change in direction into account.

Both the full geostrophic relations and the simple relation suggested by Simiu and Scanlan (1978) are in principle valid for a homogeneous, uniform terrain with the roughness z_0 . This is however almost never the case in reality.

One solution is to use a model of the internal boundary layer which develops after a roughness change, but these models are typically not well suited for multiple roughness transitions. Therefore some kind of effective roughness has to be used.

5.2 Applied Atmospheric Model

In the work of Troen (1989) both untreated data and exposure corrected data are available. The exposure corrected data are treated through a model which takes roughness, shelter effects, and stability correction into account, in order to obtain statistics above four standard roughness classes.

The exposure corrected data are an estimate on the regional wind climate, and can readily be transformed to geostrophic level through Equation 5.1. In a recent study on wind comfort, Blocken and Persoon (2009) suggest using the procedure of Verkaik et al. (2005) to take changes in roughness into account. The outline of the model is as follows:

1. Transformation of the wind from measurement height to 60 m by the normal log-law:

$$U(z) = \frac{U_{*,l}}{\kappa} \ln \left(\frac{z}{z_{0,l}} \right) \quad (5.5)$$

Where:

- U_* Friction velocity [m/s]
 - $z_{0,l}$ Local roughness height [m]
2. Transformation of $U_{*,l}$ to $U_{*,r}$ corresponding to $z_{0,r}$, where index “r” stands for regional, using Equation 5.5.
 3. Transformation from 60 m to the top of the ABL using the geostrophic relations given by Equation 5.1. The geostrophic wind can eventually be interpolated between multiple meteorological sites.

The inverse procedure can be applied at the location for each sector in question, with the effective roughness heights at that location. The procedure is sketched in Figure 5.2

The philosophy is that the local roughness field is blended in the surface layer, and the regional roughness field is blended in the Ekman layer. The reason for choosing 60 m as blending height for the local roughness is however not obvious.

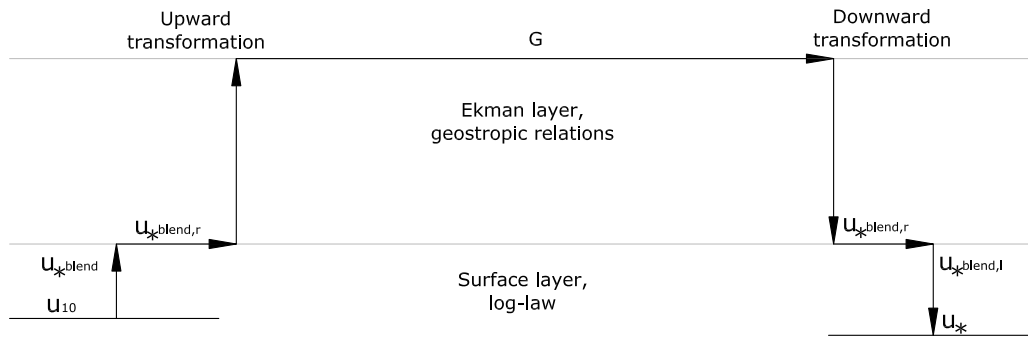


Figure 5.2 Procedure for transformation of wind from one location to another. The input is the surface wind at 10 m, which is transformed using the log-law and the local roughness field to the blending height. Hereafter an equivalent wind is determined using the regional roughness field, and the transformation is continued to geostrophic wind. The inverse procedure is applied in the downward transformation. The output is the friction velocity at the location of interest.

The height of the surface layer is normally taken as the lowest tenth of the full ABL height (Garratt 1992). A reason for fixing the blending height at 60 m is that it makes the overall calculation easier.

As the height of the surface layer actually scales with the Coriolis parameter and the friction velocity, the blending height should be determined based on latitude and a proper estimate on the friction velocity.

In the present application the top of the surface layer is fixed at 150 m roughly, corresponding to a velocity of 6 m/s, 1.7 m above a terrain with roughness height 0.03 m in Denmark.

5.2.1 Choosing the Roughness Heights

The procedure outlined by Verkaik et al. (2005) is set up to determinate surface wind speeds based on numerical weather prediction systems. Since the intention were to determine the surface wind for the entire Netherlands, a quite sophisticated treatment of the roughness heights is suggested, based on land use maps and so-called footprint models (e.g. Schmid 1994).

For the present purpose just a description of the inlet statistic at the boundary of the domain actually modelled is sought. A more simple treatment is therefore suggested in the following, based on how the procedure by Verkaik et al. (2005) operates in a single grid point.

Two directional dependent roughness heights are to be determined. To each roughness height a footprint length scale D is associated, determining the distance to the centre of the source roughness field, as showed in Figure 5.3.

The effective roughness is then estimated from the roughness field considering the following:

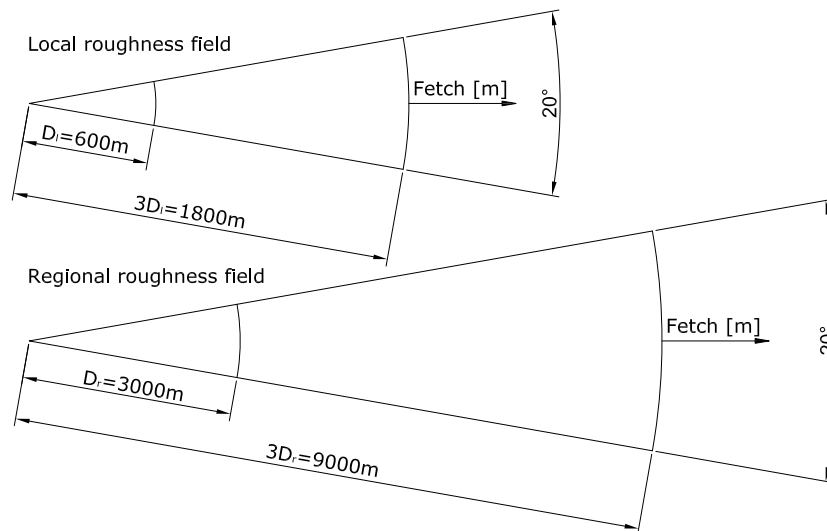


Figure 5.3 Sketch of roughness footprint length scales after Verkaik et al. (2005).

- Consider the roughness field highest at the footprint length scale, and up to a distance of three times the footprint length scale.
- Give the larger roughness slightly more weight.
- In a bell shape, roughness in 10° to each side of the considered direction has influence.
- The roughness height can be estimated from the updated Davenport classification by Wieringa (1992).

In practice estimates on the roughness are made every time the roughness changes significantly, that is just before and just after, in order to interpolate between these values, as exemplified in Figure 5.4.

The local roughness determined is also applied for the inlet profiles in the CFD evaluation of the atmospheric flow.

5.3 Implementation Issues

The model is relatively simple to apply for a given wind measurement in order to transform it to another place. However treating the wind speed as a directional dependent statistical variable complicates the process significantly.

This is a result of directional roughness gradients changes the distance between two sectors, which the model is applied for. This results in changes in the probability that the wind is coming from a specific direction.

The input to the transformation procedure is the data given by Troen (1989). These are the Weibull parameters A and k for 12 equidistant sectors, and the probability that the wind is coming from a given sector P_θ .

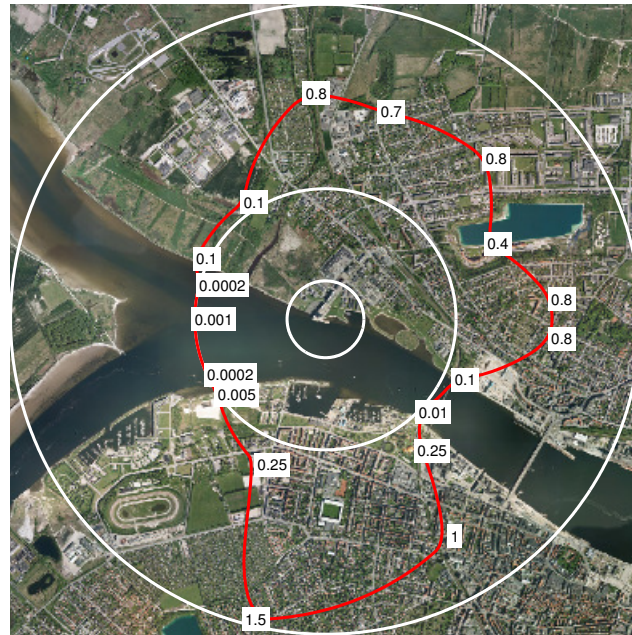


Figure 5.4 Effective local roughness applied for the case at Høje Brygge, Nørresundby. The first circle is the domain modelled explicitly by CFD, the second corresponds to the footprint length scale and the third corresponds to three times the footprint length scale. The estimated roughness is illustrated superimposed on the second circle.

More continuous data would be appropriate, but this is however what is available. In order to make the statistics continuous, spline interpolation have been applied. This results in a directional dependent probability density function.

The following procedure is applied in order to transform the wind:

1. A spline is fitted to the parameters A , k and P_θ , in order to increase the directional resolution to n_θ sectors.
2. The transformation procedure is calculated for each sector.
3. The procedure is linear and is therefore calculated as a factor, which is multiplied with the scale parameter A for each sector.
4. The change in direction is likewise determined for each sector.
5. The change in direction for each sector determines the change in P_θ .
6. The parameters A , k and P_θ , are fitted to a new directional grid.
7. The determined parameters are smoothed by a running average covering 30° as this is the resolution of the original data.
8. Representative values of the parameters A , k , and P_θ are determined for the sector each CFD realisation covers.

The last item gives the opportunity for making CFD realisations for another number of directions than the 12 given in the input data, or for sectors of different width but covering the same probability of occurrence.

5.4 Verification and Validation of Transformation Procedure

In order to verify that the model is implemented right, it is tested whether transformation up and down yields the same result as the initial data. This is showed in Figure 5.5 with the Tirstrup data.

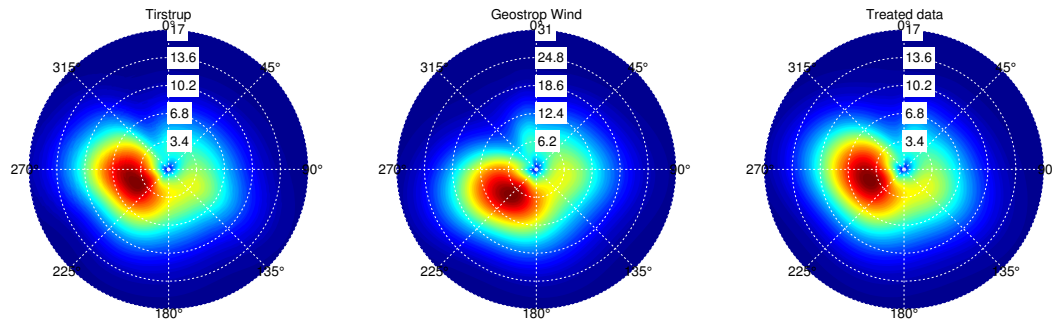


Figure 5.5 Verification of upward and downward transformation.

The procedure is intended to do the same as the procedure Troen (1989) applied in order to correct that data for local effects. The procedure is therefore validated with the untreated data as input and compared with the treated data of Troen (1989).

Troen (1989) has validated his results by transformation and interpolation of the statistics to another site where wind measurements are available, with excellent results. The quality of the data which is validated against should therefore be quite adequate.

Systematic errors can however be present in both models, as they are based on the same principles, although additional submodels are present in the procedure by Troen (1989). In Figure 5.6 the obtained A -parameters are compared with those of Troen (1989) and in Figure 5.7 the values of P_θ are compared.

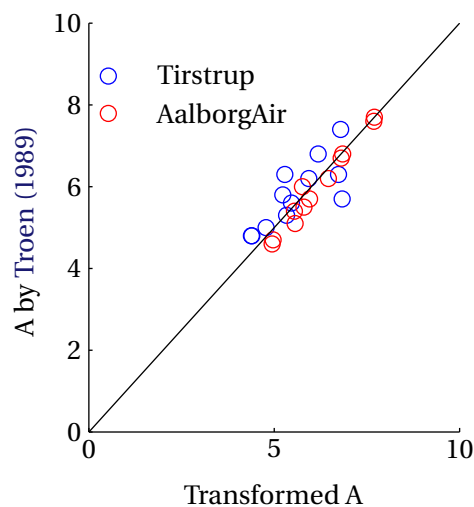


Figure 5.6 Comparison of A obtained by transformation and by Troen (1989).

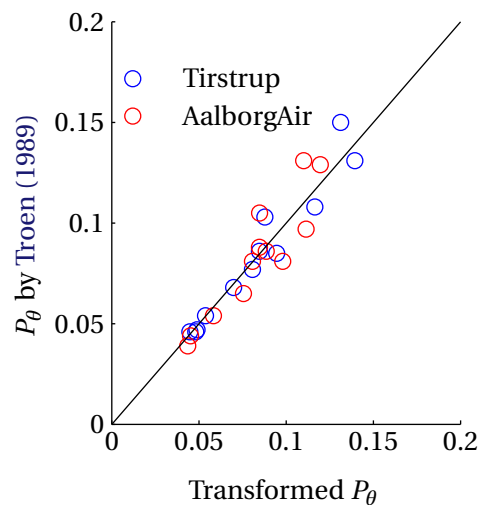


Figure 5.7 Comparison of P_θ obtained by transformation and by Troen (1989).

The level of agreement is quite good. In particular the agreement on the Aalborg transformation is very good. The errors in the Tirstrup data can be attributed to the significant shelter effects at measurement site, as the area is quite forested.

Introducing the shelter submodel Troen (1989) applies in the procedure, will however not gain anything in the present application, as it is the downward transformation that is interesting.

5.5 Conclusion and Perspectives on Statistical Treatment

The statistical treatment is overall satisfactory. However the final conclusion on the wind conditions is extremely sensitive to the actual parameters. Care therefore has to be taken in the process.

Although the quality of the input data is quite good, the directional discretisation is somewhat limited for the present application. It would be appropriate to apply data with higher directional resolution.

The procedure of Verkaik et al. (2005) where land use maps have been applied to estimating the roughness fields, would have quite good perspectives if wind conditions are to be evaluated on a routine basis.

Especially because the sole dependent parameter in the transformation process is the roughness height, care has to be taken in estimating the right values. Furthermore interpolation of the geostrophic wind statistics between meteorological sites would be appropriate if the horizontal transformation is significant.

5.6 Linearity with Respect to the Velocity

A direct coupling between a CFD model and wind statistics require that the wind speeds can be normalised. This is only physical meaningful if the flow pattern is independent of the free wind speed. The flow is strongly dependent on the Re number at very low wind speeds. However, according to Jensen (1959), the flow is independent of the Reynolds number for wind speeds found in atmospheric flows.

In order to investigate the dependency of the Re number, the flow around a $4 \times 4 \times 1$ cube and a cylinder is investigated with different inlet velocities.

5.6.1 Study on a $4 \times 4 \times 1$ Cube

Two identical models with different wind speed are conducted and compared. One with a reference wind speed of 5 m/s and one with 10 m/s in a height of 0.2 m.

A regression plot of the normalised velocity and turbulent kinetic energy are showed in Figure 5.8 and 5.9. From these plots it is clear that the velocity behaves almost complete linear with the wind speed.

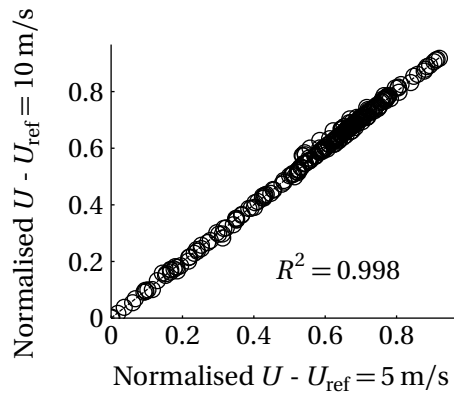


Figure 5.8 Regression plot of normalised velocities.

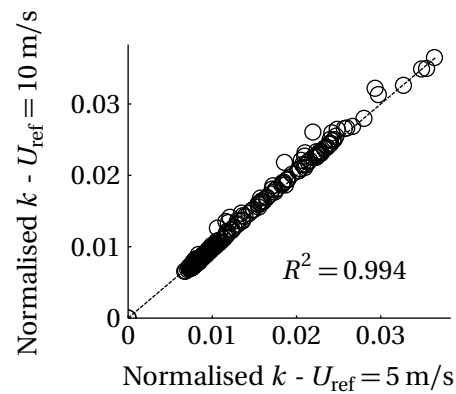


Figure 5.9 Regression plot of normalised k .

Because both the velocity and the standard deviation hereof behave linear with a change in wind speed, it is possible to normalise the velocities without making further considerations about the free stream velocity.

5.6.2 Study on a Cylinder

In flows with sharp edged geometry the separation points are well defined. On cylinders however the point of separation moves further upstream with increasing Re number, which could change the flow pattern with a change in free stream wind speed.

Two identical models are run with different reference speed, one with 1 m/s and one with 15 m/s, which is considered as appropriate limits when evaluating wind conditions.

A regression plot of the normalised velocity and turbulent kinetic energy can be seen in [Figure 5.10](#) and [Figure 5.11](#). From the figures it is clear that the wind around a cylinder behaves quite linear as well, at least for the velocities present in atmospheric flows.

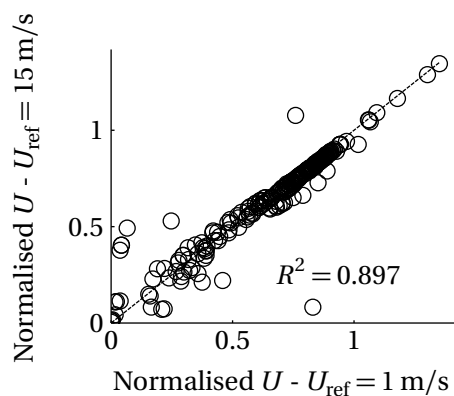


Figure 5.10 Regression plot of normalised velocities for the cylinder.

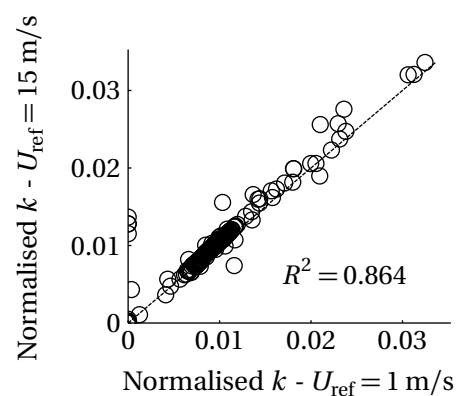


Figure 5.11 Regression plot of normalised k for the cylinder.

It is thereby concluded, that a single realisation of the wind statistics is adequate for each direction.

5.7 Coupling between Wind Statistics and CFD Calculations

The coupling between the wind statistics and the actual CFD calculations is made through the friction velocity U_* . The applied inlet condition is fully described through the friction velocity and the inlet roughness height.

The inlet roughness height is a deterministic variable, while the friction velocity U_* is a directional depended statistical variable.

A number of realisations are made for U_* through the CFD calculations and appropriate statistics are determined for the realisations. The output of the CFD calculations are normalised by the U_* used for the calculation by the following relation:

$$\frac{\text{Friction velocity}}{\text{Friction velocity in model}} = \frac{\text{Threshold}}{\text{Effective wind speed at ground level}} \quad (5.6)$$

Where the left hand side designates the normalisation by the friction velocity applied in the given realisation, and the right hand side is a fraction of “how much is the threshold exceeded”. In practice the friction velocity in the model is transferred to the right hand side.

Combined with the cumulative distribution function of the Weibull distribution describing the friction velocity, the exceedance probability of the evaluation criteria can be determined. By this procedure statistics are determined for the entire computational domain.

6 Validation of CFD Model

In order to validate the numerical flow model presented in Chapter 4, full scale measurements are conducted in the area around Høje Brygge, Nørresundby. The measurements are conducted using ultrasonic anemometers.

Furthermore considerations on the anisotropy of the turbulence are conducted. It is demonstrated that the numerical model makes adequate estimates for the actual flow and turbulence.

The location investigated to validate the CFD models is Høje Brygge in Nørresundby. A view of the surrounding area is seen in Figure 6.1. In the area of investigation it is known that there already are problems with the wind conditions.



Figure 6.1 View of the surrounding area of Høje Brygge, Nørresundby. (Picture from Cowi A/S)

The measurements are conducted with three 2D and two 3D ultrasonic anemometers showed in Figure 6.2, which makes it possible to make measurements in several positions at the same time. Thereby it is possible to measure in a large number of spatial points over a short period of time, while the wind is coming from the same direction.

6.1 Calibration of anemometers

Calibration of the anemometers is conducted by placing the anemometers at the outlet of a wind tunnel, and relate the values measured in the wind tunnel and on the anemometer.

The wind speed in the tunnel is determined from pressure measured on each side of an aperture placed inside the wind tunnel. From the pressure difference it is possible to find the speed of the wind by use of formulas for the given aperture. Three apertures are used where each aperture is used in different ranges of wind speeds. The larger the aperture the higher speed.



Figure 6.2 Illustration of ultrasonic anemometers. The left is the 3D and the right is the 2D anemometer. (Pictures from Gill Instruments and Rehn Instruments.)

Each anemometer is exposed to a wind speed from 1.5 m/s to 28 m/s which covers the wind speeds that will be measured in the area at Høje Brygge.

Together with the wind speeds found in the wind tunnel, the signal from the anemometers is measured. The signal from the anemometer is a Voltage signal and from the calibration a parameter is found that translates the measured Voltage signal to a wind speed. The data is collected by use of the program Catman 4.5.

The relation between the wind speed and the output Voltage signal is seen in [Figure 6.3](#) for one of the anemometers. Details of the calibration procedure are given in [Chapter C](#).

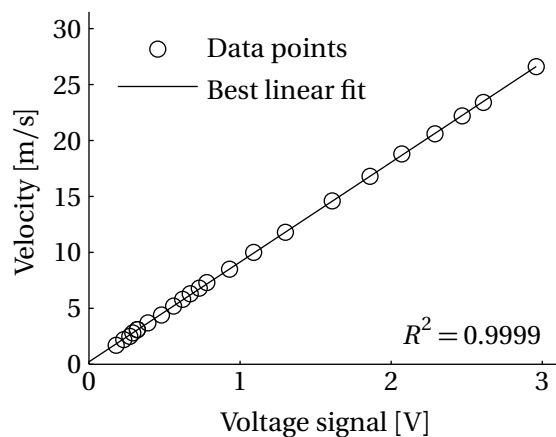


Figure 6.3 Relation between measured Voltage signal and wind speed. The calibration coefficient is given by the slope of the best linear fit.

6.1.1 Uncertainties in Calibration

The main source of error is the limited size of the wind tunnel applied in the calibration. The measuring area of the 3D anemometers is of the same size as the outlet of the wind tunnel, whereby uncertainty about the flow field imposed in the calibration process arises. For the 2D anemometers the measuring area is much smaller.

It has been verified that the 2D and 3D anemometers yield the same result if they are placed next to each other in an outdoor flow field.

6.2 Preparation of Equipment

For the measurements one anemometer is placed in a height of 11 m, and the four others are placed on stands in a measuring height of 1.7 m. Pictures of the reference anemometer and the anemometers at pedestrian height is seen in [Figure 6.4](#) and [6.5](#).



Figure 6.4 Reference anemometer in lift.



Figure 6.5 Anemometers at 1.7 m height.

The reference anemometer positioned in 11 m height is a 3D anemometer, and is used to normalise the values given for the other four anemometers. Ideally the reference is placed at a location where the wind is not interfered of nearby obstacles. The other four anemometers are used to measure the wind conditions around the buildings at pedestrian level.

A control test of the equipment is conducted and long measurement series are saved for analysis of the necessary time-averaging period. A list of equipment is given in [Appendix C.4](#).

6.3 Choosing Time-Averaging Period

Choosing a time-averaging period for the measurements is essential to get reliable results for both mean wind speed and the standard deviation hereof. A too short averaging period can cause bad agreement between the reference and ground level anemometers due to wind gusts only passing one of the anemometers.

In principle a longer averaging period will give a better agreement, however there is a risk of a change in the free wind direction during long measurements. Field measurements are therefore conducted on days with steady wind from one direction.

Based on a continuous measurement of 1 hour and 45 minutes, regression plots between a pedestrian level anemometer and the reference are given in Figure 6.6 for an averaging period of 1, 2, 5 and 10 min.

A longer measurement increases the statistical reliability for the averaging periods of 5 and 10 min, as these plots are based on only 21 and 10 measurements respectively.

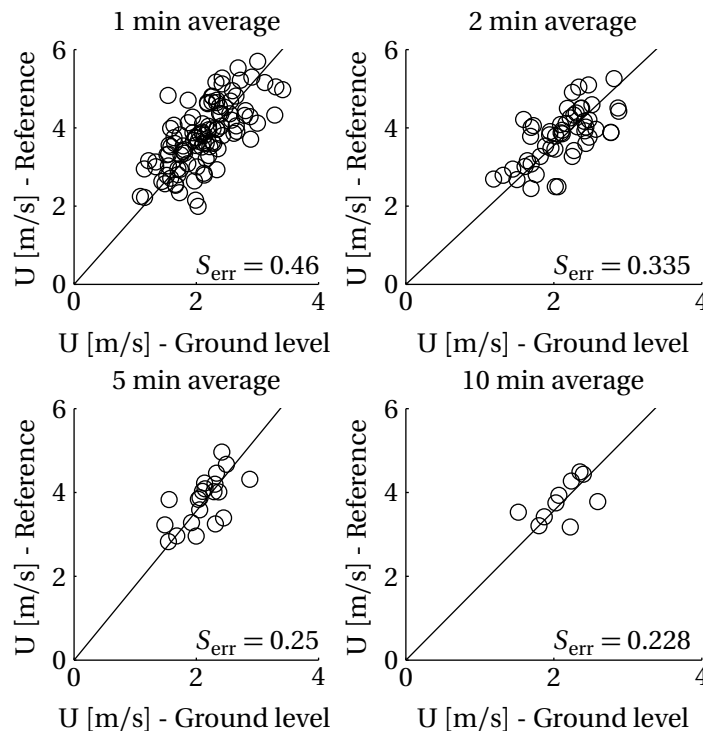


Figure 6.6 Agreement of simultaneous measurements of the mean velocity at reference height and at pedestrian level. Time averaging period is 1, 2, 5, and 10 min respectively.

From Figure 6.6 it is seen that the agreement increases as the averaging period increases. Both 5 min and 10 min shows good agreement, however 10 min seems to have fewer outliers. Based on this analysis a time-averaging period of 10 min is chosen which also is a practical convenient averaging-time as the positioning of the anemometers between each measurement at Høje Brygge takes approximately 10 min.

6.4 Measurements at Høje Brygge

Field measurements is conducted on two different days. On the 10th of February 2010 measurements were conducted with wind from NE and on the 9th of April 2010 with wind from west. The positions of the anemometers are showed in Figure 6.7.

As seen in Figure 6.7 the anemometers are not pointing in the north direction. This is because the Voltage signal jumps between 0° and 360° with a delay in the output signal, and thereby some data are erroneous if the wind switches between each side of the north

direction of the anemometers. Therefore the anemometers on the first day are pointing their north direction parallel to the quay. On day two the anemometers are pointing to two of the reference points used.

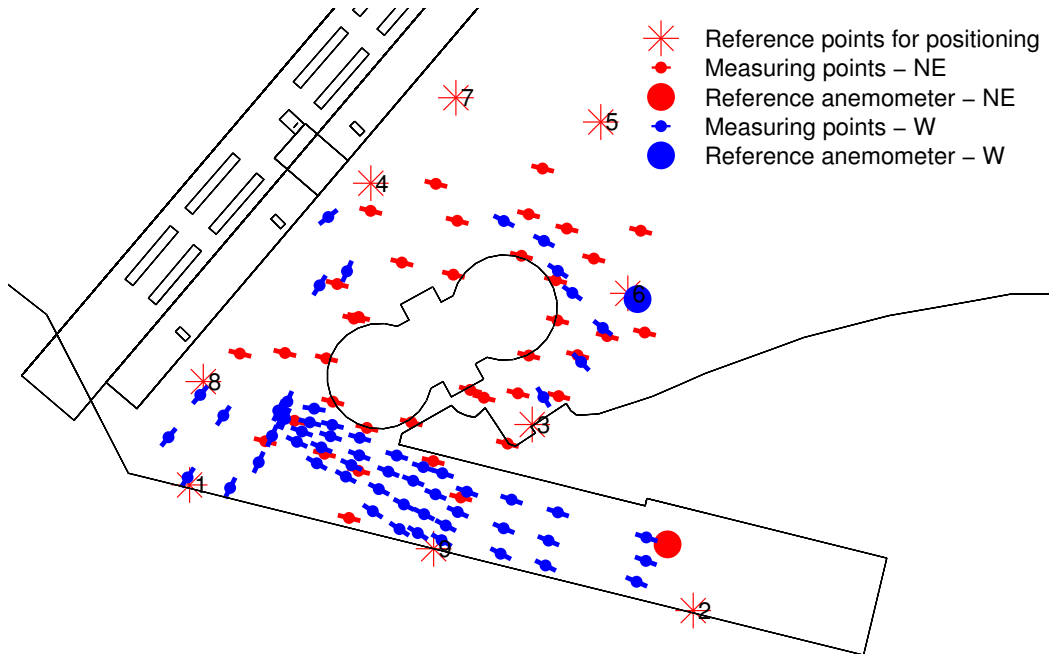


Figure 6.7 Map of Høje Brygge with positions of anemometers, trailer with reference anemometer, and reference points. Directions of the anemometers are illustrated by a north-south indicator.

Before the measurements the reference anemometer is mounted on the lift and raised to 11 m. The computer is connected to all of the equipment. The following procedure is used for each measurement:

1. Put up anemometers on ground level on chosen positions.
2. Conduct measurement in 10 min.
3. Move anemometers to the next measuring point.
4. Use levelling instrument or GPS to find the precise position of the anemometers from last measuring period.
5. Repeat point 1-4 until all measurements are conducted.

The positions of the anemometers are determined with a levelling instrument on the day with wind from NE, and a precision GPS is used on the day with wind from west.

For the levelling instrument three lengths are found to the reference points and a least square method is used to find the measuring point. Details of this method are given in [Section C.4.1.](#)

The GPS can measure a position with a precision of approximately 1 cm, when it is connection to all local masts and satellites. However it was not possible to get a satisfactory precision between and very close to the buildings and therefore some of the results are discarded.

6.5 Comparison of Mean Wind Speed and Direction

The reference anemometer should be placed in a free wind stream if possible. With wind from NE the pier is a suitable place. With wind from west the wind is affected by the buildings in every area that the cables reach. It is therefore not possible to have a reference measurement independent of all building geometries. The wind pattern at 11 m height can be seen in Figure 6.8 and 6.9 for wind from NE and west respectively.

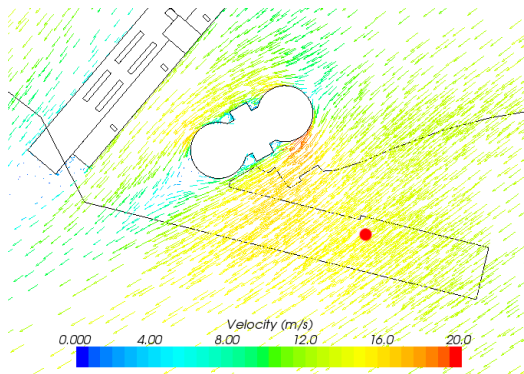


Figure 6.8 Wind pattern at 11 m with wind from NE. The red dot indicates the position of the reference anemometer.

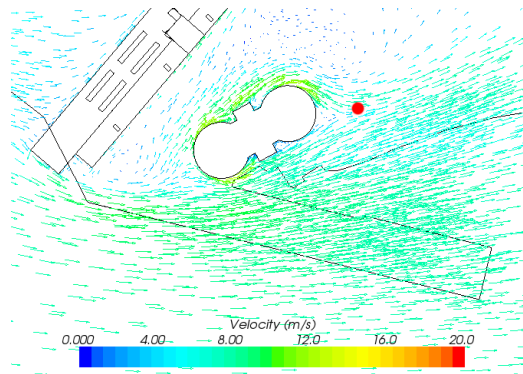


Figure 6.9 Wind pattern at 11 m with wind from west. The red dot indicates the position of the reference anemometer.

The wind speed and direction are given for each data series in Figure 6.10 for both days. With wind from NE the reference is placed in an almost free stream and the direction corresponds approximately to the free stream direction. The wind does not vary a lot neither in direction nor wind speed. This is seen by the red dots, which indicates deviation from the mean direction during a measuring period of 10 min for each measurement. No change in wind direction is indicated by the dot in the end of the arrow.

With wind from west the reference is more influenced by building geometries and the direction does not correspond to neither the free stream direction nor the expected direction based on a CFD model with wind from west. Furthermore the direction varies between each measurement, this is seen as the red dots are not in the end of the arrows. This is attributed to the fact that the wind direction at the reference changes significantly with a small change in direction of the free stream.

6.5.1 Evaluation of Wind from North-east

The mean wind is approaching from 41° with respect to north at the reference. According to the CFD calculation this corresponds to wind approaching from 60° with respect to north in the free stream. The difference between these angles suggests that the wind at the reference is not unaffected by the building geometries.

The mean wind speed of each data series are normalised by the value at the reference anemometer, as the flow is independent of the Re number according to Section 5.6. In Figure 6.11 the calculated and measured wind vectors are showed.

Some of the measured velocities clearly stand out from the general wind pattern. This is, among others, measurement number 28, 35, and 39. For measurement number 28

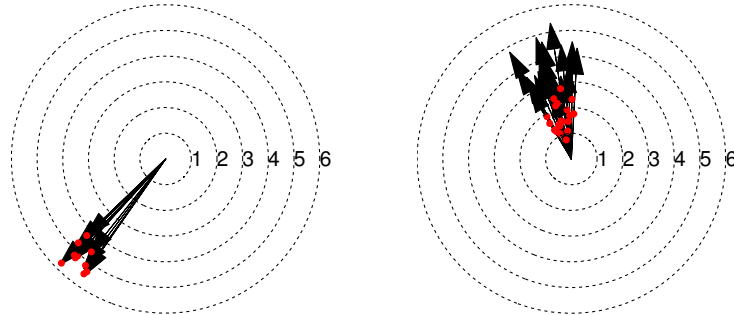


Figure 6.10 Wind speed and direction for the reference anemometer for wind from NE and west respectively. The deviation from the mean direction during a measuring period of 10 min is indicated by a red circle for each measurement. Great variations of the wind direction takes place at the reference with wind from west which is attributed to building induced turbulence.

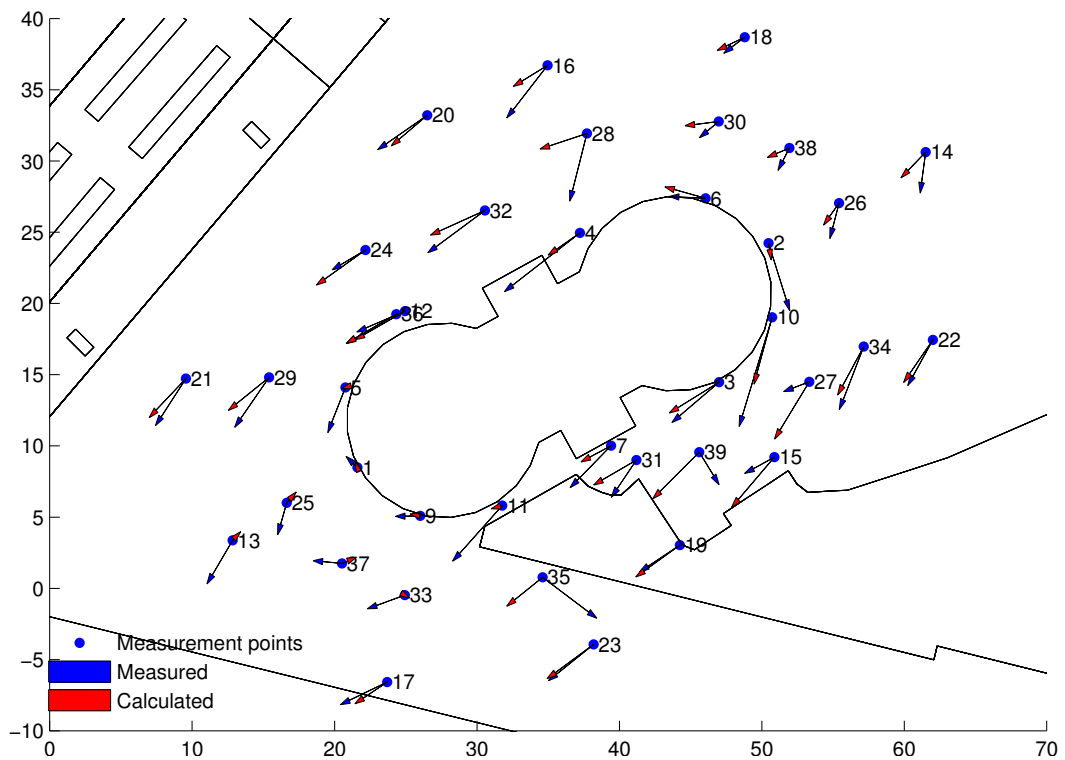


Figure 6.11 Vector plot of normalised wind speeds for both the CFD model and the measurements. Origo of the Coordinate system is chosen from the first reference point.

it was registered that it was in between two cars which are not modelled in the CFD calculations. Problems with the stands resulted in some problems with anemometers turning during the measuring period.

The overall agreement between measurements and calculations is acceptable. The results fit best in the upstream flow and away from the buildings. In the wake zone there is less agreement between the results. The CFD model predicts a separation on the south side of the eastern tower which does not seem to happen when looking at the measurements. This separation is illustrated in [Figure 6.12](#).

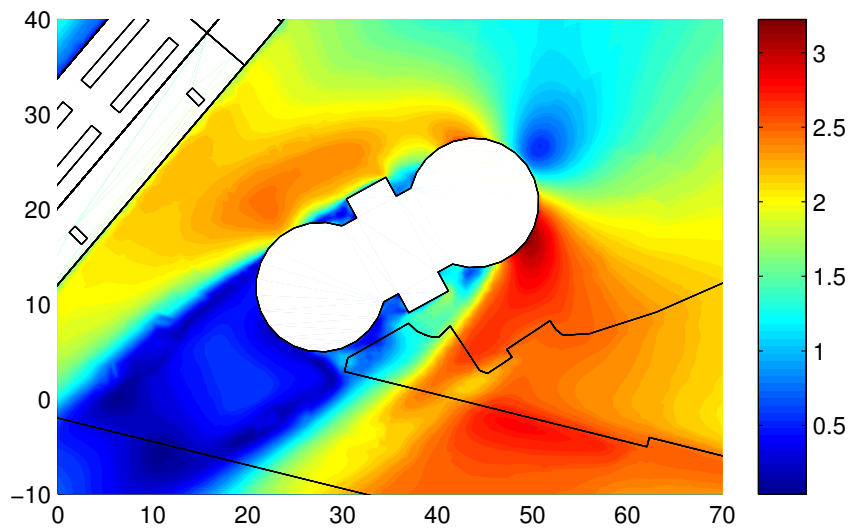


Figure 6.12 Contour plot of velocities corresponding to the wind direction at the day of the measurements. Separation seems to occur at the south side of the eastern tower.

6.5.2 Evaluation of Wind from West

The CFD calculation where the direction at the reference anemometer fits best is with wind in the free stream approaching in 280° with respect to north. In [Figure 6.13](#) the normalised velocity vectors in the CFD model and the measurements are given.

Some of the measuring points are sorted out due to inaccuracy of the GPS coordinates. Most of these points are between and close to the buildings.

From the CFD calculations it is realised that a small change in the direction of the free stream yield a significant change in the results. On the day of measuring the wind direction was changing during the day. This has affected the accuracy of results.

In general the measurements are in agreement with the calculations, and the overall flow patterns are resolved satisfactory.

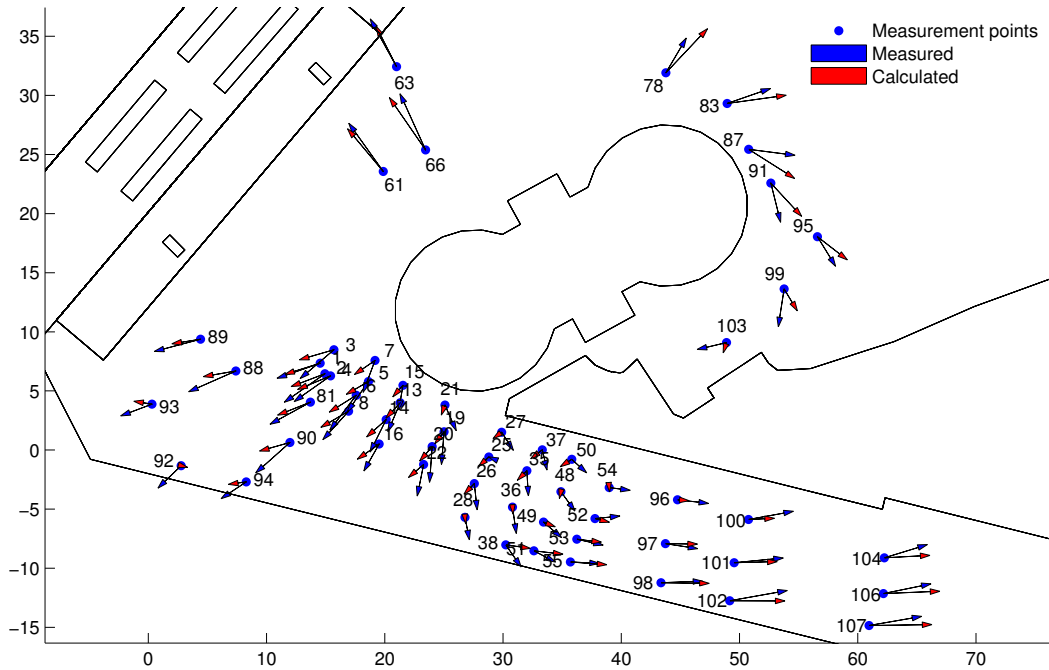


Figure 6.13 Vector plot of normalised wind speeds for both the CFD model and the measurements with wind from west. Origo of the Coordinate system is chosen from the first reference point.

6.6 Measurements of Turbulence

The turbulent part of the evaluation criteria σ can be evaluated by k , which at least for isotropic turbulence is related to the standard deviation by:

$$\sigma_{|U_i|} = \sqrt{\frac{2}{3}k} \quad (6.1)$$

For strongly anisotropic conditions with fluctuations only in one direction, the relation is:

$$\sigma_{|U_i|} = \sqrt{2k} \quad (6.2)$$

The true relation is somewhere between these limits, but as the two limits just change the coefficient in front of \sqrt{k} , the relation is linear and thereby the exact value does not change the correlation between the measured values, and those extracted from the CFD computations.

The standard deviations are as well as the velocities normalised with the mean velocity at the reference point.

A problem with two-equation turbulence models is that it does not give results of the directional components of the turbulence. Without this knowledge the CFD results cannot be directly compared to the measurements. Instead σ is calculated in both extremes, fully isotropic turbulence and fully anisotropic with the results from wind from NE. A regression plot of these results is seen in [Figure 6.14](#).

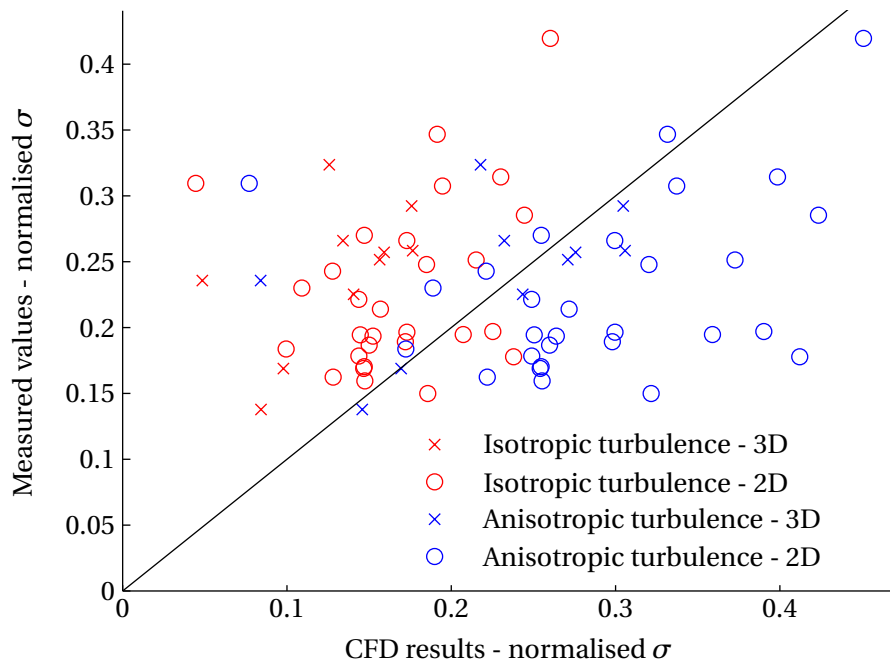


Figure 6.14 Regression plot of the measured and calculated standard deviation of the velocity. This plot shows the results for both fully isotropic and anisotropic turbulence.

When considering the isotropic turbulence the CFD model underestimates σ , while considering fully anisotropic turbulence the CFD results overestimates σ . As expected the real value should be somewhere in between these two limits.

Not all points should have the same amount of anisotropy. It is expected that the turbulence in a free stream would be more isotropic than turbulence induced by a building, because the building would cause fluctuations mostly in the horizontal plane, near the ground.

This leads to the expectation that the largest values of turbulence will be more anisotropic. This is in agreement with Figure 6.14 where the values of σ from the CFD model has a tendency to differ more from the measured values at high turbulence levels when assuming isotropic turbulence.

In principle a value of the level of anisotropy could be used in every single point where the wind condition is evaluated. However this would demand a RSM, a DES, or a LES model which would be much more computational expensive with only a small improvement of the results. Instead an overall measure of the level of anisotropy can be used to evaluate σ by the formula:

$$\sigma = \sqrt{a \cdot k} \quad (6.3)$$

To find a , a relation between \sqrt{k} and the measured σ is required. This is showed in Figure 6.15 where also the best fit is plotted. The slope of the fit corresponds to a value of a on 1.27 which as expected is between $2/3$ and 2.

This method should be used with caution because more measuring points are used close to the building than further away. Furthermore it can be expected that in other cases

more or less anisotropic turbulence is induced by the buildings. The size of a could be adjusted for different locations. Closer to 2/3 for open areas and closer to 2 for dense building areas.

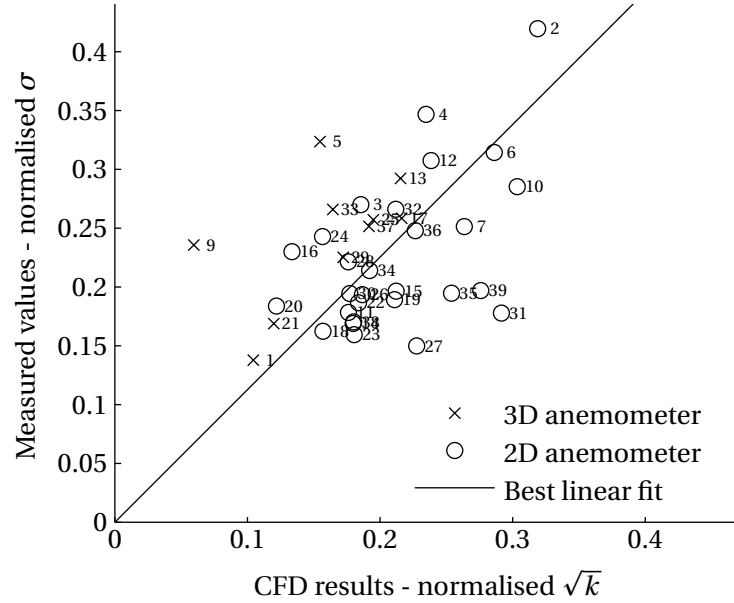


Figure 6.15 Relation between the calculated turbulent kinetic energy and the measured standard deviation of the velocity with wind from NE.

The 3D anemometers can be used to measure the degree of anisotropy. The anisotropy will be measured as the ratio between the standard deviation of the horizontal components of the velocity and the standard deviation of the vertical velocity:

$$\text{Degree of anisotropy} = \frac{\sigma_u^2 + \sigma_v^2}{\sigma_w^2} \tag{6.4}$$

Using this expression it is assumed that the anisotropy is building induced and is in a horizontal plane. The expression gives a value of 2 if the turbulence is completely isotropic. The value will increase for higher deviations of the wind velocity in a horizontal plane caused by building induced turbulence.

Calculations shows that the average value of the degree of anisotropy is 4.3 in the reference point at 11 m height with wind from NE. At ground level this value increases for some points to over 10 showing a higher level of anisotropy as expected.

Figure 6.16 shows the measured values for the level of anisotropy on a contour plot of the calculated value of the standard deviation. A good correlation between the size of σ and the degree of anisotropy is seen which supports the assumption that building induced turbulence is more anisotropic than free stream turbulence.

The correlation between the calculated value of k and the measured value of the anisotropy is showed in Figure 6.17. A tendency of increasing anisotropy with increasing k is seen. A clear connection between the anisotropy and k would demand a lot more measurement points.

For the time being isotropic turbulence is assumed, but some of the indications stated here should be investigated further in a future study.

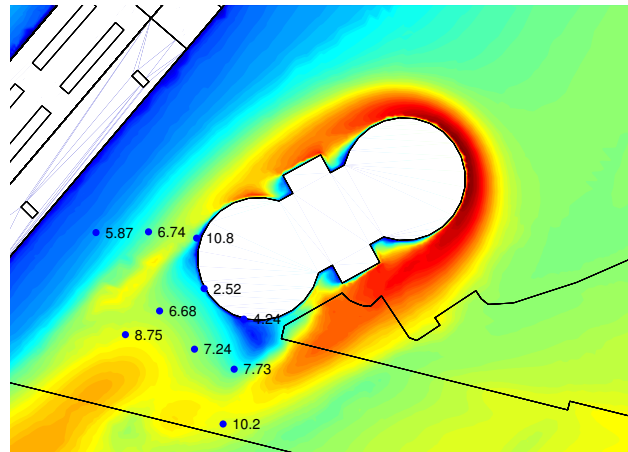


Figure 6.16 Calculated values of σ_u with measured values of the anisotropy of the turbulence.

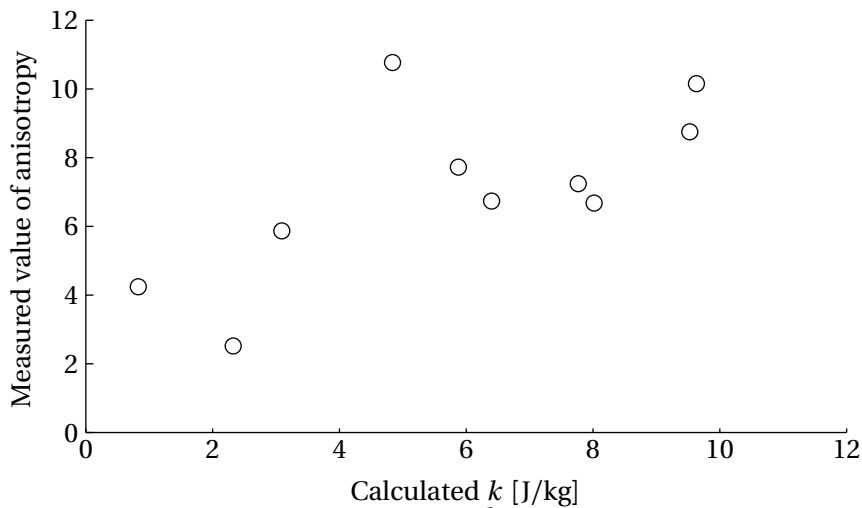


Figure 6.17 Regression plot of the calculated k and the measured value of the anisotropy with wind from NE.

6.7 Conclusions on Comparison Between CFD and Measurements

Measurements have been conducted at Høje Brygge, Nørresundby, on two different days with wind from NE and west respectively. The measurements were conducted using ultrasonic anemometers.

The measurements are compared with the numerical model in Figure 6.11 and 6.13 the overall results are satisfactory, and the numerical model appears to resolve the both the flow field, the magnitude, and direction of the wind to the order of precision of the measurement equipment and methodology applied. In general the results are better in the approaching flow than in the wake zone.

Investigation on the connection between the turbulence denoted by the kinetic energy, and the standard deviations on the measurements are investigated. It is found that the

turbulence is anisotropic, with the largest variations in the horizontal plane, and with larger anisotropy near buildings than in the free stream.

Indications on a coupling between the turbulent kinetic energy and the standard deviations are presented. The coupling is not linear as it scales with the turbulence itself. Applying those results requires a larger number of measurements, however.

7 Procedure for Evaluating Wind Conditions based on CFD

In the following a suggested procedure for evaluating wind conditions is outlined. The procedure is based on recommendations in the literature and the studies performed in the present thesis.

The procedure can be considered as an attempt to make a proper compromise between precision and time consumption in the process of evaluating the wind conditions at a given location, at least for the time being.

7.1 Outline of Procedure

The suggested procedure for evaluating wind conditions at a given location is given by the flow diagram in Figure 7.1. In the following the recommendations are listed starting with the initial steps.

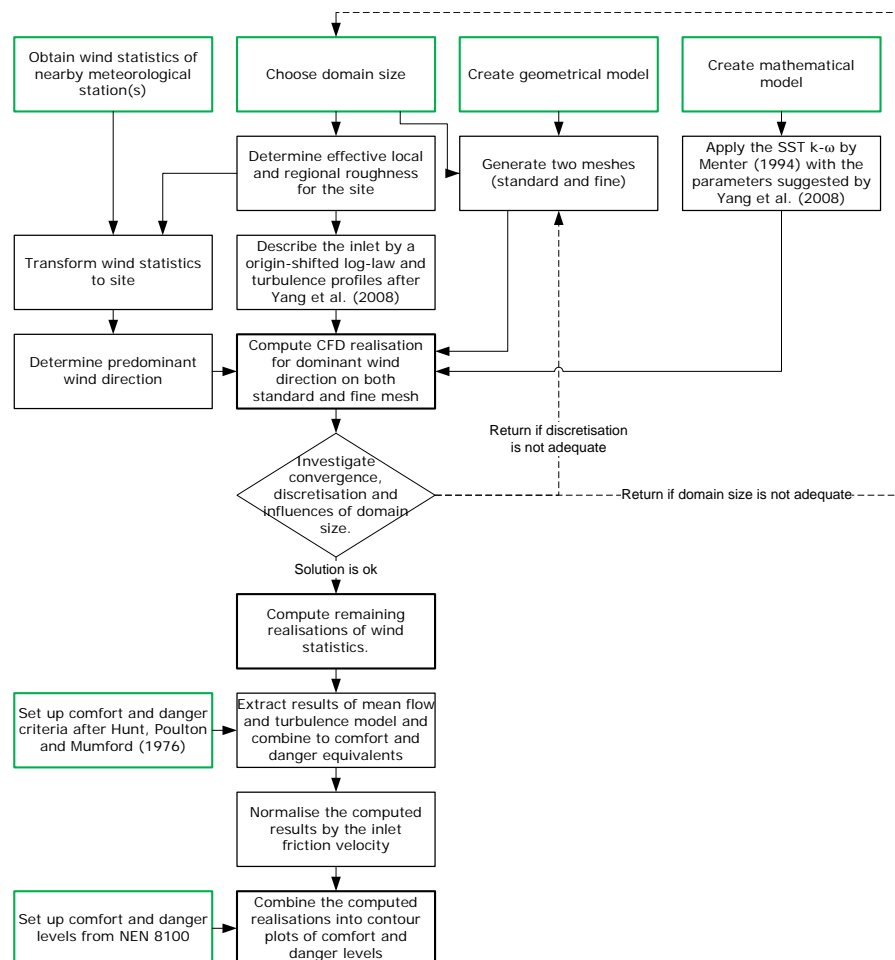


Figure 7.1 Overview of procedure for evaluating wind conditions by CFD. The starting points are the green boxes.

Obtain Wind Statistics

The wind statistics exposure corrected for nearby features is obtained from e.g. Troen (1989) for a nearby meteorological station. Data with higher directional discretisation is preferable, if available.

Determine roughness

The effective local and regional roughness is determined based on ortho photos or land use maps. Verkaik et al. (2005) have suggested a model for automatic determination of roughness based on land use maps. This model is preferable if wind conditions are to be determined on a routine basis.

Transform Wind Statistics

The wind statistics is transformed to the location in question by the procedure outlined in Chapter 5 based on Wieringa (1986) and Verkaik et al. (2005). Input to the transformation is the statistics of the meteorological site.

The output of the transformation procedure is the directional depended probability distribution function of the friction velocity for the location at the inlet boundary. The implementation procedure outlined in Section 5.3 can be applied to perform the calculation. Simpler procedures for transformation to the site are described by Simiu and Scanlan (1978) and Troen (1989), but they are less precise.

At least the same care as in the actual CFD calculation has to be taken in this part, as the resulting danger and comfort levels are very sensitive to the statistical parameters obtained at this step.

Determine Predominant Wind Direction

From the directional wind statistics the predominant wind direction is determined.

Choose Domain Size

The domain size should be selected so all relevant flow features are resolved and the free stream boundaries not interfere with the flow at pedestrian level. Franke et al. (2007) states the following guidelines, that have seem to comply with the simulations conducted in the present thesis:

- The top boundary should be $2H-3H$ above ground level, where H is the height of the tallest building.
- The region of interest should be placed in the middle of the domain.
- The blockage ratio should be less than 3 %.
- The horizontal extend of the domain should be $5H-10H$ downstream and $2H$ upstream, where H is the height of the tallest building in the domain. Large horizontal extend is most important for simple building configurations.

The same domain size is applied in all directions, that is the side boundaries in a given flow calculation is placed at the same distance from the rotation point as the inlet and outlet. This serves to limit the blockage ratio of the buildings facing the flow from a given direction.

Create Geometrical Model

The geometrical model of the site in request is constructed, either from scratch or based on existing 3D models if they are of acceptable quality. [Yoshie et al. \(2005\)](#) have showed that at least two rows of preceding buildings should be constructed. The ground level is determined from a terrain model, based on orographic maps.

Boundary Conditions

The inlet conditions are described by an origin shifted log-law turbulence profile derived for a stable atmospheric boundary layer, as suggested by [Yang et al. \(2008\)](#).

The velocity inlet profile is described by:

$$U(z) = \frac{U_*}{\kappa} \ln \left(\frac{z-d}{z_0} \right) \quad (7.1)$$

Where the parameter d is set to 3 times z_0 . The velocity lower than the origin of the log profile is set to zero. The realisation is computed with the friction velocity U_* determined so the velocity profile yields 6 m/s at z equals 1.7 m above the origin of the log profile. This value is chosen to minimize the dependency of the Re number for the part of the probability distribution that lies above the thresholds.

The profile of the turbulent kinetic energy and specific dissipation rate is given by:

$$k(z) = \frac{U_*^2}{\sqrt{C_\mu}} \sqrt{C_1 \ln \left(\frac{z-d}{z_0} \right) + C_2} \quad (7.2)$$

$$\omega(z) = \frac{U_*^3}{\kappa \sqrt{C_\mu}} \frac{1}{z-d} \quad (7.3)$$

The part of the profiles that lies below $z = z_0 + d$ are given the values at $z = z_0 + d$. When the k -profile reaches zero at top where $z > z_0 \exp \left(\frac{-C_2}{C_1} \right) + d$, the profile is set to zero.

The outlet is described by pressure outlet. On the sides and top boundaries symmetry conditions are applied. On the ground a suitable roughness for the ground surface should be applied, by the procedure outlined in [Section 3.2.3](#).

Generate Mesh

The literature only states a few tangible guidelines, as the mesh generation is highly problem specific. However the following recommendations would produce adequate meshes for the case studies presented in this thesis:

- Franke et al. (2007) suggest using at least ten meshes per cube root building volume in the central area of interest, and at least ten meshes along the side of the smallest dimension of the building of interest. This figure is however in the presented studies found to be too coarse and 15 meshes seems to be more appropriate.
- Refinement to the above level is more important in the horizontal direction than in the vertical. The extent of the high resolution area is one building width and about 15 m in the vertical. The mesh size should only change slowly away from the high resolution area.
- Refinement should be made along all feature edges describing the geometry.
- Franke et al. (2007) and Tominaga et al. (2008) recommends at least three meshes between the ground and evaluation level. This figure is probably a result of the limit imposed by the wall function problem (Blocken, Stathopoulos and Carmeliet 2007; Hargreaves and Wright 2007).

It is however found to be a major error source if the discretisation is so low. Somewhere between 7–10 meshes seems more appropriate. This is only possible if the remedial procedure described in Section 3.2.3 is possible in the given CFD code.

- Make the mesh size proportional to the log-law. That is fine mesh at ground, coarse at the top.
- Prismatic meshes should be applied on walls, and on the ground surface it should extend up above evaluation level, in order to get cell centroids in the evaluation plane.

Franke et al. (2007) recommends generalised Richardson interpolation in order to estimate grid convergence. While this process might seem tempting, systematic refined meshes are difficult to apply since all mesh sizes do not necessary scale linearly with respect to a single parameter, and the wall function procedure will limit the problem at a certain point.

Create Mathematical Model

The mathematical model consist of a given flow solver to solve the Navier Stokes equations for incompressible fluids coupled with the turbulence model.

Set up of Turbulence Model

As showed in Chapter 4 the k - ω SST model by Menter (1994) with the parameters suggested by Yang et al. (2008) is the best model for evaluating atmospheric flow. The model coefficients are listed in Chapter A.

Compute CFD Realisation from Dominant Wind Direction

The first CFD simulation is calculated from the dominant wind direction on both the standard and fine mesh. This covers two purposes:

- The computation from the dominant wind direction gives a first guess on the actual wind conditions.
- Investigation of the adequateness of chosen discretisation and domain size.

Investigate Solution

The solutions computed on the standard and fine mesh are investigated in order to verify the solution. The following points are considered:

- Convergence of results at pedestrian level.
- Significant signs of high-rise buildings in the flow in the top boundary.
- Evaluation of the approaching flow for signs of erroneous flow developments that can be attributed to mistakes in the inlet or ground conditions, or wrong inlet distances.

If the mesh or domain size is not adequate then the process is returned to the mesh generation or domain size selection steps respectively.

Compute remaining Realisations

If the mesh and domain are acceptable the remaining realisations are computed. The number of resolutions is somewhat problem dependent and depend on the threshold of the criteria evaluated. Considerations on selecting the directions of the realisation are presented in [Chapter 10](#).

Set up Evaluation Criteria

The evaluation criteria are based on thorough experiments by [Hunt, Poulton and Mumford \(1976\)](#) and the discussion by [Bottema \(2000\)](#), suggesting the equivalent wind speeds for human comfort and danger:

$$U_{\text{eq,c}} = U + \sigma_U < 6 \text{ m/s} \quad (7.4)$$

$$U_{\text{eq,d}} = U + 3\sigma_U < 20 \text{ m/s} \quad (7.5)$$

Extract Results

The results are extracted from the CFD models. The wind conditions are evaluated through the comfort and danger criteria, therefore equivalent danger and comfort wind speeds are computed by [Equation 7.4](#) and [7.5](#). The amount of turbulence is evaluated through the k equation in the turbulence model.

The relation between σ and k is based on fully isotropic turbulence whereby the relation is as follows:

$$\sigma = \sqrt{\frac{2}{3} \cdot k} \quad (7.6)$$

Further studies on this coupling are advisable.

Normalise Results by Friction Velocity

The results are normalised by the friction velocity in order to convert the wind statistics for the friction velocity to statistics for the evaluation plane.

Set up Levels of Danger and Comfort

The danger and comfort levels are based on the Dutch code of practice NEN 8100. This code of practice defines five comfort levels and three danger levels given in [Table 7.1](#) and [Table 7.2](#).

Table 7.1 Levels of comfort divided after probability of exceedance (%) in the Dutch code of practice for NEN 8100 (after [Willemsen and Wisse 2007](#)).

| Exc. prop. | Designation | Traversing | Strolling | Sitting |
|------------|-------------|------------|-----------|----------|
| <2.5 | A | Good | Good | Good |
| 2.5-5.0 | B | Good | Good | Moderate |
| 5.0-10.0 | C | Good | Moderate | Poor |
| 10-20 | D | Moderate | Poor | Poor |
| >20 | E | Poor | Poor | Poor |

Table 7.2 Levels of danger divided after probability of exceedance (%) in the Dutch code of practice NEN 8100 (after [Willemsen and Wisse 2007](#)).

| Exc. prop. | Designation | Level |
|------------|-------------|--------------|
| <0.05 | A | Safe |
| 0.05 – 0.3 | B | Limited risk |
| >0.3 | C | Dangerous |

For the danger criterion these levels are a matter of convention, and are in principle a political decision. If any local restrictions apply, the danger criterion should be based on these. The wind climate of the Netherlands are however comparable to the Danish, so the Dutch code would form a proper basis for any Danish restrictions.

Combine the Results

The results are combined for each realisation in order to obtain contours of the comfort and danger levels. This ends the evaluation process and conclusion on the wind conditions are made based on the contours and relevant flow phenomena.

7.2 Method for Automate the Calculation Procedure

To be able to couple the CFD results with the wind statistics, results from different directions are needed. The changes between the models for each direction are small but very time consuming to change. This makes it suitable to make an automated process in Star-CCM+ using the opportunity for writing a JavaScript.

The procedure consist of a loop containing the following steps:

- Creating a local coordinate system with the x-axis in the direction of the wind.
- Creating a box containing the computational domain.
- Defining boundary conditions on the box surface.
- Creating a volume mesh of the domain.
- Run simulation until convergence of the equivalent velocity.
- Export results for velocities and turbulent kinetic energy.

After each run the box is removed before a new is created. In order to save computational time the previous solution is used as an initial guess in the next calculation where the wind direction is turned.

7.3 Sensibility of Parameters in Evaluation Procedure

The process of evaluating wind conditions consists of multiple submodels. Each of these submodels introduces an uncertainty on the overall results of the calculation. The calculation procedure can be divided into two parts, one which consists of describing and evaluating the flow and its statistic, and another which consists of analysing the flow statistic by given evaluation criteria.

The first part is an objective description of the flow, and the second is a subjective assessment of a given wind climate. Numerous uncertainties lie in the subjective evaluation, which at the best is an evaluation of an average person's performance and comfort in a given wind flow.

The uncertainties coupled with how we are affected by wind can in principle be described by refined evaluation criteria. On the other hand the uncertainties coupled with how the flow is evaluated can be investigated by considerations on the submodels applied.

7.3.1 Uncertainties in the Mathematical Submodels

The starting point of the evaluation is the exposure corrected wind statistic at a meteorological station. This is an estimate on the regional wind climate over a uniform terrain. Troen (1989) has validated the procedure applied in the exposure correction, with excellent results. A very little uncertainty on this data is therefore to be expected, if the regional wind climate is assumed constant.

While the quality of the input wind statistics is excellent the directional discretisation is limited to 12 sectors. As showed in Chapter 10 the directional discretisation is quite important in order to evaluate the overall statistics of the flow. In the present application spline fitting is applied to the wind statistics in order to increase the directional discretisation, but this is at best an approximation.

The transformation of the wind statistics in order to obtain a realisation of U_* at the domain boundary, is based on the geostrophic relation and the roughness field, collapsed into two effective roughness describing the flow upstream of the domain boundary.

The winds of interest are those which add most to the exceedance probability, which are mostly appearing in clouded, near-stable conditions. The transformation is therefore based on similarity theory valid for stable conditions, but arguably some of the comfort issues arise in more unstable conditions.

The flow evaluated in the domain is based on the RANS approach. The results presented in [Chapter 4](#) and [6](#) suggest that the overall flow is modelled satisfactory. The most important uncertainty arises in the turbulence modelling.

7.3.2 **Assessment of Uncertainties in Evaluation of the Flow**

A higher friction velocity results in higher A -parameters in the Weibull distribution coupled to each CFD realisation. This change in the statistics is counteracted by the changed shape of the inlet profile.

In order to evaluate the uncertainty it can be tested what happens if the roughness field is assumed one class to low or to high. This requires recomputing of the statistics, but also new CFD calculations, which makes the process quite computational costly. In [Section 9.6](#) such an investigation is conducted for the case at Viborgvej/Bredskiftevej.

Part III

Evaluation of Wind Comfort in Practice

8 Evaluation of Wind Conditions at Høje Brygge

A procedure for evaluating wind conditions is proposed in Chapter 7. In the following the procedure is applied to an area where problematic wind conditions have been registered, in order to investigate which levels of comfort and danger the procedure determines. The evaluation gives important information on the exceedance probability in an existing case, to compare with future evaluations of building proposals.

The wind phenomena driving the registered wind conditions are analysed and remedial actions are suggested in order to counter the wind phenomena. A suggestion that will eliminate the problems at the location is presented.

In Nørresundby near the Limfjord two former silos has been rebuild and is now housing exclusive apartments. The silos, named Høje Brygge are located next to a building which in the following is denoted the Siemens building. In Figure 8.1 a picture of the two buildings is seen.

Both buildings are located at the shoreline of the Limfjord, and are therefore exposed to wind coming from wide open areas on the Limfjord.

The apartments at Høje Brygge are sold on basis of their large balconies and the excellent view over the Limfjord seen in Figure 8.2. Problems with wind conditions around the building has however scattered the success.



Figure 8.1 Picture from the site. Høje Brygge at the left and the Siemens building to the right.



Figure 8.2 View from apartment in Høje Brygge.

8.1 Stories From Residents

When the measurements presented in [Chapter 6](#) were conducted at the location, the residents were quite interested in discussing the wind conditions at the location. Several stories on the residents' experience with the wind at the location were told. In our report, we recount the residents' experiences with the wind at the location:

- Pebbles flying in the air have smashed car windows.
- While neighbours in the buildings to the NE have been barbecuing on their terrace, residents have been unable to open doors and windows due to the wind.
- On the balconies, tables are chained in order to stand still.
- A rail has been attached to the building in order to get around the building easier.
- An elderly resident has been caught in the wind, forced to clutch the rail, until other people assisted him getting away.
- When the area is salted during wintertime, the salt is blown away by the wind before it hits the ground.
- At wintertime there is a remarkably small amount of snow compared to the nearby areas.

An illustration of the wind effect at the location is given in [Figure 8.3](#).



Figure 8.3 Violent wind conditions experienced at Høje Brygge.

8.2 Surrounding Areas

Figure 8.4 shows an ortho photo of the area around Høje Brygge and in Figure 8.5 a bird's eye view of the area of interest is seen. The location is characterised by the high-rise building Høje Brygge and the Siemens building NW of Høje Brygge. The surroundings can be characterised as following:

- In south is the Limfjord. Directly south there is about 500 m to the city centre of Aalborg which consists mainly of city blocks.
- In NW there is a relatively open area with some trees.
- In NE is the city of Nørresundby which is generally low-rise buildings.

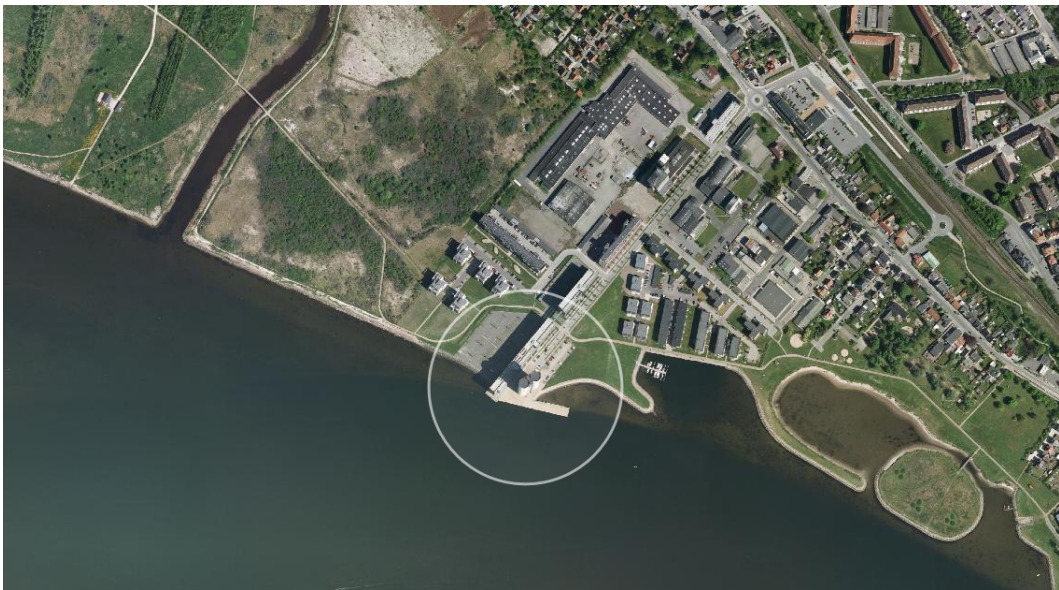


Figure 8.4 Ortho photo of the silos at Høje Brygge and the surrounding area. (Photo by COWI A/S.)



Figure 8.5 Bird's eye view of the area of interest. (Photo by COWI A/S.)

8.3 Build-up of Model for Høje Brygge

The model for Høje Brygge is based on the procedure given in Chapter 7. The setup and the case-specific parameters are listed in Table 8.1.

Table 8.1 Setup for the model at Høje Brygge.

| Parameter | Given by |
|----------------------------|--|
| Comfort criterion | $U_{eq,c} = U + \sigma_U \geq 6$ m/s. |
| Danger criterion | $U_{eq,d} = U + 3\sigma_U \geq 20$ m/s. |
| Classes for exc. prop. | After NEN 8100 (Willemsen and Wisse 2007). |
| Turbulence model | Menter (1994) $k-\omega$ SST with parameters by Yang et al. (2008). |
| Inlet | Origin shifted log-law and turbulence profiles derived for stable ABL with z_0 based on Figure 8.7 (Section 3.2.1). |
| Outlet | Zero gradient of all flow parameters. |
| Ground | Rough wall equal to $z_0 = 0.01$ m (Section 3.2.3). |
| Buildings | Smooth wall. |
| Free stream | Symmetry. |
| Mesh | Described in Section 8.4. |
| Wind statistic | Exposure corrected data of Troen (1989) from Aalborg Airport, transformed by the procedure in Chapter 5 illustrated by Figure 8.6. |
| Roughness | Given by Figure 8.7 and 8.8. |
| Directional discretisation | 12 directions equally parted by angle are used. |

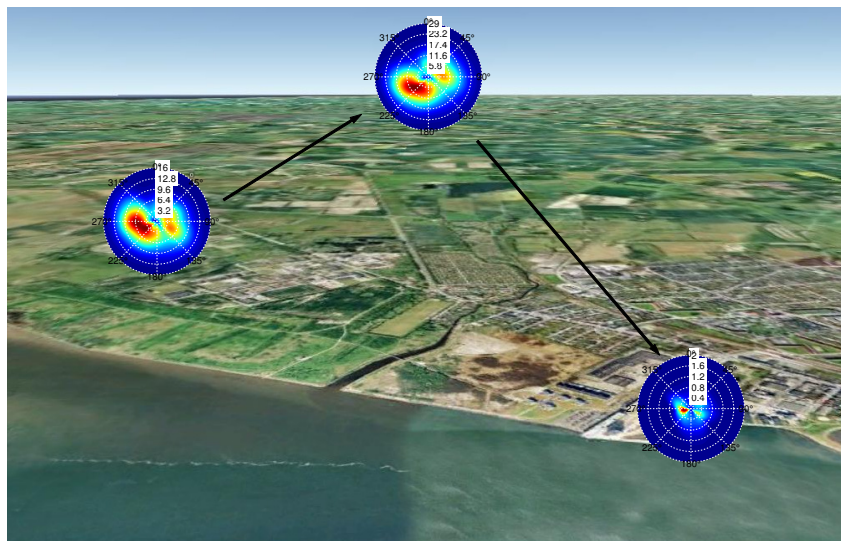


Figure 8.6 Illustration of the transformation procedure used to transform the wind statistics from one location to another.

8.4 Geometrical Model and Spatial Discretisation

The geometrical model is based on the 3D model by Aalborg Kommune (2009). This model contains the most of the buildings at Høje Brygge and the shore line.

The terrain is almost flat at the site and for simplicity the ground will be modelled as completely flat except for the quay which is 2 m high.

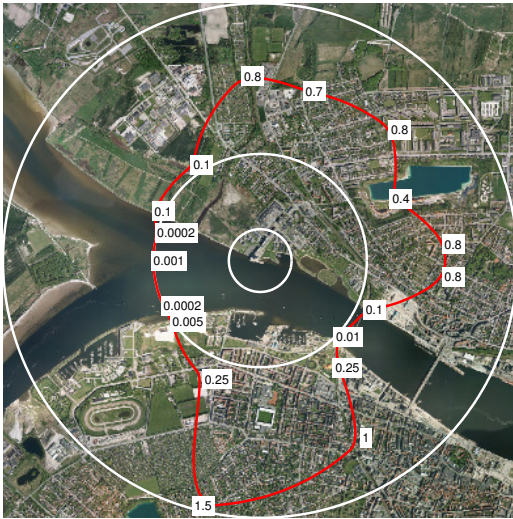


Figure 8.7 Local roughness (photo by COWI A/S).

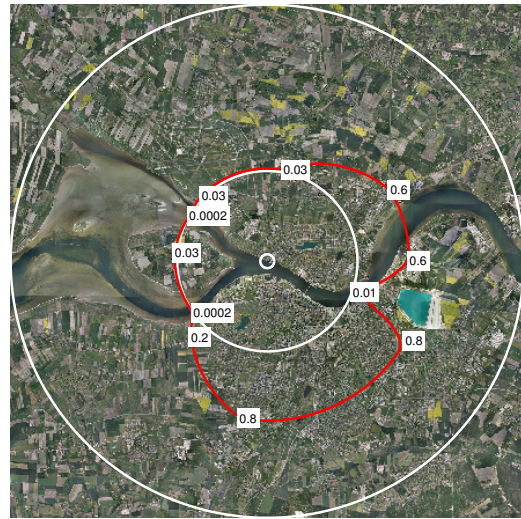


Figure 8.8 Regional roughness (photo by COWI A/S).

The buildings missing in the 3D model are modelled as boxes with approximately the same size as the buildings at the site. As well Høje Brygge itself is remodelled with a more correct description than the one given in the 3D model.

The geometry is imported as a surface mesh with the ground lying in $z=0$. The geometry is split up to different groups containing Høje Brygge, the Siemens building, other small buildings near the area of interest, and finally the ground surfaces. The different groups can be seen in Figure 8.9.

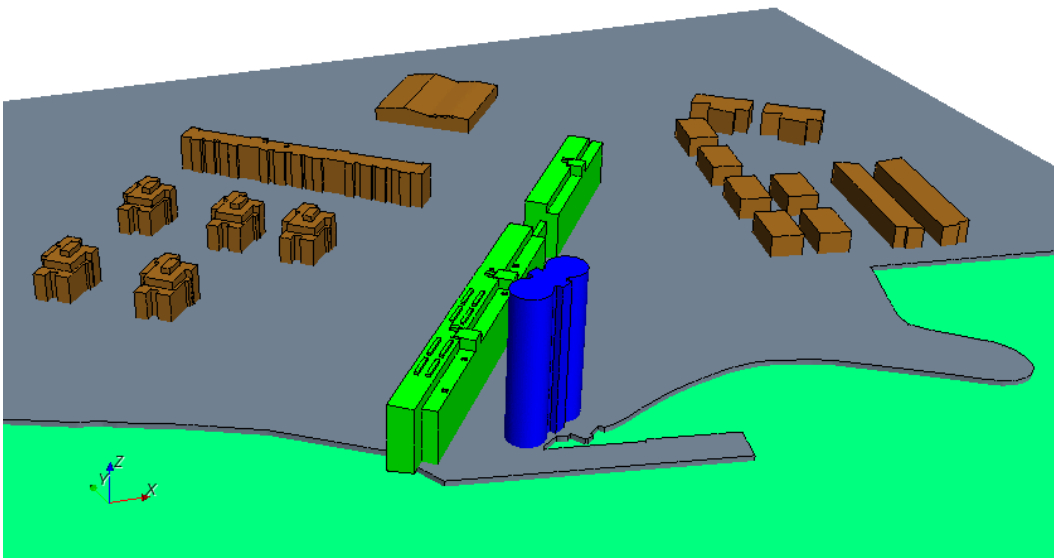


Figure 8.9 Imported surface coloured by group.

In order to be able to generate the surface mesh some surfaces are repaired manually in Star-CCM+ filling holes using the repair tools.

To get a proper description of edges between buildings and the ground, feature curves are added in the intersections. As well feature curves are added to each group of buildings and the quay as seen in [Figure 8.10](#). These curves are used when defining the mesh parameters, so a more refined mesh is used around sharp corners, e.g. the quay or a building corner. Furthermore a cylindrical volume is added around Høje Brygge for further refinement in this area.

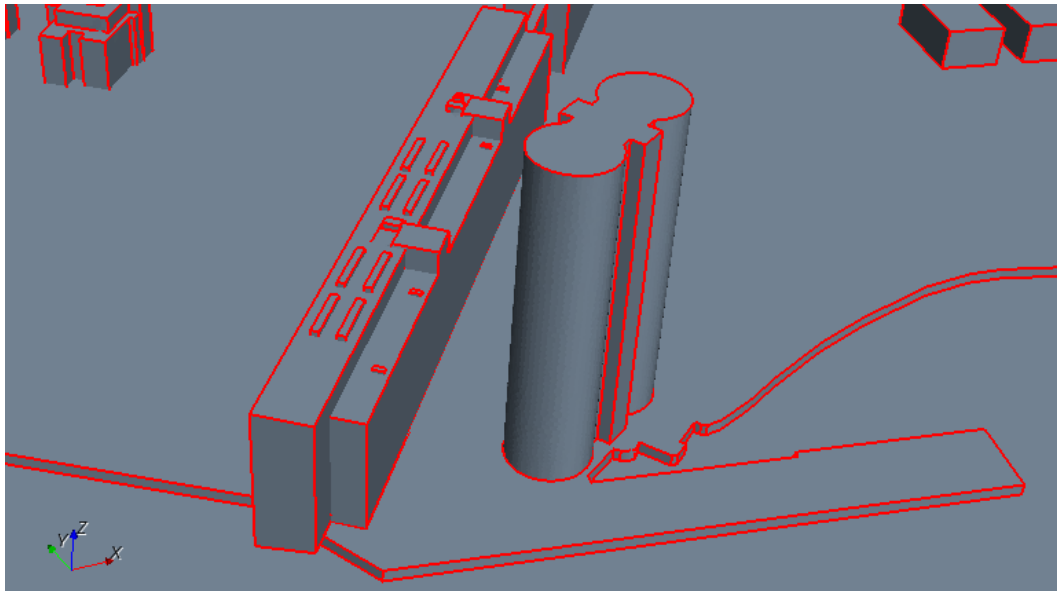


Figure 8.10 Feature curves at sharp edges in the computational domain.

The mesh parameters are set according to the recommendations in [Chapter 7](#). The applied mesh is seen in [Figure 8.11](#), and a close-up of the building with highlighted feature curves and refinement volume are showed in [Figure 8.12](#).

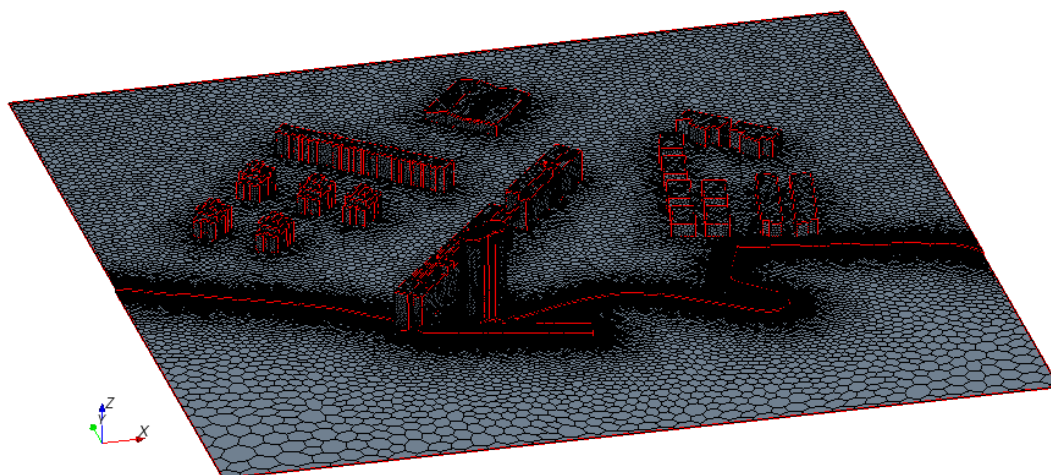


Figure 8.11 Generated volume mesh for the model of Høje Brygge.

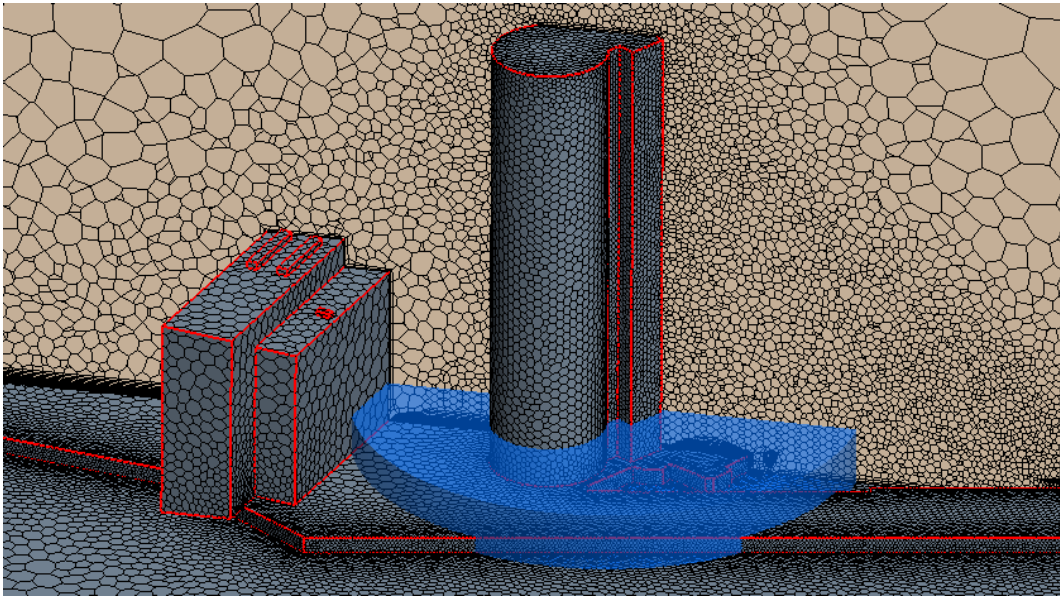


Figure 8.12 Close-up of the mesh around the area of interest. The refinement along the feature curve at the quay is seen and the refinement volume is highlighted in blue. The mesh is also showed on a vertical section through the domain.

8.5 Wind Phenomena at Høje Brygge

The wind conditions at Høje Brygge are due to a number of different flow phenomena. At the location corner streams, the Venturi effect, and a high next to low building combination is present.

8.5.1 Venturi Effect

At Høje Brygge a Venturi effect occur between the Siemens building and Høje Brygge with wind from NE as the buildings are not parallel which can be seen in [Figure 8.13](#).

The Venturi effect describes the increased wind speed that will occur at a narrowing of the surrounding geometry. The increased wind speed is simply a result of the continuity conditions, as the area gets smaller the speed increases.

8.5.2 Flow Around Cylinders

The phenomenon with flow around cylinders can be seen on the south part of the eastern tower in [Figure 8.13](#). Here it is seen that the wind accelerates around Høje Brygge.

Flow around cylinders is a well described phenomenon in fluid dynamics. Theoretically the amplification factor is 2 close to a smooth cylinder in a laminar flow.

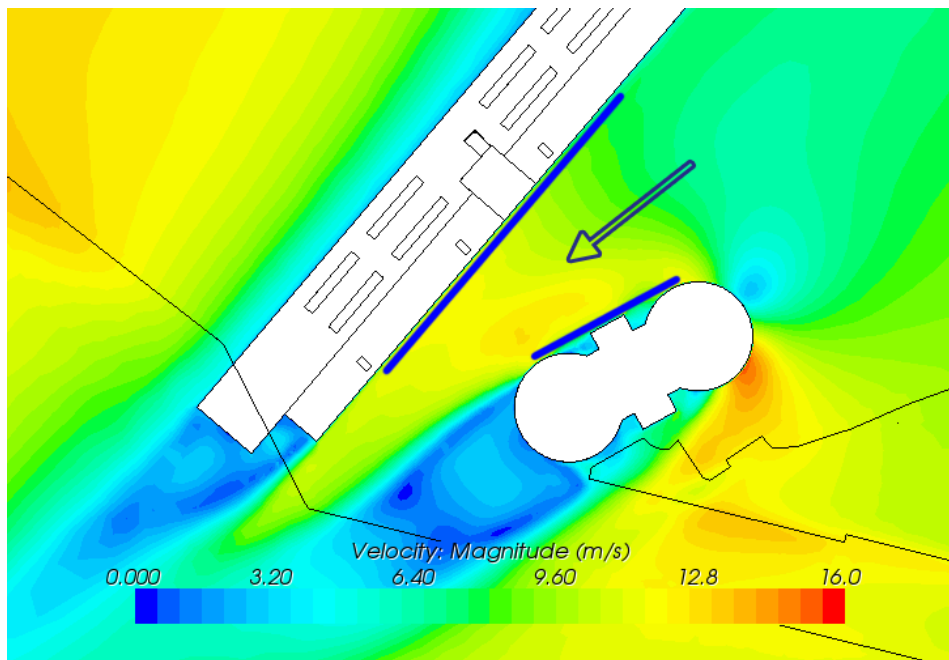


Figure 8.13 Venturi effect at Høje Brygge. As the two buildings are not parallel the wind from NE accelerates through the passage. Also it is seen that the wind speed is bigger at the south side of the eastern tower due to the flow around the cylinders.

8.5.3 High Building Behind Low Building

The problem with a high building behind a low building is pronounced at the site of Høje Brygge with wind from west to NW. [Figure 8.14](#) shows a contour plot of the pressure on a vertical section. It shows a high pressure at the top and low pressure at the bottom which drives the flow.

The tendency is also clear from the streamlines seen in [Figure 8.15](#). The lines are seeded at pedestrian level, and it is seen that all contribution to the wind velocity at these points comes from above the Siemens building when the wind is coming from west.

When wind passes a building a high pressure is formed on the front and low pressure on the back. On the back side of the building a back flow occurs. This is in itself not a problem; however when a high building is located behind a low building the effect is pronounced.

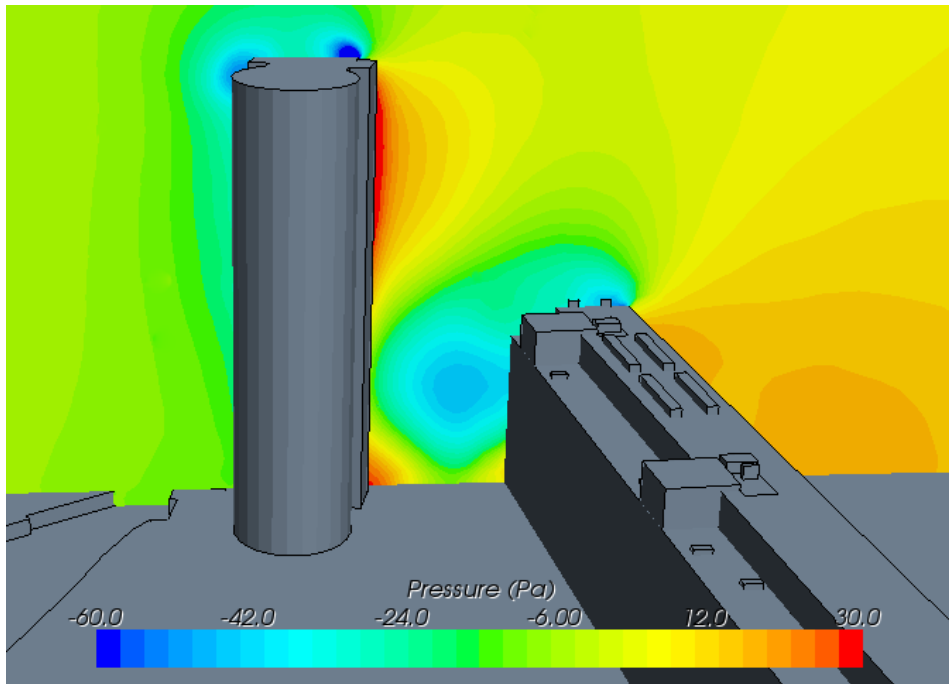


Figure 8.14 Relative pressure in a vertical section. A large pressure difference between the top and bottom of the building drives a downward flow.

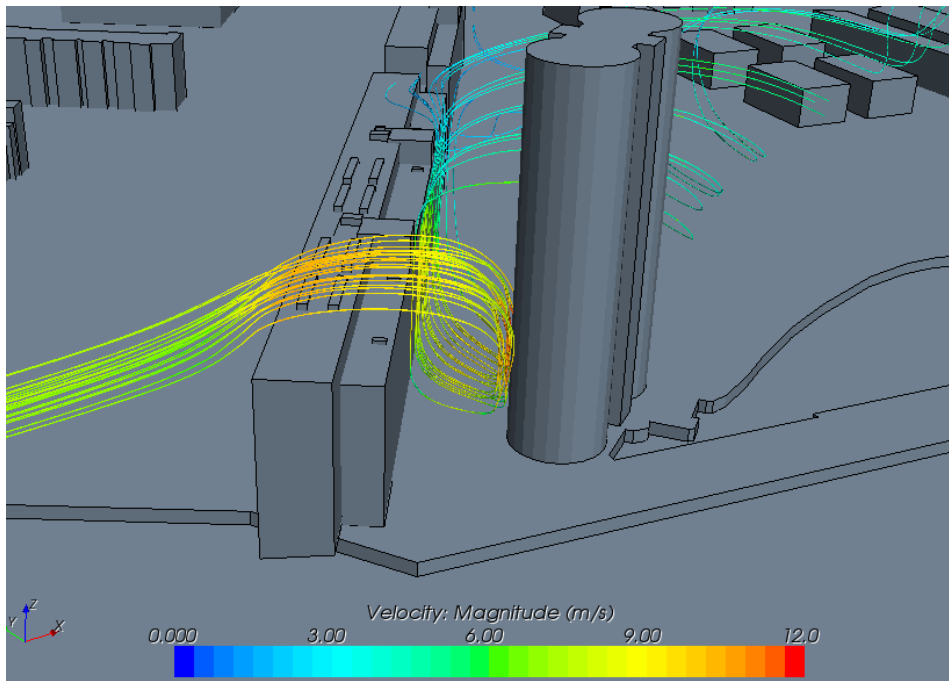


Figure 8.15 The streamlines shows that contributions to the wind speed at pedestrian level are from above the Siemens building.

8.5.4 Corner Streams

At the site around Høje Brygge the most pronounced corner stream is around the Siemens building with wind from west to NW.

High wind speeds occur over the water, and when the wind hits the Siemens Building a corner stream is also formed when the wind is from SW. In this case the amplification factor is not so significant because the wind is parallel with the Siemens building.

A road goes underneath a walking bridge between the two sections of the Siemens building. In this case strong winds can occur as a sum of three corner streams; one from the side of each section and one underneath the walking bridge. This phenomenon can also be seen as pressure short circuiting.

The two corner streams appear when wind is from west are illustrated in [Figure 8.16](#).

Near the quay another corner stream occurs as the quay is a 2 m high edge. This makes the wind speed near the quay a little higher at pedestrian level as seen in [Figure 8.17](#).

Corner streams occur at building edges and other sharp corners. Increased velocities occur as the wind is forced to pass around corners. The phenomenon is more pronounced at high-rise buildings as less of the wind will flow over the roof.

The effect is difficult to avoid, but considerations could be made regarding the placement of buildings close to each other. The effect of corner streams can be increased in passages between parallel buildings if the corner streams intersect.

If the buildings are close together the resistance is large enough that the wind speed decreases as well as the wind speed decreases if the buildings are moved far away from each other. This study has been made by [Blocken, Carmeliet and Stathopoulos \(2007\)](#) who made a study of a critical distance between parallel buildings.

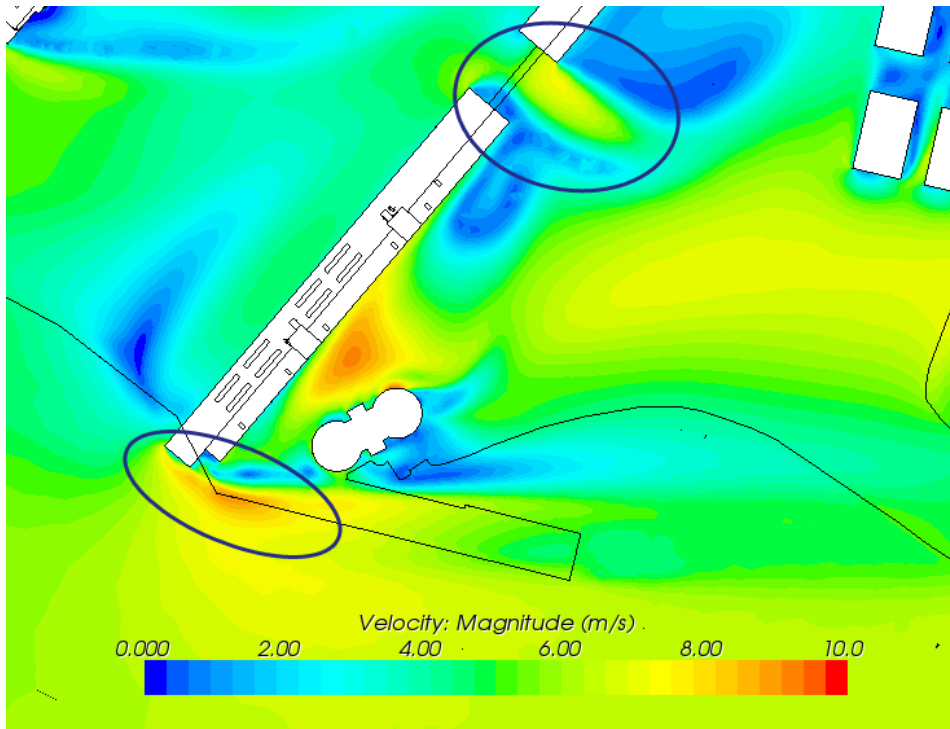


Figure 8.16 Illustration of corner streams with wind from west.

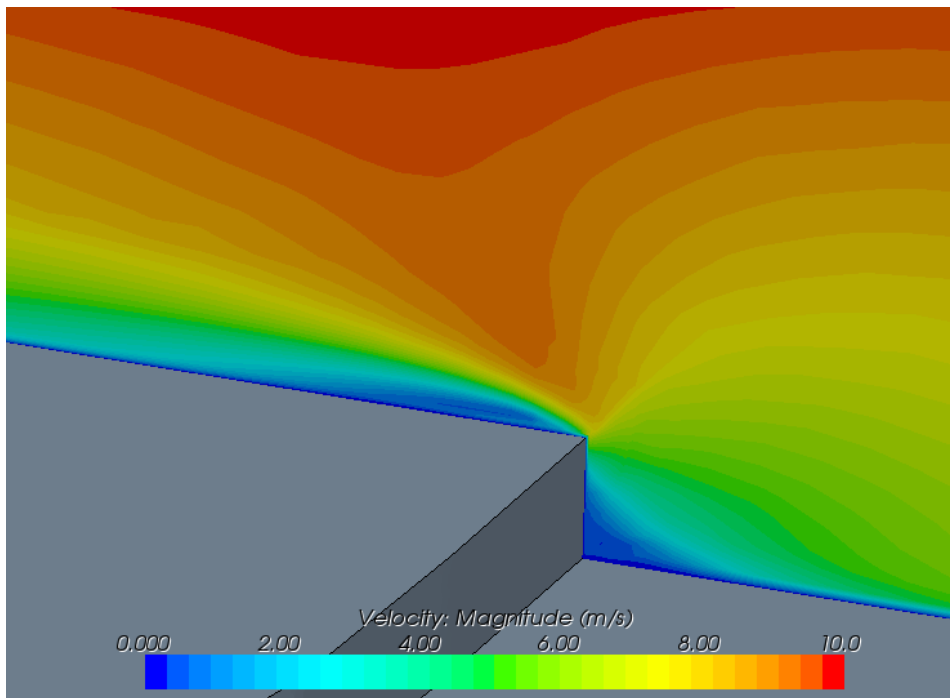


Figure 8.17 Illustration of corner stream above the quay.

8.6 Level of Comfort and Safety

Based on the comfort and danger criteria and the wind statistics given in Table 8.1, the exceedance probability of the comfort and danger criteria can be determined.

In Figure 8.18 and 8.19 the exceedance probability of the comfort and danger criteria respectively is given. The levels of comfort and danger given in the Dutch code of practice NEN 8100 is applied (Willemsen and Wisse 2007).

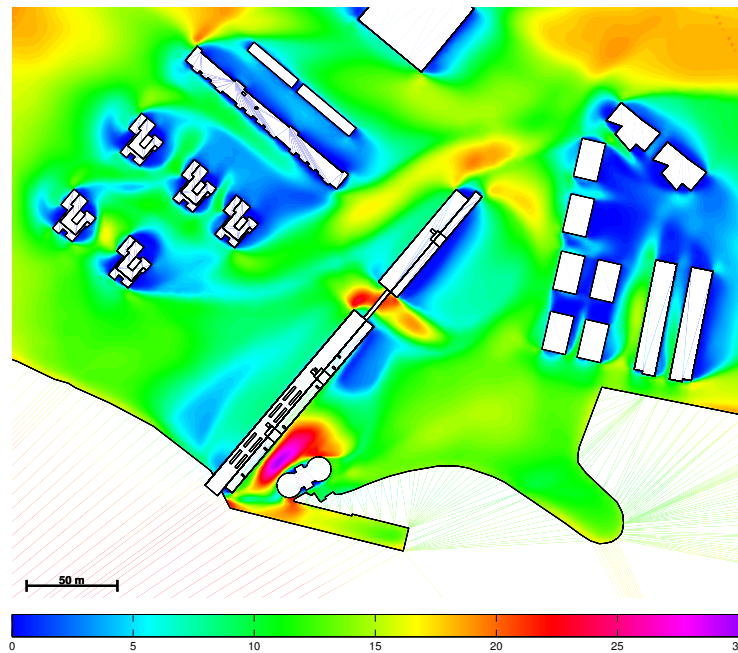


Figure 8.18 Contour plot showing the comfort in the area.

Given the maximum exceedance probabilities in Chapter 2 it is clear that there are problems with the comfort and danger at the site.

In the zone between the Siemens building and Høje Brygge the comfort criterion is exceeded up to 30 % of the time. In the same zone the danger criterion is exceeded 3 % of the time corresponding to approximately 260 h per year, which compared to the recommended maximum of 26 h is a huge exceedance.

It is clear that the danger criterion in the area as exceeded in huge areas, and therefore solutions to decrease the violent wind conditions should be sought.

In Figure 8.20 the evaluation after the 5 m/s-criterion stated in SBI-direction 128 is showed.

The limit for dangerous wind in the SBI-direction is stated as 53 % (Bjerregaard and Nielsen 1981). Thereby the wind conditions are not dangerous at Høje Brygge according to this criterion. As the wind conditions at the site are known to be dangerous, this is an example where the criterion in the SBI-direction fails.

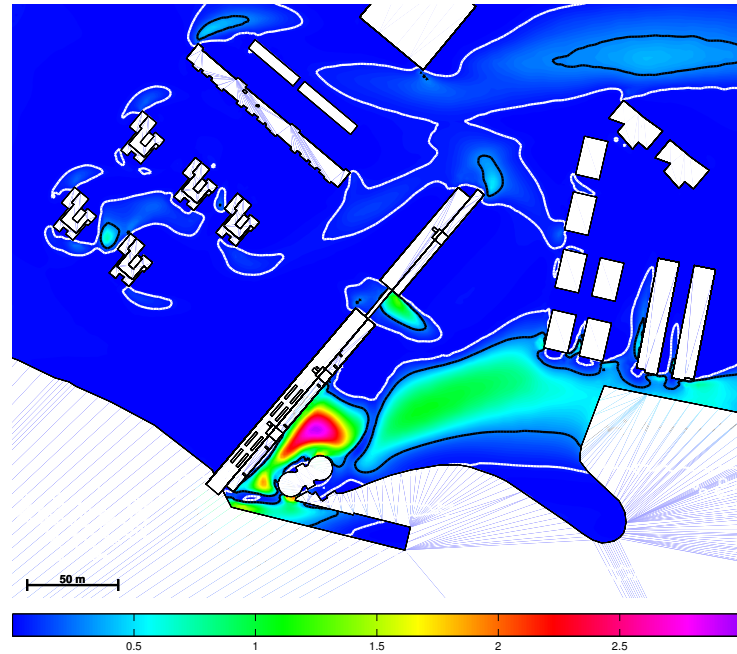


Figure 8.19 Contour plot showing the danger in the area.

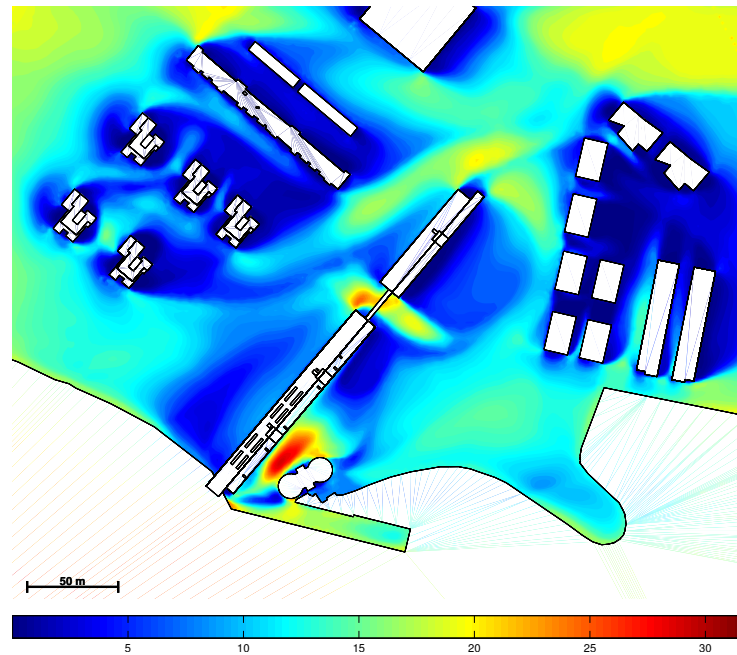


Figure 8.20 Contour plot showing the probability that the mean wind exceeds 5 m/s.

8.7 Suggested Solutions for Høje Brygge

The identified flow phenomena call for remedial measures countering the effects. In the following a number of different proposals are given, improving the wind conditions at the location.

8.7.1 Changing Location of Entrance

The wind conditions at the north-western side where the entrance is located are quite severe. On the south-eastern side the wind conditions are much more proper. Therefore a direct remedial measure is to change the location of the entrance. At the SE side an elevator is located. An entrance can be placed just next to it or made directly into the elevator.

8.7.2 Minimising the Wind Speed

Due to the wind coming from the wide areas of the Limfjord, a solution to decrease the wind coming from this direction is investigated. This is done by making a simple model of the quay as it is today, one that has a rounded corner at the water line, and one that accelerates the wind in the vertical direction by making a channel. The models can be seen in Figure 8.21, and for the evaluation the velocity 1.7 m over the ground level are plotted.

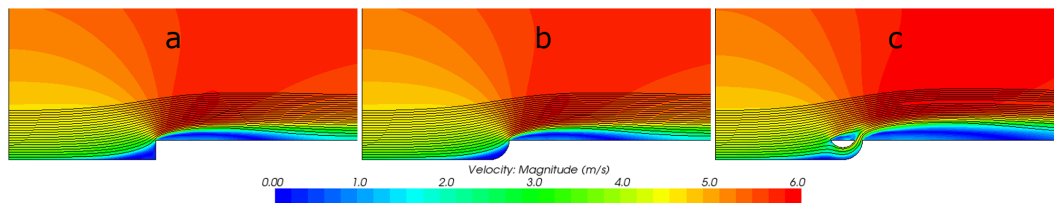


Figure 8.21 Sketch of different quay designs. **a** is the present design, **b** has a rounded shape, and **c** has an extra attachment which accelerates the wind upwards.

In Figure 8.22 it is seen that the velocities from the quay that is at Høje Brygge at the moment and the quay with rounded corner gives approximately the same at pedestrian level.

On the other hand the quay where a tunnel is modelled by making a half circle that accelerates the wind in the vertical direction, gives much smaller velocities at evaluation height and could therefore be a solution, or part of a solution to decrease the violent wind conditions.

However solution c induces a lot more turbulence as seen in Figure 8.22. The solution should therefore be evaluated based on the comfort and danger criteria. The equivalent velocity for comfort and danger respectively are showed in Figure 8.23. The comfort increases but the extra induced turbulence makes it just as dangerous as with no new features. The solution can therefore not be used to decrease the dangerous wind conditions in the area.

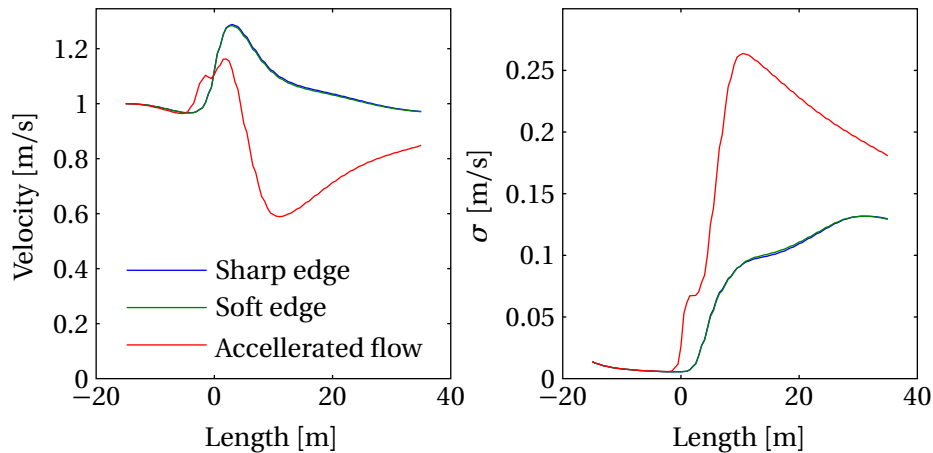


Figure 8.22 Comparison of normalised U and σ at $z=1.7$ m on the three models with sharp edge, rounded edge, and accelerated flow at the waterline respectively. The edge of the quay is at $x=0$ m. It is seen that the velocity for the sharp edged and soft edged are the same.

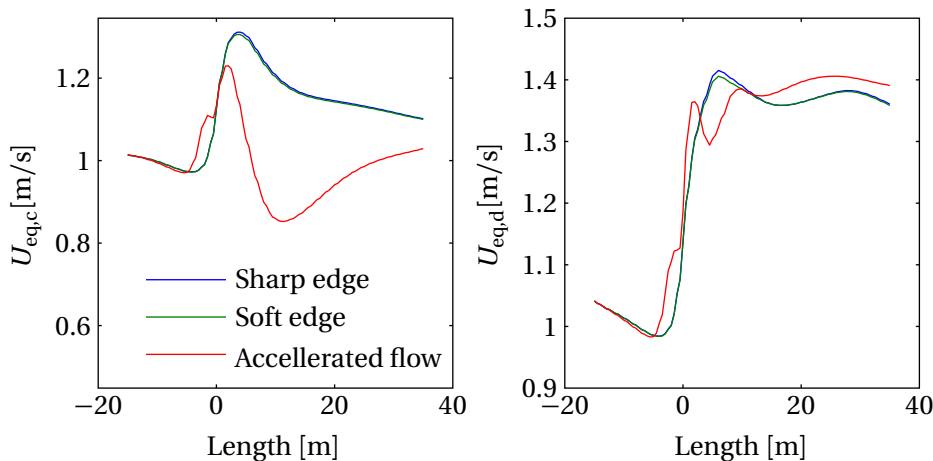


Figure 8.23 Comparison of the normalised equivalent velocity, $U_{eq} = U + k_p \sigma$, at $z=1.7$ m for both comfort and danger. The edge of the quay is at $x=0$ m.

8.7.3 Pent Roof

For the dominant wind direction the problem with strong winds occurs as a large pressure difference is formed between the top and bottom of Høje Brygge. Downward facing winds could be blocked by a pent roof attached to each tower. A model of the pent roof can be seen in [Figure 8.24](#).

As a proof of concept two identical models are made, except that the pent roof is implemented in one of the models. A smaller section of the full model of Høje Brygge is used to save some computational time.

In the analysis a rather large pent roof of 4 m is used. The analysis is made from two different directions; wind from WNW which is almost perpendicular to the Siemens building, and wind from west which is the dominant wind direction.

The results of the analysis with wind from west can be seen in [Figure 8.25](#) to [8.28](#) for both a horizontal section at pedestrian level, and a vertical section.

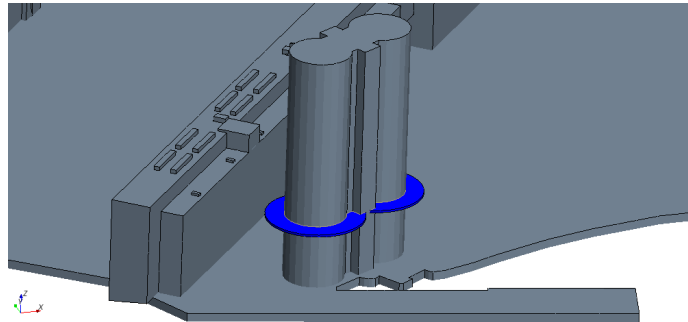


Figure 8.24 On each tower a pent roof is attached in order to block the downwards pointing wind.

At pedestrian level the wind speed decreases by 47%, but more important it should be noted that the changed wind pattern means that the velocity is in the other direction than before the attachment of the roof. The change in direction is seen by comparing Figure 8.25 and Figure 8.26.

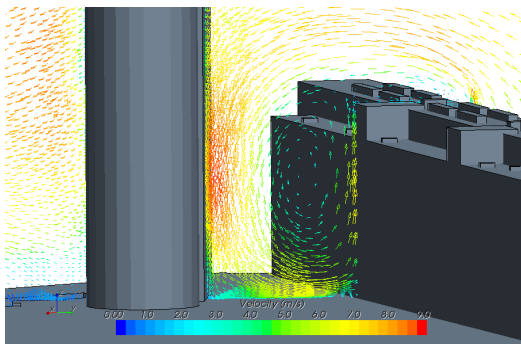


Figure 8.25 Vector plot of the velocity on a vertical section without the pent roof.

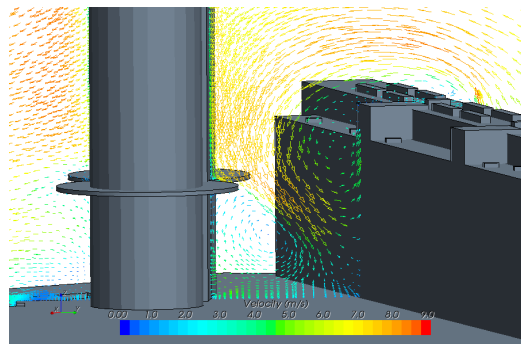


Figure 8.26 Vector plot of the velocity on a vertical section with the pent roof.

This leads to the conclusion that for the given wind direction the size of the pent roof is too large. The wind component along the buildings cannot be decreased much with this solution, but the component orthogonal to the building is almost removed, as seen in Figure 8.27 and 8.28.

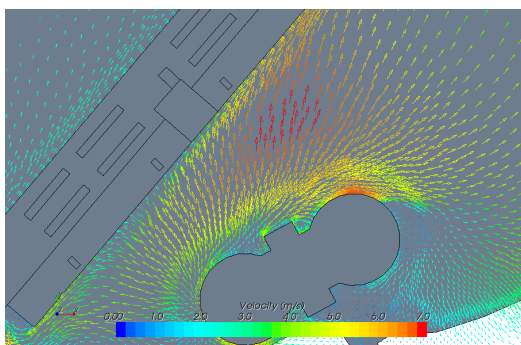


Figure 8.27 Vector plot of the velocity on a horizontal section without the pent roof.

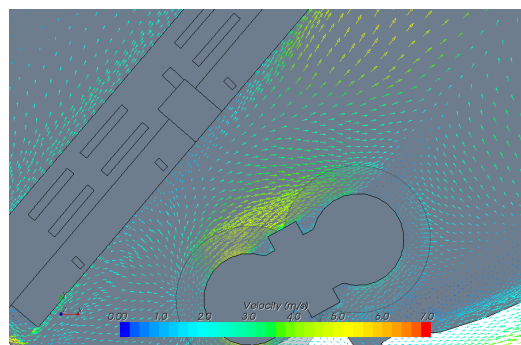


Figure 8.28 Vector plot of the velocity on a horizontal section with the pent roof.

Unfortunately the pent roof induces a lot more turbulence than without the roof. This increase should be weighted against the reduction of the wind speed to determine if the solution would make a better wind climate. A contour plot of the turbulent kinetic energy with and without the pent roof can be seen in Figure 8.29 and 8.30.

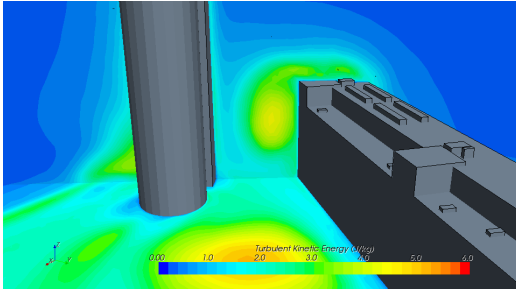


Figure 8.29 Contour plot of the turbulent kinetic energy without the pent roof.

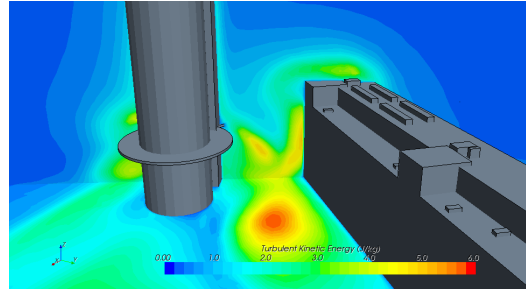


Figure 8.30 Contour plot of the turbulent kinetic energy with the pent roof.

Conclusions on Pent Roof

The results are compared on the average speed and k in a grid in the area between the entrances of both buildings. The result of the analysis can be seen in Table 8.2.

Table 8.2 Average wind speed and k in front of the entrances before and after attachment of the pent roof.

| Wind direction | With pent roof | | Without pent roof | | Ratio | |
|----------------|----------------|-------------|-------------------|-------------|--------------|-------------|
| | Speed m/s | k J/kg | Speed m/s | k J/kg | Comfort % | Danger % |
| WNW | 1 | 0.17 | 0.639 | 0.212 | 76 | 88 |
| W | 1 | 0.048 | 0.529 | 0.083 | 65 | 80 |

As seen a large reduction in mean wind speed is achieved, unfortunately with an increase in turbulence. To evaluate the total improvement of the wind climate the comfort and danger criteria should be evaluated before and after attachment of the pent roof. This shows an improvement for both criteria. The equivalent velocity decreases to 65% of the wind given without the pent roof for the comfort criterion with wind from west.

As the buildings are not parallel, the wind pattern changes with the distance between the buildings. Together with changing wind direction it is not possible to reduce the wind speed to zero over the whole area.

As well the pent roof will not have a large effect on the wind component along the buildings. However the method would be ideal in the case with parallel buildings of different height placed orthogonal to the dominant wind direction.

Further investigations would include an optimisation on the size and position of the pent roof.

8.7.4 Application of Windbreak

Another possibility for reducing the wind speed is to put up one or more windbreaks, which could be modelled as either solid or porous structures. When making a typical windbreak a porous structure gives the most shelter effect because a back flow behind the windbreak is avoided. This could have a good effect with wind from south where the area is free to the open fetch over the Limfjord.

In the case of Høje Brygge, windbreaks can also be used to build up a higher pressure at pedestrian level between the buildings and lead the wind flow around the building to a greater extent.

In this case the windbreak should not be porous. However this leads to a problem of creating a passage around the windbreak where the wind could be accelerated and make an even more dangerous zone than without the windbreak.

A setup with two solid windbreaks placed as showed in [Figure 8.31](#) are tested with wind from west. A direct comparison of mean wind speeds can be seen in [Figure 8.32](#) and [8.33](#).

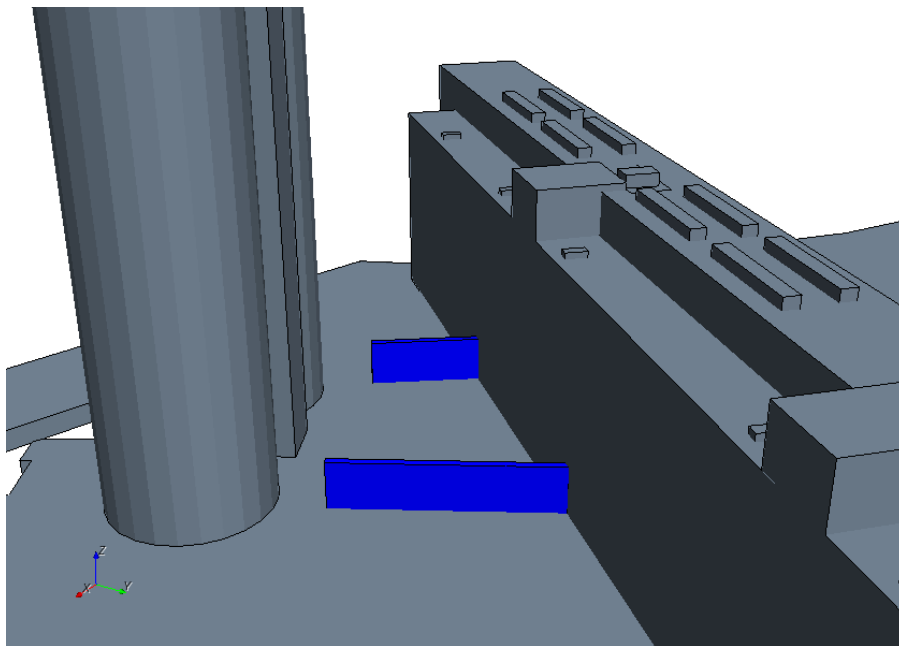


Figure 8.31 Positions of the windbreaks at Høje Brygge.

It is clear that the wind speeds are reduced in a large area. The passage through the windbreak is however more exposed than before, which is critical as the residents are forced to choose that way because of the position of the entrance to Høje Brygge.

A closer look at the streamlines, which is seen in [Figure 8.34](#) passing through this opening, reveals that the problem occurs because of the height difference between the Siemens building and Høje Brygge.

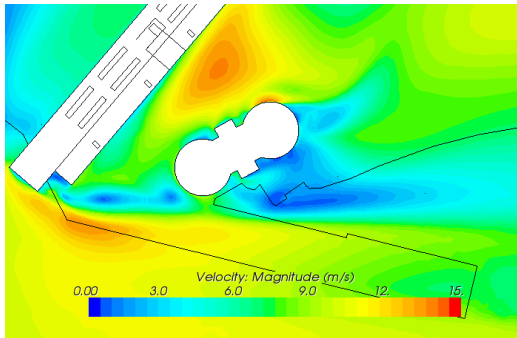


Figure 8.32 Mean wind speeds before the establishment of windbreaks.

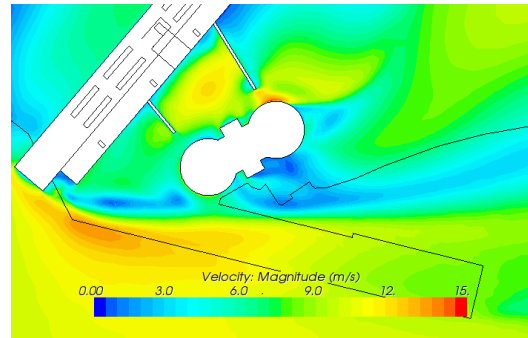


Figure 8.33 Mean wind speeds after the establishment of windbreaks.

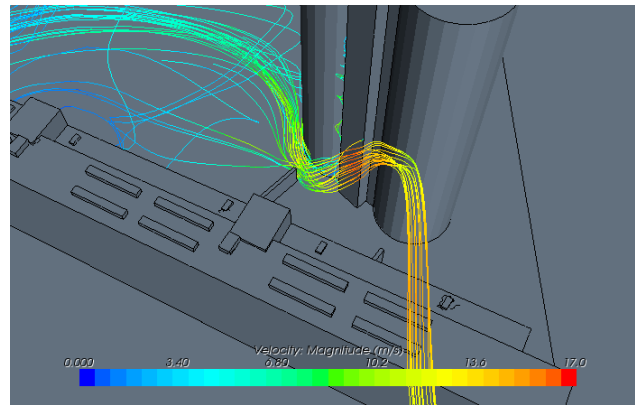


Figure 8.34 Streamlines through passage between windbreak and building.

8.7.5 Combination of Pent Roof and Windbreaks

The windbreaks establish a greater pressure, but there are still problems with downward facing wind, which the pent roof decreased. A combination of the two solutions is therefore investigated.

The wind pattern with this solution is compared with the model with windbreaks only. Contour plots of the equivalent velocity for both comfort and danger are showed for both models in Figure 8.35 to 8.38.

From the figures it is clear that the combination of windbreaks and pent roof significantly decreases the equivalent velocity for both comfort and danger. This is a result of the fact that the wind entering the passage between the windbreak and building has changed direction several times after passing the roof of the Siemens building.

In Figure 8.39 and 8.40 the level of danger and comfort is given with the combination of windbreaks and pent roof. The model is based on a directional resolution of 12 sectors of equal size.

As showed in the figures, the problem with wind right next to Høje Brygge has disappeared. In fact the problem in the passage under the Siemens Building is the most severe location in the domain. However the pent roof and the wind breaks do not solve the problem west of Høje Brygge, although the wind conditions here also are heavily influenced by Høje Brygge.

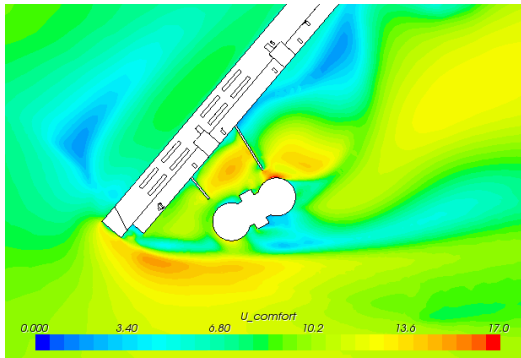


Figure 8.35 Equivalent velocity for comfort criterion with windbreaks.

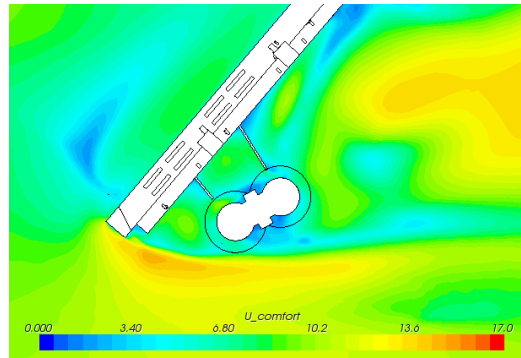


Figure 8.36 Equivalent velocity for comfort criterion with windbreaks and pent roof.

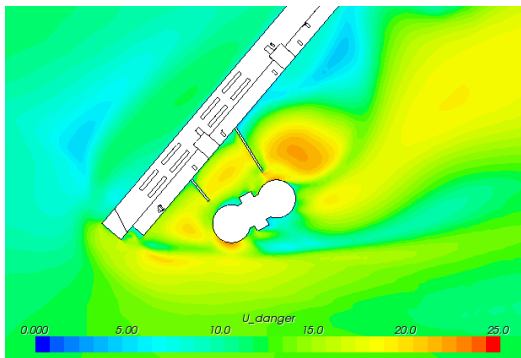


Figure 8.37 Equivalent velocity for danger criterion with windbreaks.

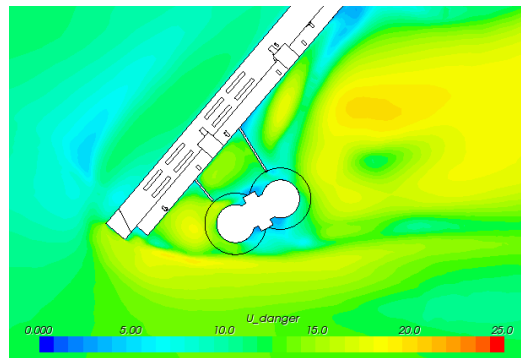


Figure 8.38 Equivalent velocity for danger criterion with windbreaks and pent roof.

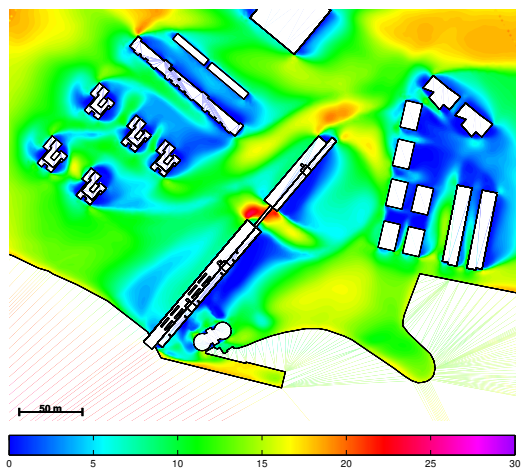


Figure 8.39 Contour plot showing the comfort in the area.

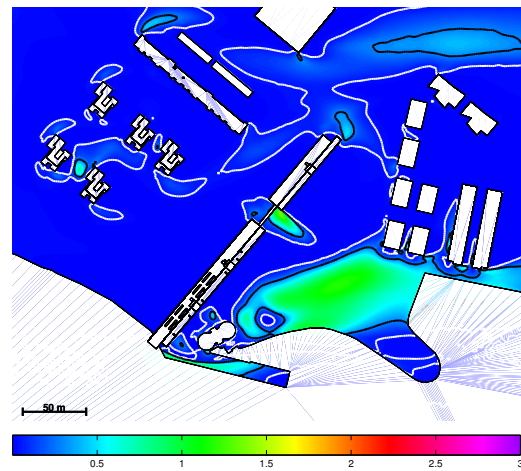


Figure 8.40 Contour plot showing the danger in the area.

8.7.6 Other Solutions

Other solutions could as well reduce the violent wind conditions in the area:

- Making the Siemens building higher in front of Høje Brygge, in order to leave the facade of Høje Brygge less exposed.
- Altering the geometry of the Siemens building to allow some flow through, in order to increase the pressure on the lee side.
- Construction of a building higher than the Siemens building on the western side, which decrease the exposed facade area of Høje Brygge
- Combining the Siemens building and Høje Brygge by a corridor.
- Foresting the area west of the Siemens building in order to decrease the wind speed of the approaching flow.
- Setting up a system of windbreaks, which forces the wind at ground level to make so many shifts in direction as possible.

The solutions given in this section is not further investigated by calculations.

8.8 Conclusions on Wind Evaluation at Høje Brygge

The wind conditions at Høje Brygge is evaluated according the procedure established in [Chapter 7](#), by means of CFD, exposure corrected wind statistic of Aalborg Airport transformed to the location of interest, and evaluated by criteria for comfort and danger.

The calculations document the severe wind conditions in the area, which residents have complained about. In the Dutch code of practice NEN 8100 the area around Høje Brygge are in the worst category in both comfort and danger. The danger criterion is exceeded around 11 days per year, which is ten times as much as allowed in NEN 8100.

By evaluation with the 5 m/s criterion given in SBI-direction 128, the area does not fall into the category for danger. This is seen as major discrepancy of this criterion as there are multiple incidents of dangerous winds reported in the area.

Three solutions are investigated by calculations, and it is found that combination of a pent roof and a windbreak gives better wind conditions in the surrounding area at Høje Brygge. The aims of these initiatives are to limit the down-flow in front of Høje Brygge and to increase the pressure behind the Siemens building, respectively.

This combination removes the violent wind conditions next to Høje Brygge, but some of the other flow phenomena induced by Høje Brygge remains. According to the calculation the area between the Siemens Building and Høje Brygge actually become a decent zone with respect to wind conditions. Further optimisation on the location of the windbreaks and the size of the pent roof remains.

A number of other solutions are suggested without any further study.

9 Evaluation of Wind Conditions at Viborgvej

The procedure for evaluating wind conditions proposed in Chapter 7 is used to evaluate the wind conditions at a location on Viborgvej/Bredskiftevej in Århus.

Århus municipality demand an evaluation of the wind conditions when high-rise buildings are planned for. Therefore an evaluation based on the comfort and danger criteria given in Chapter 2, is made to give information on the exceedance probability of the wind in the area of interest.

The wind phenomena driving the registered wind conditions are analysed and remedial actions are suggested in order to counter the wind phenomena.

In the western end of Århus in an area located at Viborgvej/Bredskiftevej, a new hotel and congress centre is proposed. This centre includes eight high-rise buildings with different heights, the tallest with a height of 70 m. The eight high-rise buildings will be placed on each side of Viborgvej as seen in Figure 9.1.



Figure 9.1 Development plan for the area at Viborgvej where the hotel and congress centre will be placed. The eight buildings that are planned for are marked with dark gray colour. Graphics from Dansk Erhvervsprojekt A/S.

Five of the high-rise buildings are placed on the north side of Viborgvej and the last three are positioned on the south side of the road. In [Figure 9.2](#) and [9.3](#) the proposed buildings are seen along Viborgvej.



Figure 9.2 Illustration of the view from west on Viborgvej. Graphics from Dansk Erhvervsprojekt A/S.



Figure 9.3 Illustration of the view from east on Viborgvej. Graphics from Dansk Erhvervsprojekt A/S.

9.1 Surrounding Areas

The area is, as seen in [Figure 9.1](#), parted by Viborgvej that goes from west to east through the area of investigation.

The north side of Viborgvej is mainly covered with domiciles of several different companies, among other the owner of the hotel and congress centre project, Dansk Erhvervsprojekt A/S. These are buildings of a considerable size. Further away, on the north side of Viborgvej, is an open area with recreational facilities and agriculture areas.

On the south side of Viborgvej is an area, which is mainly dominated by one family houses.

9.2 Build-up of Model for Viborgvej

The model for Viborgvej is based on the procedure given in Chapter 7. The setup and the case-specific parameters are listed in Table 9.1.

Table 9.1 Setup for the model at Viborgvej.

| Parameter | Given by |
|----------------------------|---|
| Comfort criterion | $U_{eq,c} = U + \sigma_U \geq 6 \text{ m/s.}$ |
| Danger criterion | $U_{eq,d} = U + 3\sigma_U \geq 20 \text{ m/s.}$ |
| Classes for exc. prop. | After NEN 8100 (Willemsen and Wisse 2007). |
| Turbulence model | Menter (1994) $k-\omega$ SST with parameters by Yang et al. (2008). |
| Inlet | Origin shifted log-law and turbulence profiles derived for stable ABL with z_0 based on Figure 9.5 (Section 3.2.1). |
| Outlet | Zero gradient of all flow parameters. |
| Ground | Rough wall equal to $z_0 = 0.03 \text{ m}$ in the central domain, and $z_0 = 1 \text{ m}$ in the area of parcels (Section 3.2.3). |
| Buildings | Smooth wall. |
| Free stream | Symmetry. |
| Mesh | Described in Section 9.3. |
| Wind statistic | Exposure corrected data of Troen (1989) from Tirstrup, transformed by the procedure in Chapter 5 illustrated by Figure 9.4. |
| Roughness | Given by Figure 9.5 and 9.6. |
| Directional discretisation | 12 directions equally parted by angle are used. |

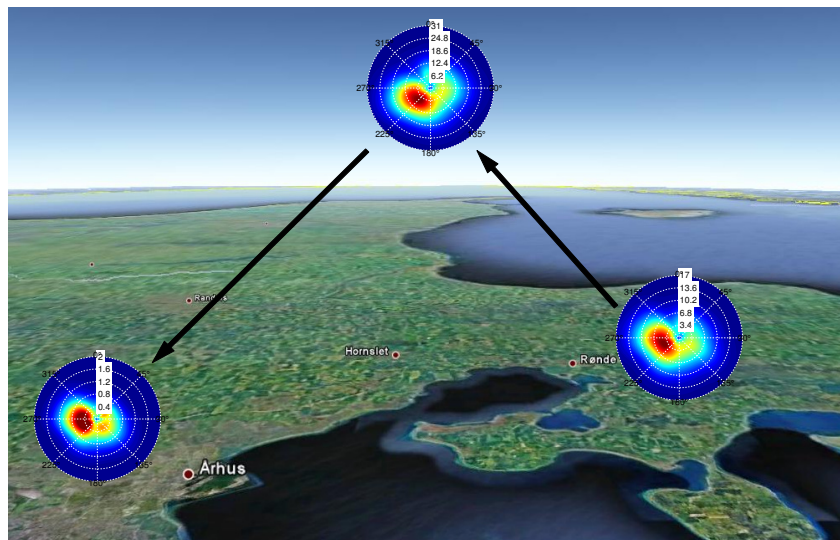


Figure 9.4 Illustration of procedure for transformation of wind. The wind at 10 m height at the airport in Tirstrup is transformed to geostrophic level, and from the geostrophic level transformed down to a realisation of the friction velocity at Viborgvej. (Photo by COWI A/S)

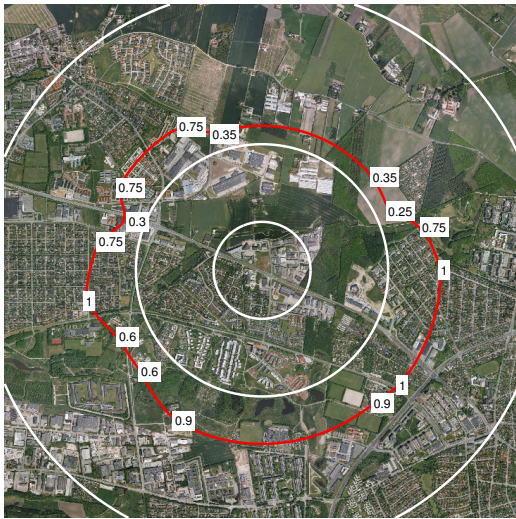


Figure 9.5 Local roughness. (Photo by COWI A/S).



Figure 9.6 Regional roughness. (Photo by COWI A/S).

9.3 Geometrical model and Spatial Discretisation

The computational domain at Viborgvej consists of a terrain model, the existing buildings, and the new high-rise buildings. The buildings are divided into different groups, showed by different colours in Figure 9.7.

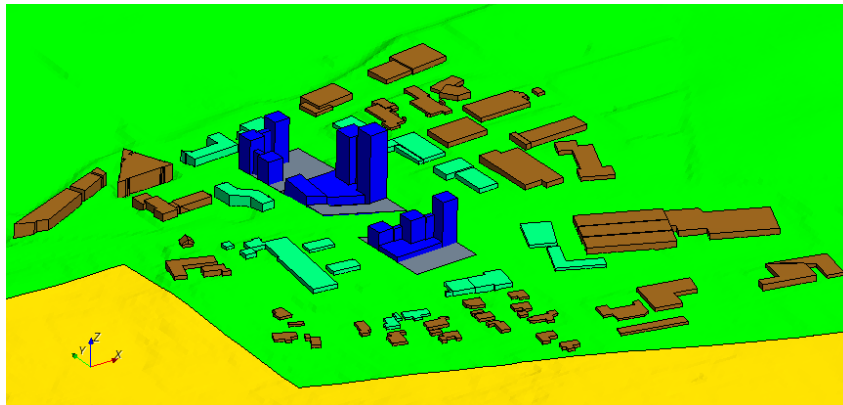


Figure 9.7 Geometry used for Viborgvej divided by different parts. The blue part is the high-rise buildings evaluated, the green buildings are included with fine grid, the brown buildings with a coarser grid. The yellow ground area has a greater roughness than the green ground area due to a residential area.

The surrounding buildings are divided into two groups; near located buildings and far located buildings on which different mesh sizes will be used. Furthermore a volume covering the bottom 20 m of the domain around the high-rise buildings is refined more than the surroundings.

The mesh is illustrated in Figure 9.8 and a close-up to the high-rise buildings in Figure 9.9.

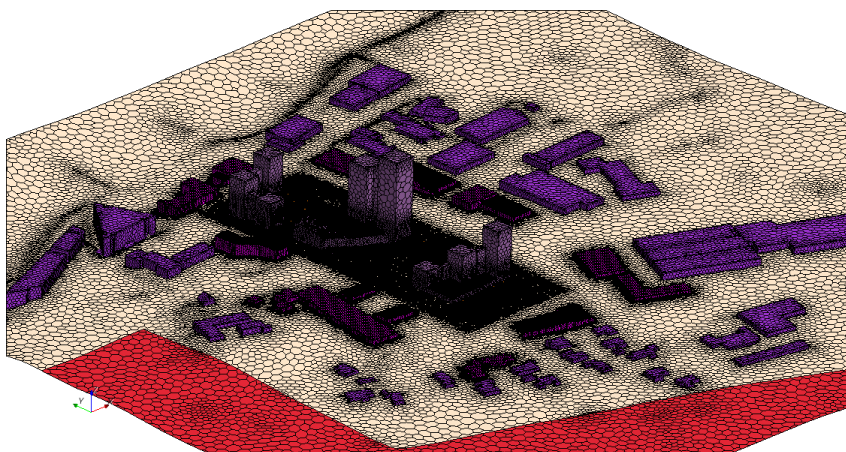


Figure 9.8 Mesh used in the calculations for Viborgvej.

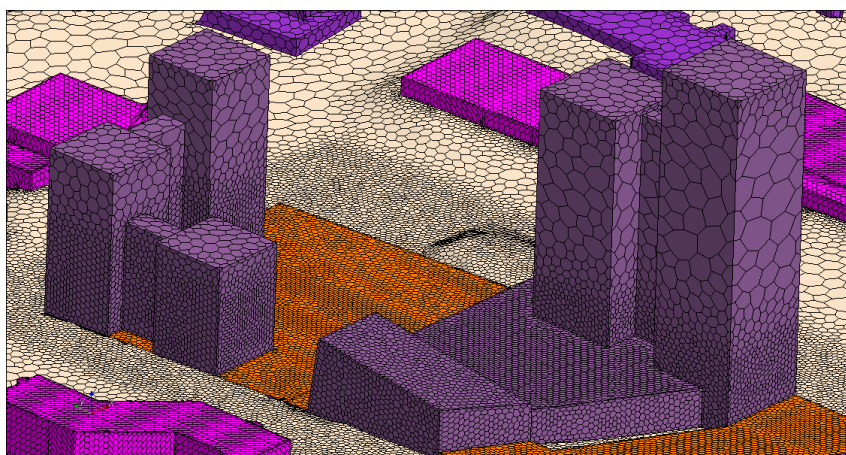


Figure 9.9 Close-up of the mesh used in the calculations for Viborgvej.

On the ground a prism layer of 7 cells is used up to a height of 2 m, in order to refine the ground layer in which large velocity gradients occur, and still be able to use the full wall roughness.

9.3.1 Convergence Analysis

As the solution will depend on mesh size, if the mesh is too coarse, a comparison of a solution is made with three different base sizes. A coarse with, 775 000 cells, a standard with 2 000 000 cells and a fine with 3 300 000 cells. Regression plots of the mean velocity are showed in [Figure 9.10](#) both compared to the finest mesh.

It can be seen that the mesh has an influence on the results for both the coarse and medium mesh. The largest deviations from the fine mesh occur at small velocities which do not contribute much on neither comfort nor danger.

An even distribution of both higher and lower velocities are seen, which indicates that the difference in solutions with different meshes is to find as small translations of the wind pattern, and not overall change of mean wind speed. For further calculations the standard mesh is accepted.

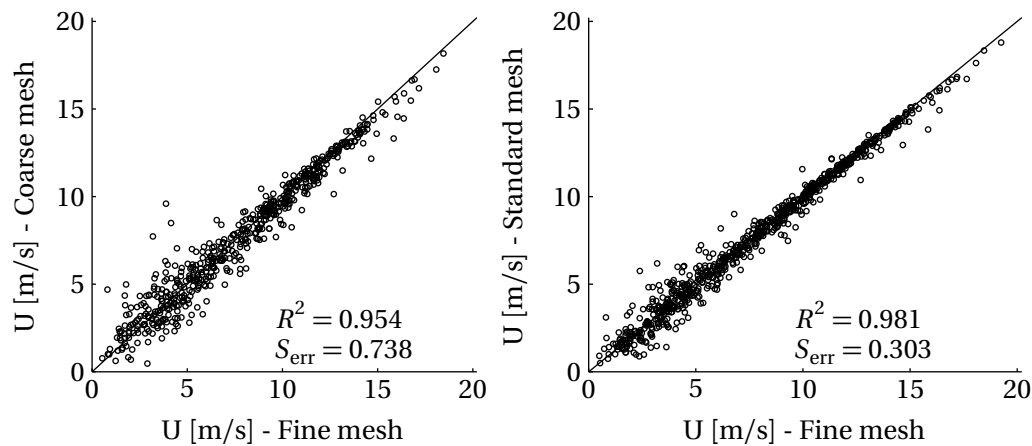


Figure 9.10 Regression plots of the mean velocity in three models with different mesh size. In both plots the fine mesh is used as reference.

9.4 Wind Phenomena at Viborgvej

The most pronounced phenomenon that is seen in the area at Viborgvej is corner streams. These are seen around the corners of building A1 and A2, and to a less extent at the corners of building B3 and B4. The corner streams around the buildings can be seen in [Figure 9.11](#).

The corner streams arise as the wind, coming from the dominant western direction, strikes into the walls of the high-rise buildings. Thereby a high pressure arises at the front of the buildings and the wind will seek around the corners of the building. Streamlines of the corner streams are seen in [Figure 9.11](#).

The passageway between building A1 and A2 increases the high pressure in front of the A buildings.

9.5 Level of Comfort and Safety

To examine the changes in the wind conditions the proposed building induces, a reference model without the new buildings is made along with the model where the new buildings are introduced.

This leads to four plots of the area; two plots are showing the wind conditions in connection with the comfort criterion and two with the conditions based on the danger criterion. The criteria used are the ones found in [Chapter 2](#).

9.5.1 Comfort Criterion

The comfort criterion is evaluated by comparing the exceedance probability before and after the high-rise buildings is built. In [Figure 9.12](#) the comfort criterion is seen with the terrain as it is today and in [Figure 9.13](#) with the high-rise buildings.

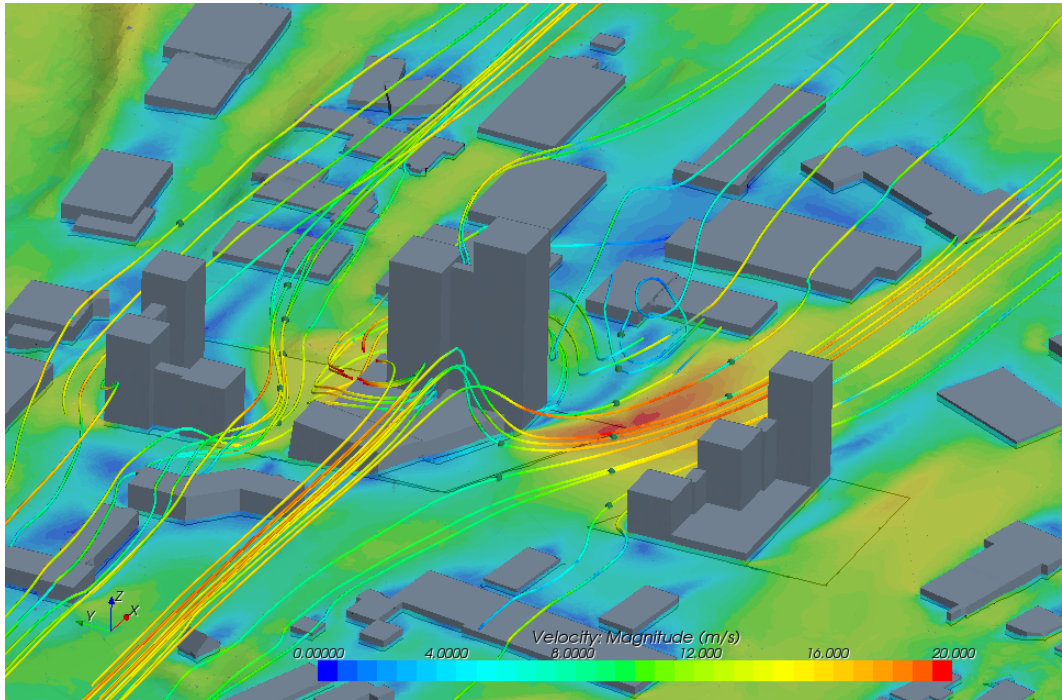


Figure 9.11 Streamlines of the wind coming from west and striking into the walls of buildings A and B.

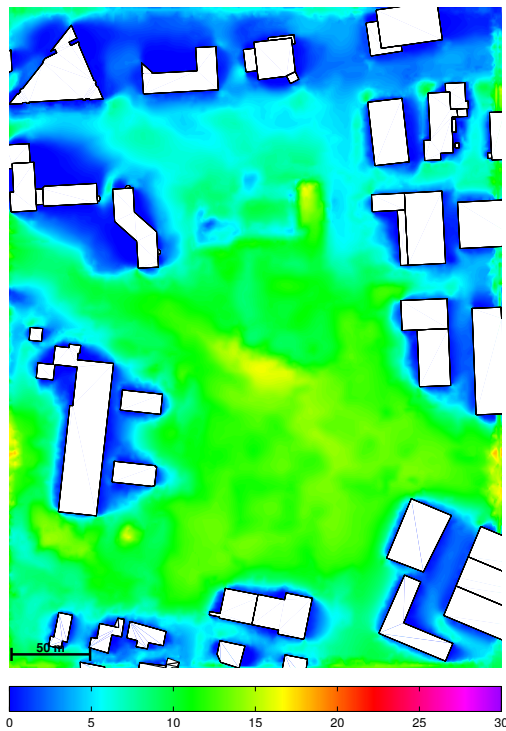


Figure 9.12 Plot of the comfort without the high-rise buildings.

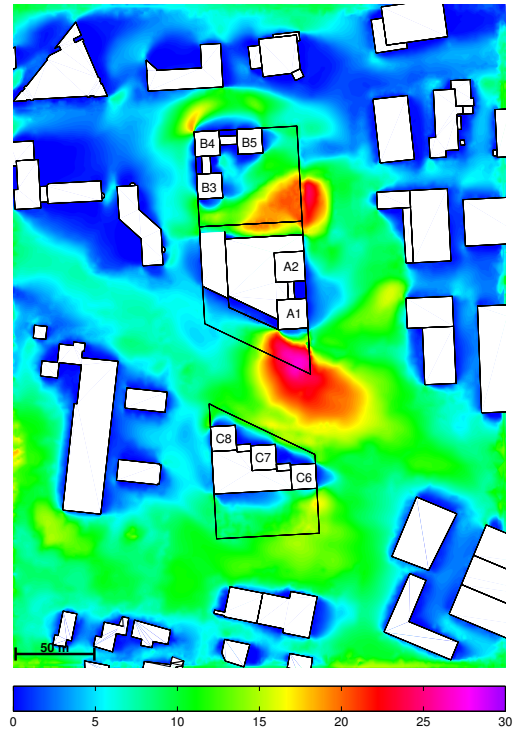


Figure 9.13 Plot of the comfort with the high-rise buildings included.

When the high-rise buildings are put up the comfort level is decreased in several places on the north side of Viborgvej. Though there are some areas, especially close to the new buildings, where the comfort increases due to sheltered zones behind the buildings.

The corner streams that arise around the corners of building A1 and A2 and B3 and B4 can be seen as well. In the corner stream produced by A1 the worst level of comfort is found. In this area the comfort criterion is exceeded 27 % of the time as indicated in Figure 9.13.

9.5.2 Danger Criterion

In Figure 9.14 the danger criterion is evaluated in the reference model, and in Figure 9.15 the danger criterion is evaluated with the new building introduced

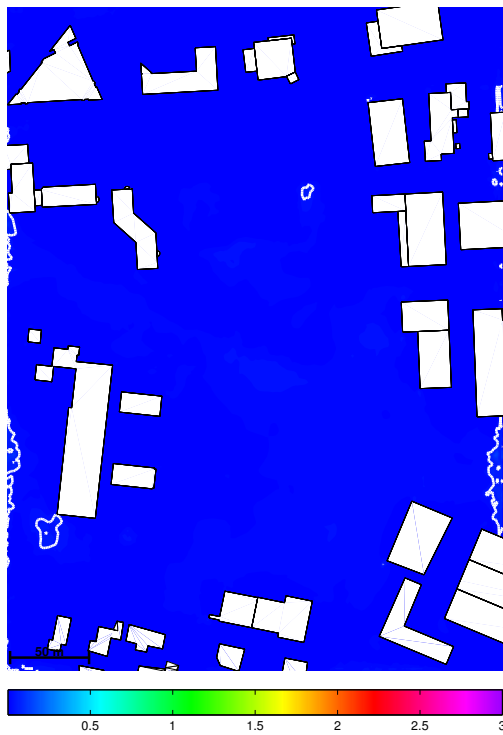


Figure 9.14 Plot of the danger without the high-rise buildings.

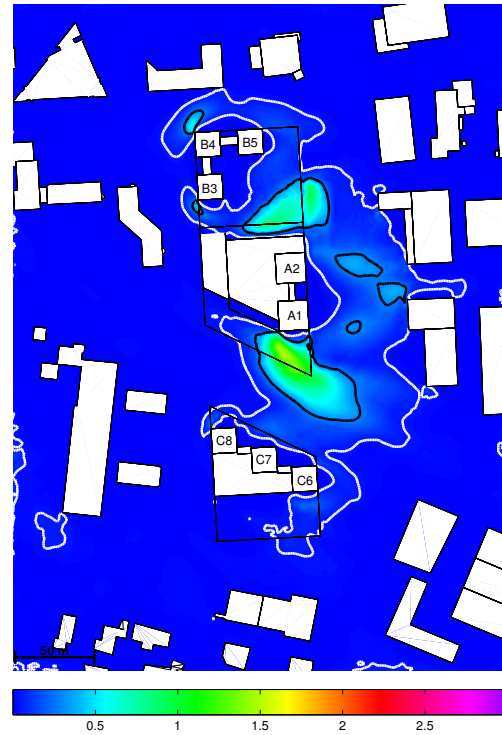


Figure 9.15 Plot of the danger with the high-rise buildings included.

It is seen that dangerous wind are almost never encountered in the reference model. The new buildings induce a number of areas with significant exceedance probability, especially around the buildings A1 and A2 and to a lower extend around the B-buildings.

At the C-buildings however no significant problems are introduced. This is attributed to the fact that the towers C8 to C6 are gradually increasing in height seen from the predominant western direction.

The criterion is exceeded in 1.6 % of the time in the corner stream coursed by A1, which is much higher than the limit of 0.3 % of the time.

9.5.3 Evaluation after SBI-direction

In order to demonstrate the sensitivity to the evaluation criterion an evaluation by the 5 m/s-criterion based on the SBI-direction is showed in Figure 9.16. Two conclusions can be made: The exceedance probability is not near the 53 % that the SBI-direction states as dangerous, but it is well above the 20 % level, which the direction states for when remedial actions should be carried out.

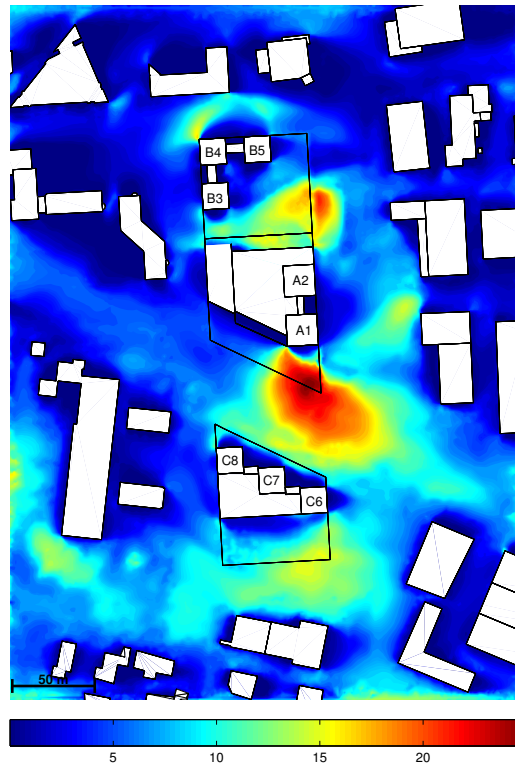


Figure 9.16 Plot of the probability that the mean wind exceeds 5 m/s.

9.6 Sensibility of the Roughness length

In order to evaluate the sensibility of the exceedance probability to the estimated local roughness used to determine the inlet profiles, a model with the double roughness is run. A higher roughness yields a higher friction velocity which would overestimate the exceedance probability. However, this overestimation is counteracted by a lower velocity gradient with higher roughness.

Figure 9.17 to Figure 9.20 shows the exceedance of the comfort and danger criteria for a model with the original estimated roughness and a model with the double roughness. In both models the exceedance probability is found by applying the corresponding wind statistics adjusted to the roughness.

The influence of the estimated roughness does not have a great influence on the exceedance probability as long as the same roughness is used in the model and to calculate the wind statistics for the location. It is assessed that the the local roughness can be estimated with higher precision than a factor two.

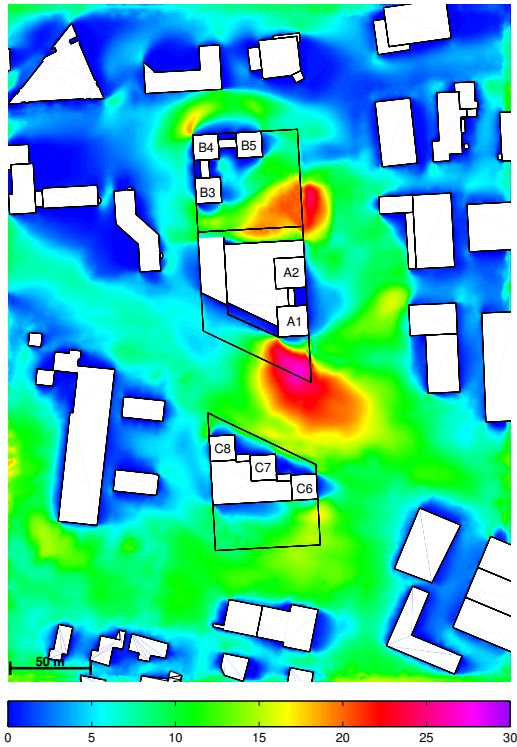


Figure 9.17 Exceedance probability of the comfort criterion with the original estimated roughness.

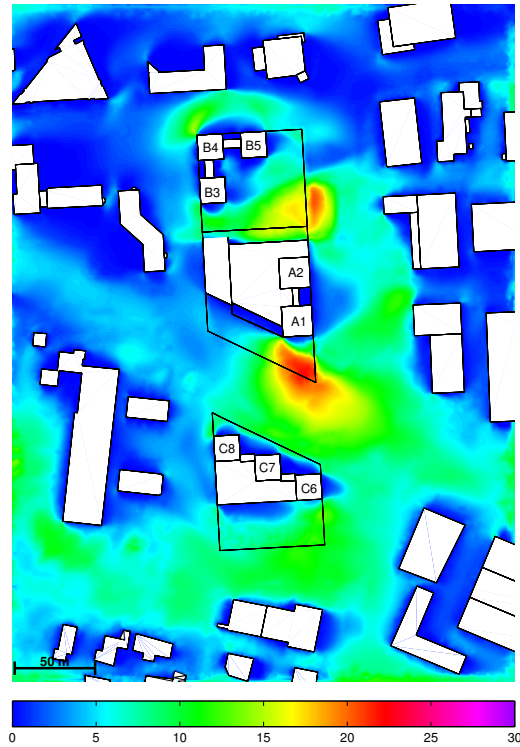


Figure 9.18 Exceedance probability of the comfort criterion with the double roughness.

9.7 Suggested Solutions for Viborgvej

As the danger criterion is exceeded more often than recommended, one or more initiatives has to be done in order to reduce the exceedance probability.

The problem with violent wind conditions occurs as large façade areas of the A and B buildings are directly exposed to the free stream. Thereby corner streams occur, and solutions for decreasing the corner streams around the A buildings could be:

1. Introducing an opening between building A1 and A2.
2. Rotate building A1 and A2 45° around their own axis.
3. Move building A1 and A2 to the east-west direction instead of the north-south direction.
4. A smaller tower can be built to the west of A1 and A2.
5. Changing the geometry of building A1 and A2, so the part that that is higher than the surrounding buildings is more aerodynamic.
6. Reduce the thickness of A1 and A2 over the level of the surrounding buildings, or increase the thickness of A1 and A2 in the level under the surrounding buildings.

Mainly the ideas given above are decreasing the wall area on the side where the wind hits. The dominant wind direction and speed is west.

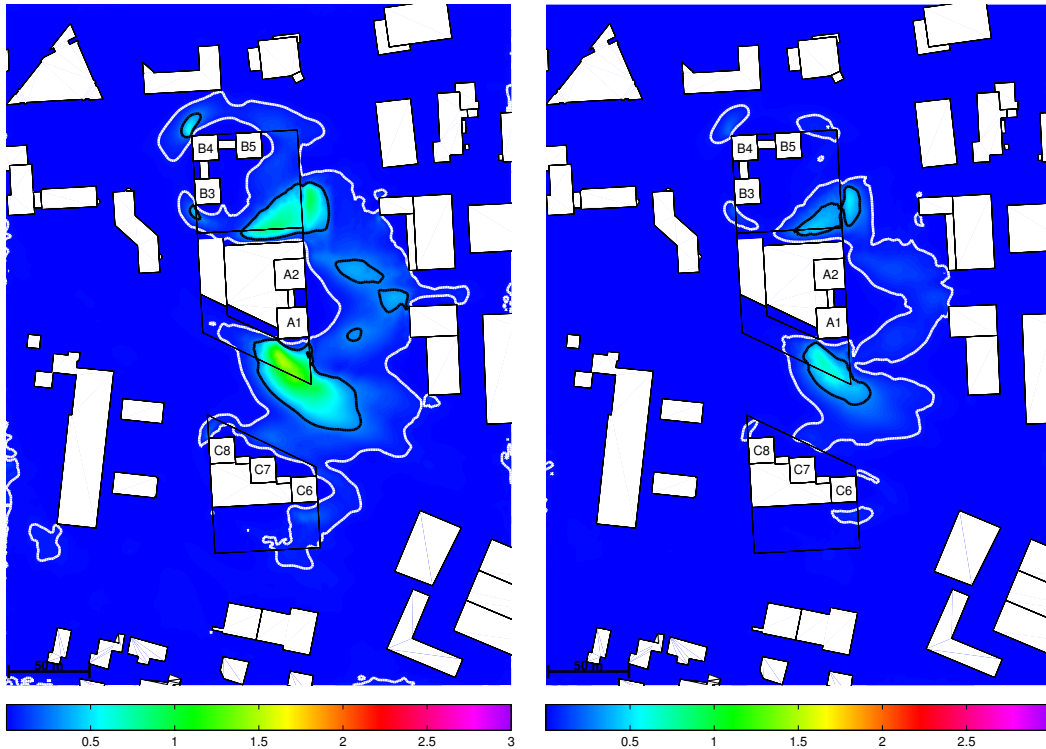


Figure 9.19 Exceedance probability of the danger criterion, original roughness.

Figure 9.20 Exceedance probability of the danger criterion with the double roughness.

The solution given in 4 is making bad wind condition on the roof in front of the A1 and A2 buildings, but as no one is walking around on the roof, this is not a problem.

The solution to change the thickness of the buildings in the height of the surrounding buildings is to give the wind a better possibility to go around the buildings and not hit down and accelerate at pedestrian level.

9.7.1 Modelling of Solution

The first solution given is analysed further. The reason for removing the passage is to decrease the pressure on the front of the towers A1 and A2, driving the corner streams around the towers.

The analysis is conducted by the same procedure as the reference models. Contour plots for the comfort and danger criterion are given in Figure 9.21 and Figure 9.22 respectively.

It is seen that the wind conditions are better after removing the passageway, but are still not acceptable. The maximum exceedance of the danger criterion is 1.4 % after the conditions is tried improved by removing the passageway.

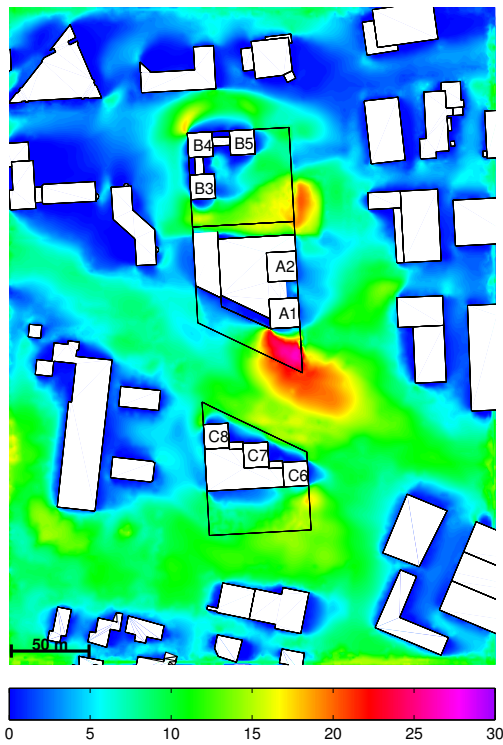


Figure 9.21 Plot of the comfort when the passageway is removed.

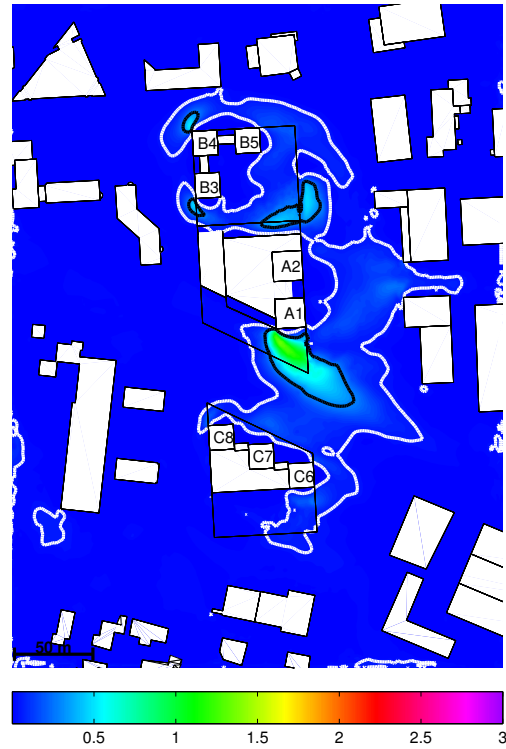


Figure 9.22 Plot of the danger when the passageway is removed.

9.8 Conclusions on Wind Evaluation at Viborgvej/Bredskiftvej

The wind conditions at Viborgvej/Bredskiftevej is evaluated according the procedure established in Chapter 7, by means of CFD, exposure corrected wind statistic of Tirstrup Airport transformed to the location of interest, and evaluated by criteria for comfort and danger.

It is concluded that the wind conditions in the area is not acceptable after the high-rise buildings are implemented according to the Dutch code of practice NEN 8100. Therefore a solution to reduce the wind in the area is investigated, where the passageway between building A1 and A2 are removed.

The proposed solution is not enough to reduce the areas with unacceptable wind conditions. A number of other solutions which involve altering the development plan are proposed.

10 Investigation of Directional Discretisation

In the calculations used to analyse the wind conditions for the cases presented in Chapter 8 and 9, 12 sectors spanning 30° are used to evaluate the problems. The 12 directions are a result of the directional discretisation chosen in the input statistical data by Troen (1989), but whether this is enough or too much is an open issue.

Two approaches for the directional discretisation exist, that is to make sectors of the same size or to make sectors with the same probability of occurrence. In the following results of both methods are presented, with different directional resolution to evaluate which discretisation should be used.

10.1 Computed realisations for Høje Brygge

For the case at Høje Brygge directional resolutions with 36 and 12 sectors of equal probability of occurrence and 16, 12, 8, and 4 sectors of the same size are used. The results are given in Figure 10.2 to 10.13, and in Figure 10.1 the resolved statistic for each directional resolution is given.

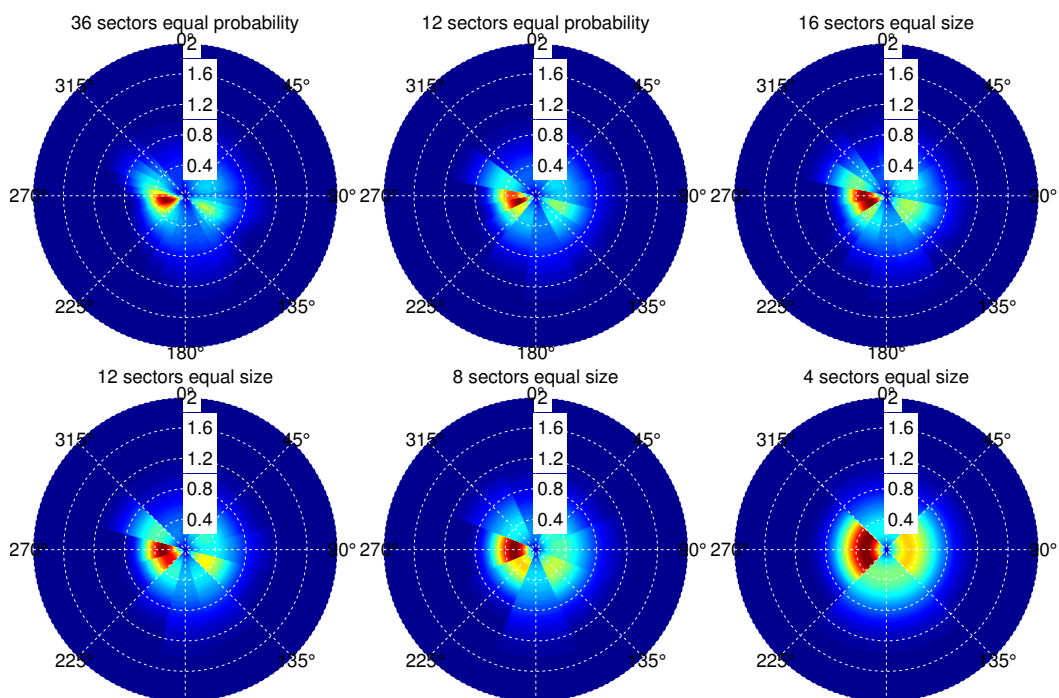


Figure 10.1 Resolved statistics for the case at Høje Brygge. For each sectoral realisation a Weibull distribution is fitted to the part of the continuous statistic, which the sector covers.

Comfort

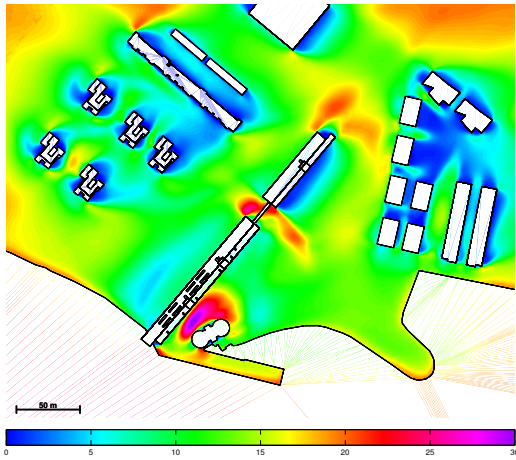


Figure 10.2 Probability of exceedance of the comfort criterion with 36 directions with equal probability of occurrence.

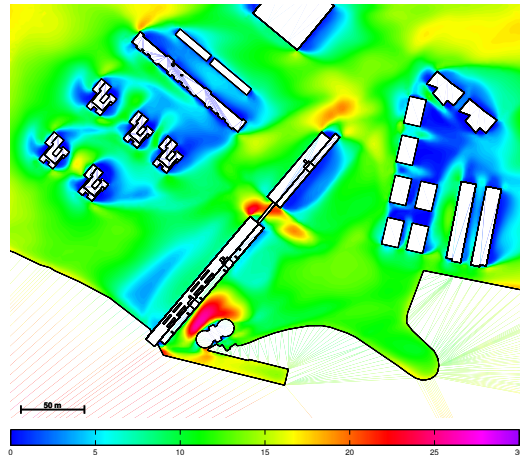


Figure 10.3 Probability of exceedance of the comfort criterion with 12 directions with equal probability of occurrence.

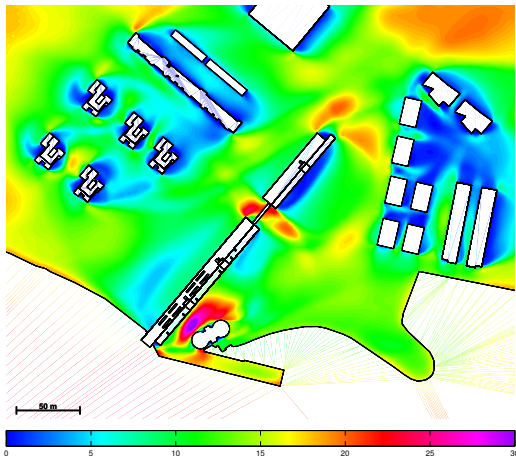


Figure 10.4 Probability of exceedance of the comfort criterion with 16 equal sized directions.

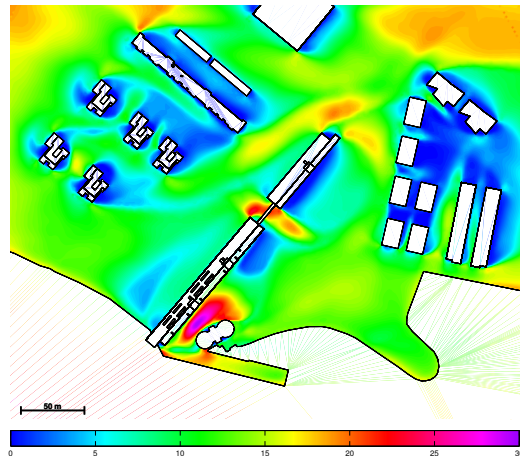


Figure 10.5 Probability of exceedance of the comfort criterion with 12 equal sized directions.

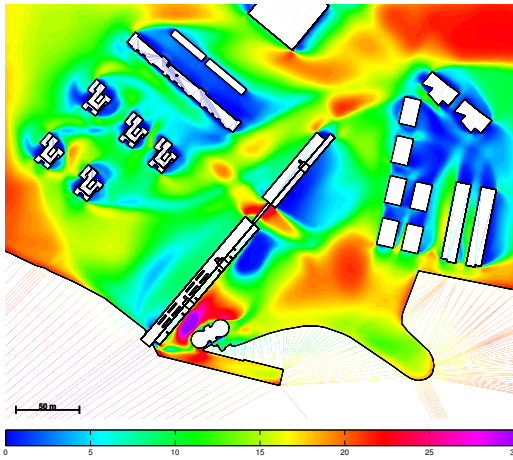


Figure 10.6 Probability of exceedance of the comfort criterion with 8 equal sized directions.

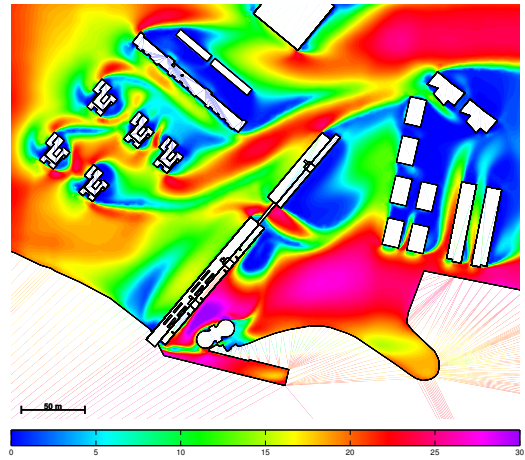


Figure 10.7 Probability of exceedance of the comfort criterion with 4 equal sized directions.

Danger

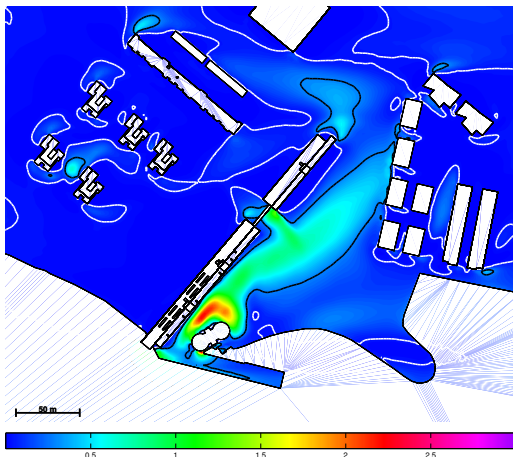


Figure 10.8 Probability of exceedance of the danger criterion with 36 directions of equal probability of occurrence.

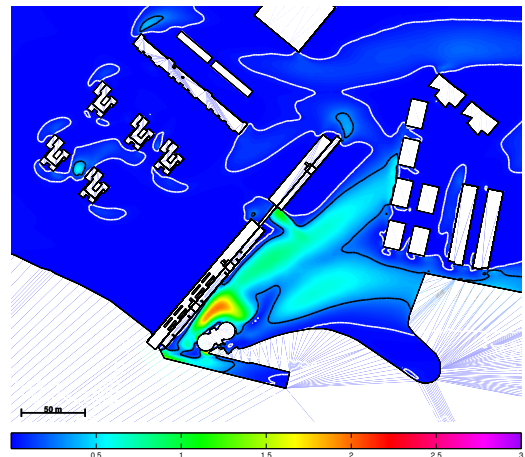


Figure 10.9 Probability of exceedance of the danger criterion with 12 directions of equal probability of occurrence.

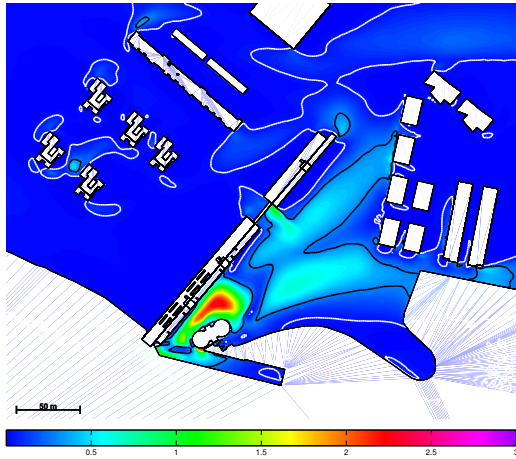


Figure 10.10 Probability of exceedance of the danger criterion with 16 equal sized directions.

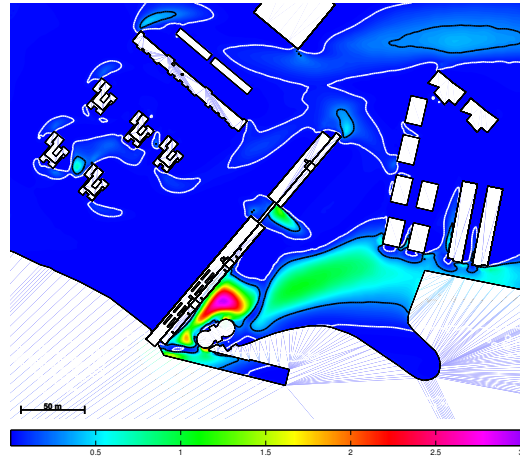


Figure 10.11 Probability of exceedance of the danger criterion with 12 equal sized directions.

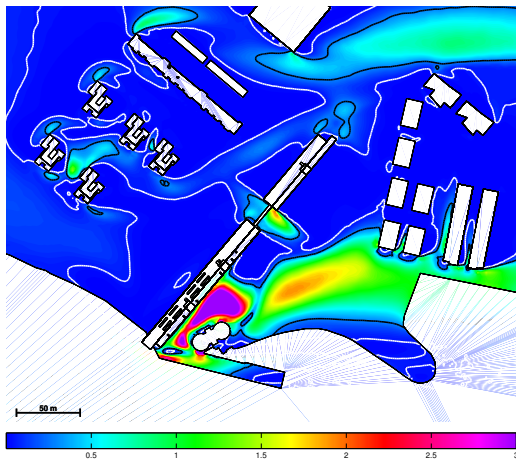


Figure 10.12 Probability of exceedance of the danger criterion with 8 equal sized directions.

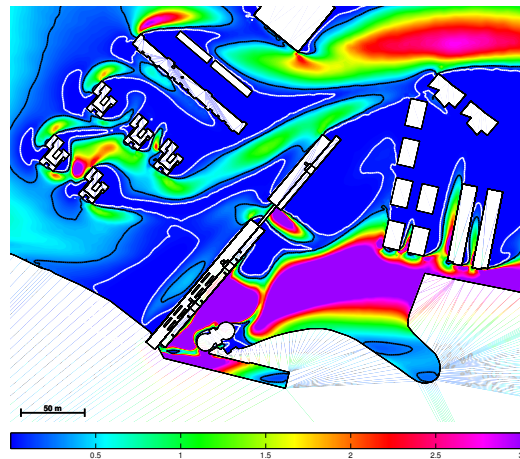


Figure 10.13 Probability of exceedance of the danger criterion with 4 equal sized directions.

10.2 Computed realisations for Viborgvej/Bredskiftevej

For the case at Viborgvej/Bredskiftevej 16, 12, 8, and 4 sectors of the same size is computed. Furthermore results of a computation which only covers the western sector is presented. The results are showed in Figure 10.15 to 10.24. In Figure 10.14 the resolved statistic for each directional resolution is given.

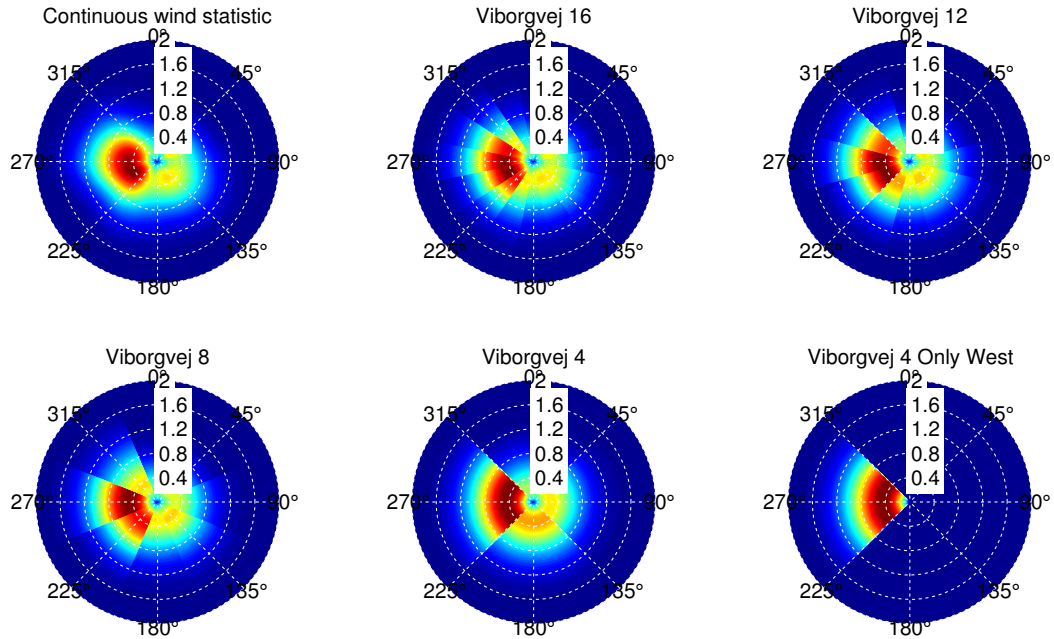


Figure 10.14 Resolved statistics for the case at Viborgvej/Bredskiftevej. For each sectoral realisation a Weibull distribution is fitted to the part of the continuous statistic which the sector covers.

Comfort

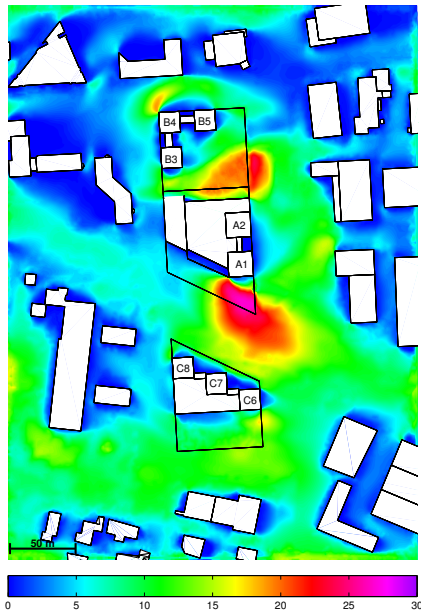


Figure 10.15 Plot of the comfort summarised for 16 directions.

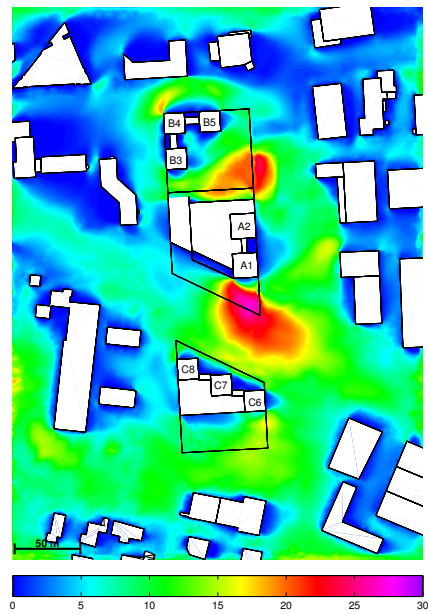


Figure 10.16 Plot of the comfort summarised for 12 directions.

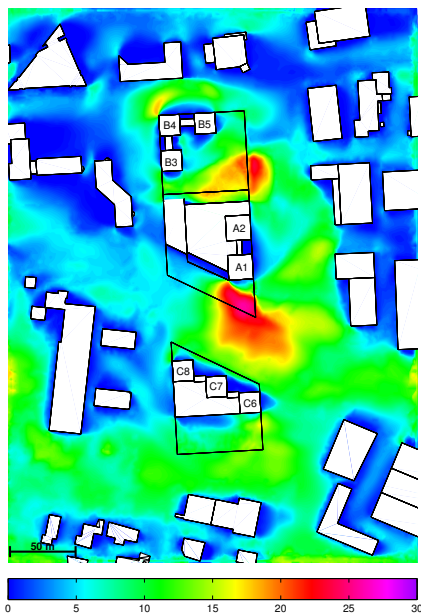


Figure 10.17 Plot of the comfort summarised for 8 directions.

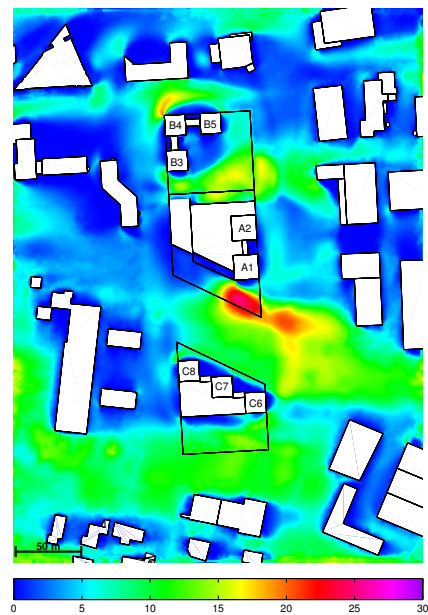


Figure 10.18 Plot of the comfort summarised for 4 directions.

Danger

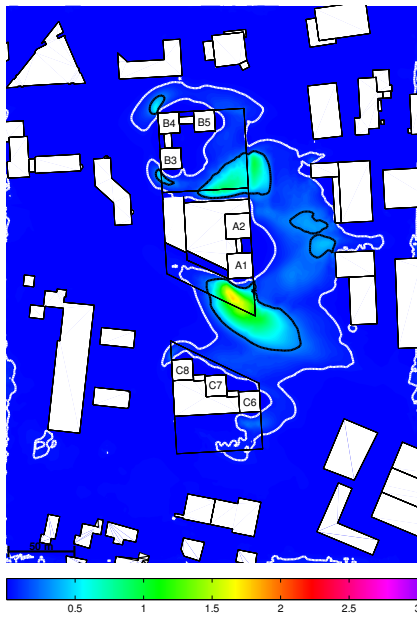


Figure 10.19 Plot of the danger summarised for 16 directions.

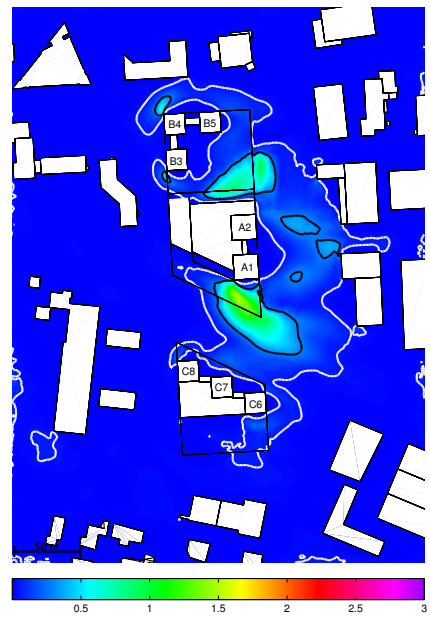


Figure 10.20 Plot of the danger summarised for 12 directions.

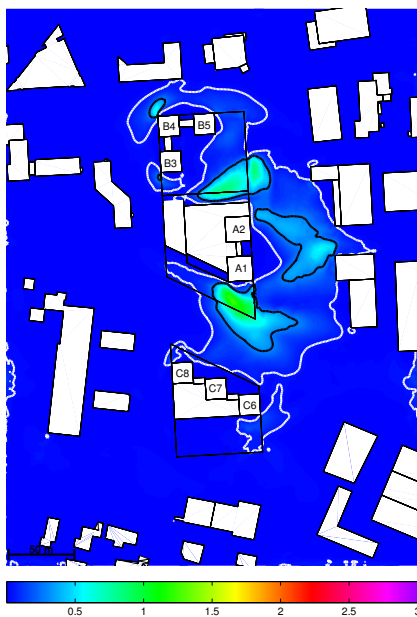


Figure 10.21 Plot of the danger summarised for 8 directions.

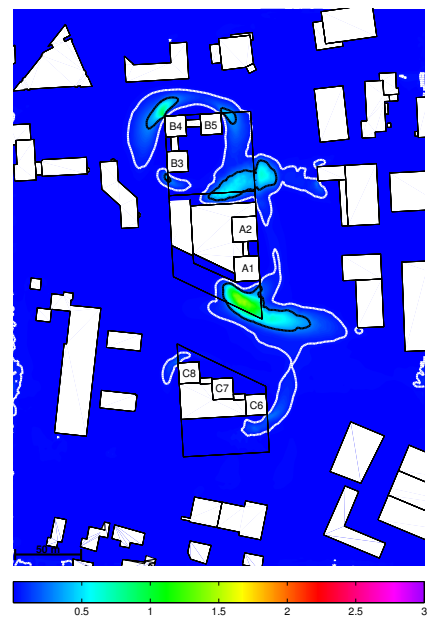


Figure 10.22 Plot of the danger summarised for 4 directions.

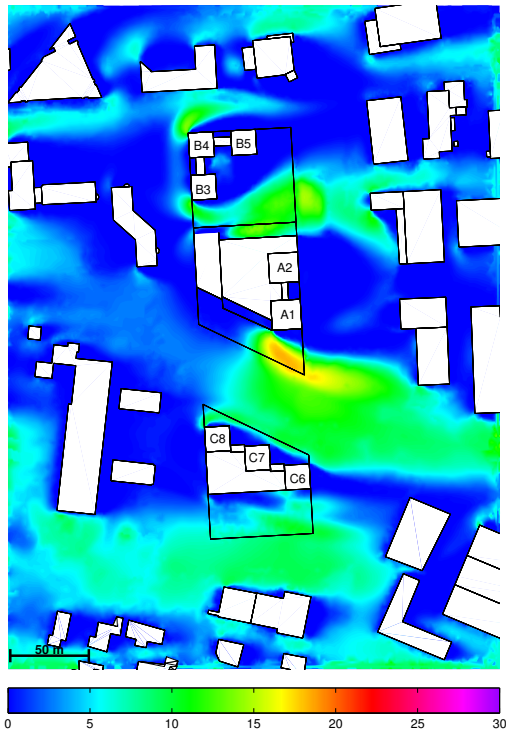
West only

Figure 10.23 Plot of the comfort given for a calculation with only wind from west.

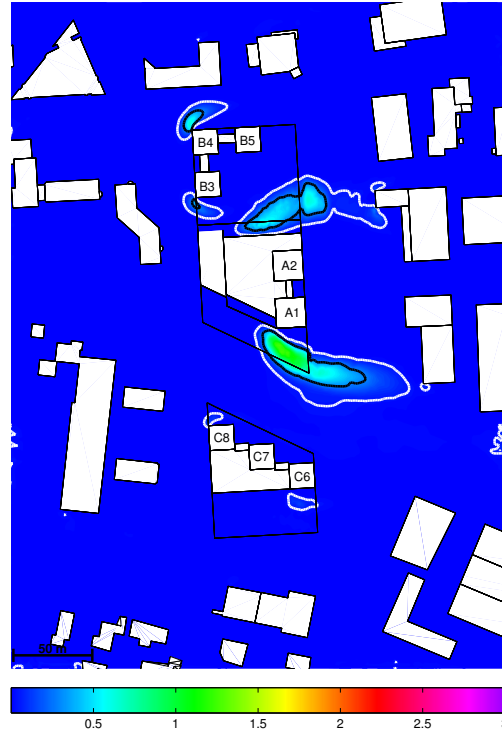


Figure 10.24 Plot of the danger given for a calculation with only wind from west.

10.3 Analysis of Directional Discretisation

A number of things stand out from the results. As seen in Figure 10.1 and 10.14 the approach where the sectors is covering the same probability resolves the continuous wind statistics better than the approach with sectors of equal size.

In the results from Høje Brygge it is clear that there is large difference in the results on the danger criterion depending on the directional resolution, even between the three best resolutions. These differences are not so pronounced in the evaluations of Viborgvej/Bredskiftevej.

On the comfort criterion the evaluations with lower directional discretisation seems to resolve the exceedance probability better than the evaluations on the danger criterion. Again the evaluations seem to be better at Viborgvej/Bredskiftevej than at Høje Brygge with lower directional resolutions.

10.3.1 Influence Roses for the Directional Discretisation

The difference in evaluating the comfort and the danger criterion can be attributed to the number of realisations, contributing to the exceedance probability, is different in the evaluation of the criteria. A higher threshold value results in a lower exceedance

probability, and for some of the directions the threshold for the danger criterion is so high that they do not contribute to the overall exceedance probability with the same order of magnitude as the worst direction.

The issue can be illustrated by an influence rose. In [Figure 10.25](#) an area of interest is specified. Integration of the exceedance probability in this area for each resolved direction gives each realisations contributing to the overall exceedance probability.

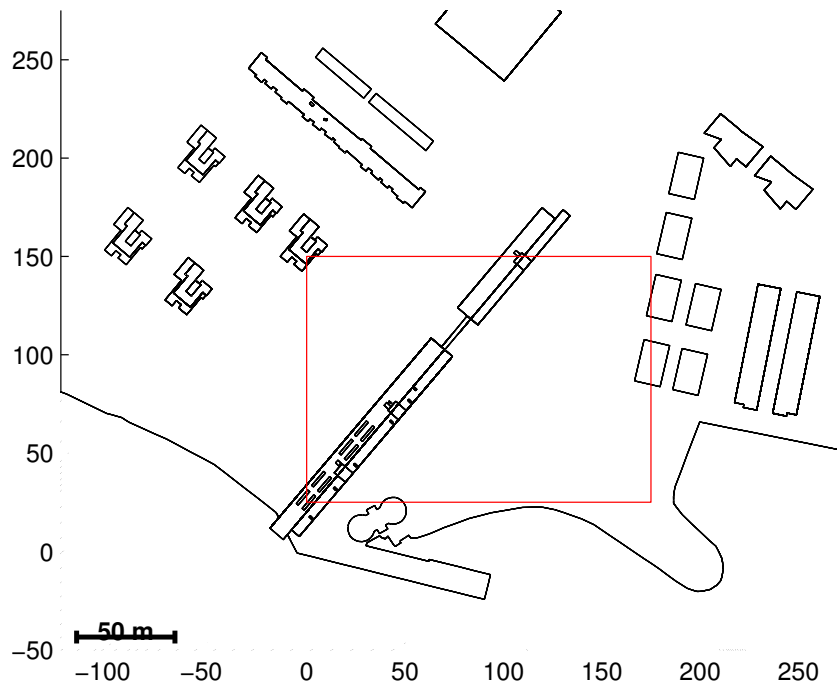


Figure 10.25 Specification of area of interest for influence rose for Høje Brygge.

In [Figure 10.26](#) and [10.27](#) the relative contribution from each realisation is given. For each directional resolution the exceedance probability is normalised with respect to the highest value.

It appears that a higher directional discretisation is required in evaluation of the danger criterion, especially from the predominant wind direction, or at least in the direction contributing most to the exceedance probability.

The approach with sectors covering the same probability was constructed to address this issue, but as seen in [Figure 10.27](#) a significant amount of computational power is wasted on directions which do not contribute, even when this approach is selected.

This also underlines the call for a higher directional resolution of the input wind statistics than those provided by [Troen \(1989\)](#).

10.3.2 New Approach to the Directional Discretisation

Based on these results, which shows that great care has to be taken in the directional evaluation of the danger criterion, some new considerations on the directional resolution can be stated.

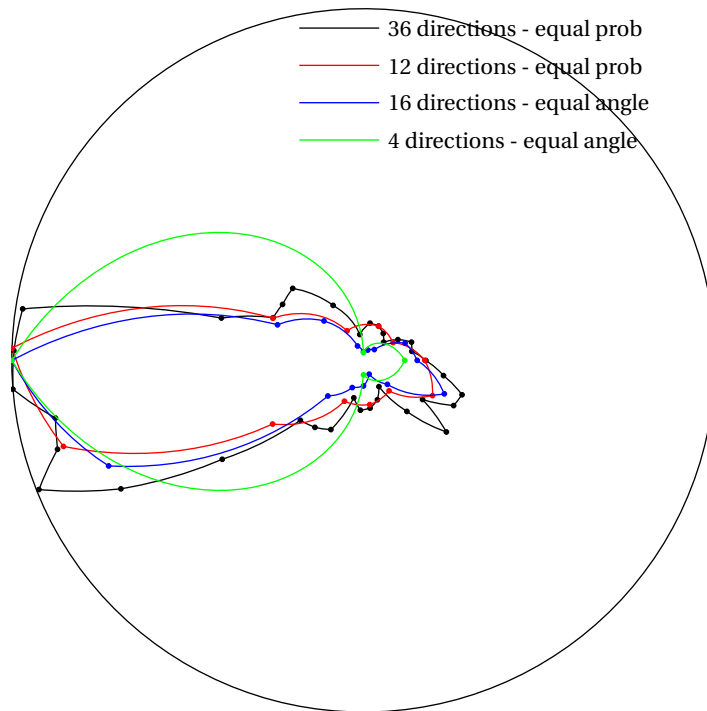


Figure 10.26 Comfort rose for Høje Brygge.

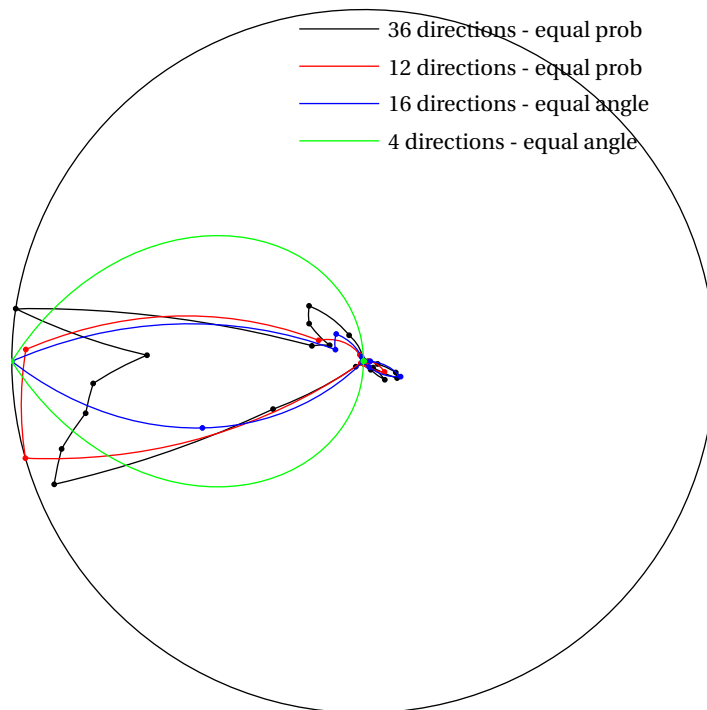


Figure 10.27 Danger rose for Høje Brygge.

The selection of directions should not only rely on which directions that are more probable than others, but also on whether these directions are probable to add to the exceedance probability. By the log-law the statistics for the friction velocity can be transformed to 1.7 m above the origin of the log-profile. The threshold of the danger criterion can be applied directly on the statistics of the 1.7 m wind, and an initial influence rose can be obtained for this 1.7 m wind.

A minimum directional resolution would still be proper, e.g. 60°, so therefore the following approach for selecting the directional resolution is suggested.

1. Select the minimum directional resolution.
2. Apply the influence rose for the 1.7 m wind and increase the directional resolution where exceedance is probable.
3. Apply the influence rose for an area of interest after the initial evaluations and compute further resolutions where the influence is very high.

It might also be proper to consider to make borders between sectors with significant changes in roughness, e.g. sea-land or city-farmland.

10.4 Conclusion on Directional Discretisation

A number of realisations of the wind statistics are computed where the directional resolution is selected by two different approaches. The following conclusions at least hold for the cases at Høje Brygge and Viborgvej/Bredskiftevej:

- The danger criterion is highly sensitive to the directional resolution.
- For the comfort criterion a directional discretisation of 12 seems adequate.
- Cases with large directional roughness changes requires a higher directional resolution.
- The concept of influence roses is introduced.
- A new approach for selecting the directional resolution is proposed.

The problem statement for the present thesis is:

To analyse and investigate the overall procedure for evaluation of wind conditions by CFD, in order to set up an operational procedure for evaluation of wind conditions at routine basis.

The work presented shows that analysing wind conditions is indeed possible by CFD, and the flow fields computed by the setup proposed are reliable for evaluating wind conditions. The procedure proposed makes it possible to evaluate wind conditions at routine basis.

In Denmark there is no code of practice for evaluating wind conditions but there is an SBI-direction. Evaluation criteria based on a survey of the literature is selected, and it is demonstrated that the criteria are better for evaluation of wind conditions than those provided in the SBI-direction. The SBI-direction yields very unacceptable results for the danger criterion, allowing too severe wind conditions.

It is demonstrated that by careful discretisation of the pedestrian level, applying the correct roughness of the ground surface, and applying the work of Yang et al. (2009) for describing the inlet conditions, the flow field can be very well modelled.

A number of different two-equation turbulence models have been applied to a test case with a $4 \times 4 \times 1$ cube where experimental data are available. The $k-\omega$ SST model by Menter (1994) with the parameters suggested by Yang et al. (2008) outperforms the other models tested.

A statistical treatment of the part of the flow which is not modelled explicitly by CFD is set up, based on the work of Wieringa (1986) and Verkaik et al. (2005), in order to transform the wind statistics at the meteorological station to the inlet of the domain.

Field measurements have been conducted at the location of Høje Brygge, Nørresundby. The results demonstrate that the CFD model computes the flow field and the turbulence satisfactory. An indication of a connection between the magnitude of the turbulent kinetic energy and the anisotropy of the turbulence is presented.

The procedure presented is applied to two different cases, in order to demonstrate the capability of the procedure and investigate remedial measures to counter undesirable flow phenomena.

The procedure is applied to the case at Høje Brygge, Nørresundby, which is known as an area with severe wind climate. The evaluation criteria selected shows that the wind conditions are severe, which is interpreted as a proof of concept for the danger levels.

The most pronounced flow phenomenon is attributed to a high-rise building behind a low-rise building. It is demonstrated that a combination of a pent roof and windbreaks at ground level reduces the areas with very severe wind conditions.

In the case at Viborgvej/Bredskiftevej, the main flow feature is a corner stream around two high interconnected buildings. It is demonstrated that a part of the problem can be removed by opening the passageway between the two buildings.

The case studies were conducted by applying a directional resolution of 12 sectors of equal size. The cases have been recomputed by a number of different directional resolution schemes. It is demonstrated that evaluation of wind comfort is evaluated adequately by 12 sectors of equal size, but the danger criterion is highly sensitive to the directional resolution. A new method is proposed for selecting the directional resolution as a part of an iterative process.

10.5 Further Studies

A number of perspectives have arisen as a part of the project, which requires further study. In general the computational method seems to be adequate but a number of the aspects leading to the input to the model, the statistical treatment, and the evaluation criteria could be refined even further.

The levels of acceptable exceedance probability are in the end a political decision, but in order to give politicians background information to set such limits, it would be desirable to model a larger part of an urban area, for instance the full area covered by the 3D model of Aalborg. Such a model is highly computational comprehensive, especially in the mesh generation, but it seems in reach with the computational power applied in the present study.

The statistical treatment could be refined further. First of all it would be desirable to extract the roughness fields directly from land use maps. More physics could be applied in the transformation procedure, for instance stability correction, or some of the models applied in siting of wind turbines (a review is given by Petersen et al. 1998). The next step could be to introduce a nested CFD model in a meteorological model covering a larger land area.

In the present project the CFD calculations is validated by field measurements, but it would be proper to conduct long term measurements in an urban area, in order to evaluate the statistics and not only the flow.

Studies on remedial measures, parameter studies, and optimisation are still open research issues, and will probably be so for a significant time to come.

- Aalborg Kommune (2009). *3D bymodel*. In Danish. URL: http://www.aalborgkommune.dk/OM_KOMMUNEN/KORT-OVER-KOMMUNEN/HOEJDEINFO/Sider/3DBymodel.aspx (visited on 20th Nov. 2009).
- Bjerregaard, E. and F. Nielsen (1981). *SBI-Anvisning 128: Vindmiljø omkring bygninger*. In Danish. Hørsholm: Statens Byggeforskningsinstitut.
- Blackadar, A. and H. Tennekes (1968). „Asymptotic similarity in neutral barotropic planetary boundary layers“. In: *Journal of the Atmospheric Sciences* 25.6, pp. 1015–1020.
- Blocken, B. and J. Carmeliet (2004). „Pedestrian wind environment around buildings: Literature review and practical examples“. In: *Journal of Building Physics* 28.2, p. 107.
- Blocken, B., J. Carmeliet and T. Stathopoulos (2007). „CFD evaluation of wind speed conditions in passages between parallel buildings—Effect of wall-function roughness modifications for the atmospheric boundary layer flow“. In: *Journal of Wind Engineering and Industrial Aerodynamics* 95.9-11, pp. 941–962.
- Blocken, B. and J. Persoon (2009). „Pedestrian wind comfort around a large football stadium in an urban environment: CFD simulation, validation and application of the new Dutch wind nuisance standard“. In: *Journal of Wind Engineering and Industrial Aerodynamics* 97.5-6, pp. 255–270.
- Blocken, B., T. Stathopoulos and J. Carmeliet (2007). „CFD simulation of the atmospheric boundary layer: wall function problems“. In: *Atmospheric Environment* 41.2, pp. 238–252.
- Bottema, M. (1992). „Wind climate and urban geometry“. PhD Thesis. Technische Universiteit Eindhoven.
- (2000). „A method for optimisation of wind discomfort criteria“. In: *Building and Environment* 35.1, pp. 1–18.
- Bottema, M., J. Leene and J. Wisse (1992). „Towards forecasting of wind comfort“. In: *Journal of Wind Engineering and Industrial Aerodynamics* 44.1-3. Special Issue 8th International Conference on Wind Engineering 1991, pp. 2365–2376.
- Catalano, P., M. Wang, G. Iaccarino and P. Moin (2003). „Numerical simulation of the flow around a circular cylinder at high Reynolds numbers“. In: *International Journal of Heat and Fluid Flow* 24.4. Selected Papers from the Fifth International Conference on Engineering Turbulence Modelling and Measurements, pp. 463–469.
- Csanady, G. (1967). „On the “resistance law” of a turbulent Ekman layer“. In: *Journal of the Atmospheric Sciences* 24, pp. 467–471.
- Davenport, A. (1976). *An approach to human comfort criteria for environmental wind conditions*. Stockholm: Swedish National Building Award Institute.
- Deardorff, J. W. (1972). „Parameterization of the Planetary Boundary layer for Use in General Circulation Models“. In: *Monthly Weather Review* 100, p. 93.
- Foken, T. (2006). „50 Years of the Monin–Obukhov Similarity Theory“. In: *Boundary-Layer Meteorology* 119.3, pp. 431–447.

- Franke, J., C. Hirsch, A. Jensen, H. Krüs, M. Schatzmann, P. Westbury, S. Miles, J. Wisse and N. Wright (2004). „Recommendations on the use of CFD in wind engineering“. In: *Proceedings of the International Conference on Urban Wind Engineering and Building Aerodynamics* 14, pp. 5–7.
- Franke, J., A. Hellsten, H. Schlünzen and B. Carissimo (2007). *Best practice guideline for the CFD simulation of flows in the urban environment*. Brussels: COST Office.
- Garratt, J. R. (1992). *The atmospheric boundary layer*. Cambridge University Press.
- Hargreaves, D. and N. Wright (2007). „On the use of the k - ϵ model in commercial CFD software to model the neutral atmospheric boundary layer“. In: *Journal of Wind Engineering and Industrial Aerodynamics* 95.5, pp. 355–369.
- Hess, G. and J. Garratt (2002). „Evaluating models of the neutral, barotropic planetary boundary layer using integral measures: Part I. Overview“. In: *Boundary-layer meteorology* 104.3, pp. 333–358.
- Hunt, J., E. Poulton and J. Mumford (1976). „The effects of wind on people: new criteria based on wind tunnel experiments“. In: *Building and Environment* 11.1, pp. 15–28.
- Jackson, P. (1978). „The evaluation of windy environments“. In: *Building and Environment* 13.4, pp. 251–260.
- Jensen, M. (1959). *Aerodynamik i den naturlige vind*. In Danish. København: Teknisk forlag.
- Johansson, C., A.-S. Smedman, U. Högström, J. Brasseur and S. Khanna (2001). „Critical test of the validity of Monin-Obukhov similarity during convective conditions“. In: *Journal of the Atmospheric Sciences* 58.12, pp. 1549–1566.
- Khanna, S. and J. Brasseur (1998). „Three-dimensional buoyancy- and shear-induced local structure of the atmospheric boundary layer“. In: *Journal of the Atmospheric Sciences* 55.5, pp. 710–743.
- Koss, H. (2006). „On differences and similarities of applied wind comfort criteria“. In: *Journal of Wind Engineering and Industrial Aerodynamics* 94.11, pp. 781–797.
- Kundu, P. K. and I. M. Cohen (2002). *Fluid Mechanics*. 2nd ed. London: Elsevier Academic Press.
- Launder, B. and D. Spalding (1974). „The Numerical Computation of Turbulent Flows“. In: *Computer Methods in Applied Mechanics and Engineering* 24.3, pp. 269–289.
- Maryland Weather (2010). URL: <http://weblogs.marylandweather.com/Wind.jpg> (visited on 21st May 2010).
- McNaughton, K. (2009). „The rise and fall of Monin-Obukhov theory“. In: *Newsletter* 30, pp. 1–5.
- Menter, F. (1994). „Two-equation eddy-viscosity turbulence models for engineering applications“. In: *AIAA journal* 32.8, pp. 1598–1605.
- Mochida, A., Y. Tominaga, S. Murakami, R. Yoshie, T. Ishihara and R. Ooka (2002). „Comparison of various k - ϵ models and DSM applied to flow around a high-rise building - report on AIJ cooperative project for CFD prediction of wind environment“. In: *Wind and structures* 5.24, pp. 227–244.
- Monin, A. and A. Obukhov (1954). „Basic laws of turbulent mixing in the ground layer of the atmosphere“. English trans. from Russian. Trans. by J. Miller. In: *Akad. Nauk SSSR Geofiz. Inst. Tr* 151, pp. 163–187.

-
- Petersen, E., N. Mortensen, L. Landberg, J. Højstrup and H. Frank (1998). „Wind power meteorology. Part I: climate and turbulence“. In: *Wind Energy* 1, pp. 2–22.
- Ratcliff, M. and J. Peterka (1990). „Comparison of pedestrian wind acceptability criteria“. In: *Journal of Wind Engineering and Industrial Aerodynamics* 36, pp. 791–800.
- Richards, P. and R. Hoxey (1993). „Appropriate boundary conditions for computational wind engineering models using the $k-\epsilon$ turbulence model.“ In: *Journal of Wind Engineering and Industrial Aerodynamics* 46, pp. 145–153.
- Rodi, W. (1991). „Experience with two-layer models combining the $k-\epsilon$ model with a one-equation model near the wall“. In: *AIAA, Aerospace Sciences Meeting*.
- Rossby, C. (1932). „A generalization of the theory of the mixing length with applications to atmospheric and oceanic turbulence“. In: *Meteorological papers* 1.4.
- Rossby, C. and R. Montgomery (1935). „The layer of frictional influence in wind and ocean currents“. In: *Papers in Physical Oceanography and Meteorology* 4.3.
- Sanz-Andres, A. and A. Cuerva (2006). „Pedestrian wind comfort: Feasibility study of criteria homogenisation“. In: *Journal of Wind Engineering & Industrial Aerodynamics* 94.11, pp. 799–813.
- Schmid, H. (1994). „Source areas for scalars and scalar fluxes“. In: *Boundary-Layer Meteorology* 67.3, pp. 293–318.
- Shih, T.-H., W. W. Liou, A. Shabbir, Z. Yang and J. Zhu (1995). „A new $k-\epsilon$ eddy viscosity model for high reynolds number turbulent flows“. In: *Computers & Fluids* 24.3, pp. 227–238.
- Shirasawa, T., A. Mochida, Y. Tominaga, R. Yoshie, H. Kataoka, T. Nozu and H. Yoshino (2003). „Development of CFD method for predicting wind environment around a high-rise building, Part2: The cross comparison of CFD results on the flow field around a 4:4:1 prism“. In Japanese. In: *AIJ Journal of Technology and Design* 18, pp. 441–446.
- Simiu, E. and R. Scanlan (1978). *Wind effects on structures: an introduction to wind engineering*. New York: Wiley Interscience.
- Spalart, P. R. (2009). „Detached-Eddy Simulation“. In: *Annual Review of Fluid Mechanics* 41.1, pp. 181–202.
- Stathopoulos, T. (2006). „Pedestrian level winds and outdoor human comfort“. In: *Journal of Wind Engineering and Industrial Aerodynamics* 94.11, pp. 769–780.
- Tominaga, Y., A. Mochida, R. Yoshie, H. Kataoka, T. Nozu, M. Yoshikawa and T. Shirasawa (2008). „AIJ guidelines for practical applications of CFD to pedestrian wind environment around buildings“. In: *Journal of Wind Engineering and Industrial Aerodynamics* 96.10-11, pp. 1749–1761.
- Tominaga, Y., A. Mochida, T. Shirasawa, R. Yoshie, H. Kataoka, K. Harimoto and T. Nozu (2004). „Cross Comparisons of CFD Results of Wind Environment at Pedestrian Level around a High-rise Building and within a Building Complex(Environmental Engineering)“. In: *Journal of Asian architecture and building engineering* 3.1, pp. 63–70.
- Troen, I. (1989). *European wind atlas*. Risø National Laboratory.
- Verkaik, J. W., A. J. M. Jacobs, A. B. C. Tijn and J. R. A. Onvlee (2005). „Local Wind Speed Estimation by Physical Downscaling of Weather model forecasts“.
-

- Von Karman, T. (1931). „Mechanical similitude and turbulence“. In: *NACA Technical Memorandums* 611.
- Wieringa, J. (1986). „Roughness-dependent geographical interpolation of surface wind speed averages“. In: *Quarterly Journal of the Royal Meteorological Society* 112.473, pp. 867–889.
- (1992). „Updating the Davenport roughness classification“. In: *Journal of Wind Engineering and Industrial Aerodynamics* 41.1-3, pp. 357–368.
- Willemsen, E. and J. Wisse (2007). „Design for wind comfort in The Netherlands: Procedures, criteria and open research issues“. In: *Journal of Wind Engineering and Industrial Aerodynamics* 95.9-11, pp. 1541–1550.
- Yang, W., Y. Quan, X. Jin, Y. Tamura and M. Gu (2008). „Influences of equilibrium atmosphere boundary layer and turbulence parameter on wind loads of low-rise buildings“. In: *Journal of Wind Engineering and Industrial Aerodynamics* 96.10-11. 4th International Symposium on Computational Wind Engineering, pp. 2080–2092.
- Yang, Y., M. Gu, S. Chen and X. Jin (2009). „New inflow boundary conditions for modeling the neutral equilibrium atmospheric boundary layer in computational wind engineering“. In: *Journal of Wind Engineering & Industrial Aerodynamics* 97.2, pp. 88–95.
- Yoshie, R., A. Mochida, Y. Tominaga, H. Kataoka and M. Yoshikawa (2005). „Cross Comparisons of CFD Prediction for Wind Environment at Pedestrian Level around Buildings: Part 1, Comparison of Results for Flow-field around a High-rise Building Located in Surrounding City Blocks“. In: *Proceedings of The Sixth Asia-Pacific Conference on Wind Engineering*, pp. 2648–2660.

List of Figures

| | | |
|------|---|----|
| 1.1 | Woman exposed to wind. | 3 |
| 1.2 | Bike pushed over by the wind | 3 |
| 1.3 | Wind conditions affected by high-rise building in Nørresundby. | 4 |
| 1.4 | Outline of project. | 6 |
| 3.1 | General definition of boundaries. | 15 |
| 3.2 | Profiles for with parameters by Launder and Spalding (1974) | 19 |
| 3.3 | Profiles for with parameters from Yang et al. (2009) | 19 |
| 3.4 | Relative change in velocity between inlet and outlet. | 19 |
| 4.1 | Computational Domain for $4 \times 4 \times 1$ cube. | 23 |
| 4.2 | Measuring points, horizontal section. | 23 |
| 4.3 | Measuring points, vertical section. | 23 |
| 4.4 | Contour plot of measured U, horizontal section. | 23 |
| 4.5 | Contour plot of measured U, vertical section. | 23 |
| 4.6 | Mesh applied for analysis of turbulence models. | 24 |
| 4.7 | Comparison of wind speed computed on fine and standard grid. | 24 |
| 4.8 | Inlet velocity profile for analysis on $4 \times 4 \times 1$ cube. | 25 |
| 4.9 | Inlet turbulence profiles for analysis on the $4 \times 4 \times 1$ cube. | 26 |
| 4.10 | Plot of turbulence intensity exceedance for hotwire anemometers. | 27 |
| 4.11 | Contour plot of U with k - ω model, vertical section. | 27 |
| 4.12 | Regression plot of U with k - ω model, vertical section. | 28 |
| 5.1 | Two-layer model of the atmospheric boundary layer | 32 |
| 5.2 | Procedure for transformation of wind from one location to another. | 35 |
| 5.3 | Sketch of roughness footprint length scales after Verkaik et al. (2005) | 36 |
| 5.4 | Effective local roughness applied for the case at Høje Brygge, Nørresundby. | 37 |
| 5.5 | Verification of upward and downward transformation. | 38 |
| 5.6 | Comparison of A obtained by transformation and by Troen (1989) | 38 |
| 5.7 | Comparison of P_θ obtained by transformation and by Troen (1989) | 38 |
| 5.8 | Regression plot of normalised velocities. | 40 |
| 5.9 | Regression plot of normalised k | 40 |
| 5.10 | Regression plot of normalised velocities for the cylinder. | 40 |
| 5.11 | Regression plot of normalised k for the cylinder. | 40 |
| 6.1 | View of the surrounding area of Høje Brygge, Nørresundby | 43 |
| 6.2 | Illustration of ultrasonic anemometers. | 44 |
| 6.3 | Relation between measured Voltage signal and wind speed. | 44 |
| 6.4 | Reference anemometer in lift. | 45 |
| 6.5 | Anemometers at 1.7 m height. | 45 |
| 6.6 | Agreement of simultaneous measurements of the mean velocity. | 46 |
| 6.7 | Map of Høje Brygge. | 47 |
| 6.8 | Wind pattern at 11 m with wind from NE. | 48 |
| 6.9 | Wind pattern at 11 m with wind from west. | 48 |
| 6.10 | Wind speed and direction for the reference anemometer. | 49 |

| | | |
|------|--|----|
| 6.11 | Vector plot of normalised wind speeds, wind from NE. | 49 |
| 6.12 | Contour plot of velocities. | 50 |
| 6.13 | Vector plot of normalised wind speeds, wind from west. | 51 |
| 6.14 | Regression plot of the measured and calculated standard deviation. | 52 |
| 6.15 | Relation between the calculated k and measured σ | 53 |
| 6.16 | Calculated values of σ_u with measured anisotropy. | 54 |
| 6.17 | Regression plot of the calculated k and the measured anisotropy. | 54 |
| 7.1 | Overview of procedure for evaluating wind conditions by CFD. | 57 |
| 8.1 | Picture from Høje Brygge. | 67 |
| 8.2 | View from apartment in Høje Brygge. | 67 |
| 8.3 | Violent wind conditions experienced at Høje Brygge. | 68 |
| 8.4 | Ortho photo of the silos at Høje Brygge and the surrounding area. | 69 |
| 8.5 | Bird's eye view of the area of interest. | 69 |
| 8.6 | Illustration of the transformation procedure for Høje Brygge | 70 |
| 8.7 | Local roughness at Høje Brygge. | 71 |
| 8.8 | Regional roughness at Høje Brygge. | 71 |
| 8.9 | Imported surface coloured by group. | 71 |
| 8.10 | Feature curves at sharp edges in the computational domain. | 72 |
| 8.11 | Generated volume mesh for the model of Høje Brygge. | 72 |
| 8.12 | Close-up of the mesh around the area of interest. | 73 |
| 8.13 | Venturi effect and flow around the towers at Høje Brygge. | 74 |
| 8.14 | Relative pressure in a vertical section. | 75 |
| 8.15 | Streamlines coming from above the roof of the Siemens building. | 75 |
| 8.16 | Illustration of corner streams with wind from west. | 77 |
| 8.17 | Illustration of corner stream above the quay. | 77 |
| 8.18 | Contour plot showing the comfort in the area. | 78 |
| 8.19 | Contour plot showing the danger in the area. | 79 |
| 8.20 | Contour plot showing the probability that the mean wind exceeds 5 m/s. | 79 |
| 8.21 | Sketch of different quay designs. | 80 |
| 8.22 | Comparison of the three quay models. | 81 |
| 8.23 | Comparison of the three quay models. | 81 |
| 8.24 | Pent roof attached to each tower. | 82 |
| 8.25 | Vector plot of the velocity on a vertical section without the pent roof. | 82 |
| 8.26 | Vector plot of the velocity on a vertical section with the pent roof. | 82 |
| 8.27 | Vector plot of the velocity on a horizontal section without the pent roof. | 82 |
| 8.28 | Vector plot of the velocity on a horizontal section with the pent roof. | 82 |
| 8.29 | Contour plot of the turbulent kinetic energy without the pent roof. | 83 |
| 8.30 | Contour plot of the turbulent kinetic energy with the pent roof. | 83 |
| 8.31 | Positions of the windbreaks at Høje Brygge. | 84 |
| 8.32 | Mean wind speeds before the establishment of windbreaks. | 85 |
| 8.33 | Mean wind speeds after the establishment of windbreaks. | 85 |
| 8.34 | Streamlines through passage between windbreak and building. | 85 |
| 8.35 | Equivalent velocity for comfort criterion with windbreaks. | 86 |
| 8.36 | Equivalent velocity for comfort criterion with windbreaks and pent roof. | 86 |
| 8.37 | Equivalent velocity for danger criterion with windbreaks. | 86 |
| 8.38 | Equivalent velocity for danger criterion with windbreaks and pent roof. | 86 |

| | | |
|-------|--|-----|
| 8.39 | Contour plot showing the comfort in the area. | 86 |
| 8.40 | Contour plot showing the danger in the area. | 86 |
| 9.1 | Development plan for Viborgvej. | 89 |
| 9.2 | Illustration of the view from west on Viborgvej. | 90 |
| 9.3 | Illustration of the view from east on Viborgvej. | 90 |
| 9.4 | Illustration of procedure for transformation of wind. | 91 |
| 9.5 | Local roughness at Viborgvej. | 92 |
| 9.6 | Regional roughness at Viborgvej. | 92 |
| 9.7 | Geometry used for Viborgvej divided by different parts. | 92 |
| 9.8 | Mesh used in the calculations for Viborgvej. | 93 |
| 9.9 | Close-up of the mesh used in the calculations for Viborgvej. | 93 |
| 9.10 | Regression plots of mean velocity in three models with different mesh size . | 94 |
| 9.11 | Streamlines showing corner streams. | 95 |
| 9.12 | Plot of comfort without high-rise Buildings. | 95 |
| 9.13 | Plot of comfort, high-rise buildings included. | 95 |
| 9.14 | Plot of danger without high-rise Buildings. | 96 |
| 9.15 | Plot of danger, high-rise buildings included. | 96 |
| 9.16 | Plot of the probability that the mean wind exceeds 5 m/s. | 97 |
| 9.17 | Exceedance probability of the comfort criterion, original roughness. | 98 |
| 9.18 | Exceedance probability of the comfort criterion with the double roughness. . | 98 |
| 9.19 | Exceedance probability of the danger criterion, original roughness. | 99 |
| 9.20 | Exceedance probability of the danger criterion with the double roughness. . | 99 |
| 9.21 | Plot of comfort with opening. | 100 |
| 9.22 | Plot of danger with opening. | 100 |
| 10.1 | Resolved statistics for the case at Høje Brygge. | 101 |
| 10.2 | Probability of exceedance for comfort with 36 directions of equal probability. | 102 |
| 10.3 | Probability of exceedance for comfort with 12 directions of equal probability. | 102 |
| 10.4 | Probability of exceedance for comfort with 16 equal sized directions. | 102 |
| 10.5 | Probability of exceedance for comfort with 12 equal sized directions. | 102 |
| 10.6 | Probability of exceedance for comfort with 8 equal sized directions. | 103 |
| 10.7 | Probability of exceedance for comfort with 4 equal sized directions. | 103 |
| 10.8 | Probability of exceedance for danger with 36 directions of equal probability. | 103 |
| 10.9 | Probability of exceedance for danger with 12 directions of equal probability. | 103 |
| 10.10 | Probability of exceedance for danger with 16 equal sized directions. | 104 |
| 10.11 | Probability of exceedance for danger with 12 equal sized directions. | 104 |
| 10.12 | Probability of exceedance for danger with 8 equal sized directions. | 104 |
| 10.13 | Probability of exceedance for danger with 4 equal sized directions. | 104 |
| 10.14 | Resolved statistics for the case at Viborgvej/Bredskiftevej. | 105 |
| 10.15 | Plot of the comfort summarised for 16 directions. | 106 |
| 10.16 | Plot of the comfort summarised for 12 directions. | 106 |
| 10.17 | Plot of the comfort summarised for 8 directions. | 106 |
| 10.18 | Plot of the comfort summarised for 4 directions. | 106 |
| 10.19 | Plot of the danger summarised for 16 directions. | 107 |
| 10.20 | Plot of the danger summarised for 12 directions. | 107 |
| 10.21 | Plot of the danger summarised for 8 directions. | 107 |
| 10.22 | Plot of the danger summarised for 4 directions. | 107 |

List of Figures

| | | |
|-------|--|-----|
| 10.23 | Comfort plot with wind from west only. | 108 |
| 10.24 | Danger plot with wind from west only. | 108 |
| 10.25 | Specification of area of interest for influence rose for Høje Brygge. | 109 |
| 10.26 | Comfort rose for Høje Brygge. | 110 |
| 10.27 | Danger rose for Høje Brygge. | 110 |
| | | |
| B.1 | Exceedance probability of the comfort criterion with $d = 3z_0$ | 129 |
| B.2 | Exceedance probability of the comfort criterion with $d = 6z_0$ | 129 |
| B.3 | Exceedance probability of the danger criterion with $d = 3z_0$ | 130 |
| B.4 | Exceedance probability of the danger criterion with $d = 6z_0$ | 130 |
| | | |
| C.1 | Calibration setup for 2D anemometer seen from the side. | 131 |
| C.2 | Calibration setup for 2D anemometer seen from the front. | 131 |
| C.3 | Definition of horizontal and vertical velocity. | 132 |
| C.4 | Setup for calibration of the 3D anemometer to determine the vertical velocity. | 133 |
| C.5 | Overview of the area and positions of reference points and anemometers. | 134 |
| C.6 | Intersection in the point of interest of three circles. | 135 |

List of Tables

| | | |
|-----|---|-----|
| 2.1 | Levels of comfort divided after probability of exceedance (%) | 10 |
| 2.2 | Levels of danger divided after probability of exceedance (%) | 10 |
| 3.1 | New parameters in the k - ε turbulence model | 18 |
| 4.1 | Different turbulence models applied on a $4 \times 4 \times 1$ cube | 22 |
| 4.2 | Boundary conditions for analysis on $4 \times 4 \times 1$ cube | 25 |
| 4.3 | Horizontal section. R^2 for the different models and parameters | 26 |
| 4.4 | Vertical section. R^2 for the different models and parameters | 27 |
| 7.1 | Levels of comfort divided after probability of exceedance (%) | 62 |
| 7.2 | Levels of danger divided after probability of exceedance (%) | 62 |
| 8.1 | Setup for the model at Høje Brygge | 70 |
| 8.2 | Average wind speed and k in front of the entrances before and after | 83 |
| 9.1 | Setup for the model at Viborgvej | 91 |
| A.1 | Closure coefficients for the k - ε model | 127 |
| A.2 | Closure coefficients for the k - ω model | 127 |

Part IV

Appendices

A Closure Coefficients for the Turbulence Models

The closure coefficients used in the turbulence models are given in Table A.1 and A.2 for both the original model and the values suggested by Yang et al. (2009). The values C_1 and C_2 are used for the velocity and turbulence profiles only.

Table A.1 Closure coefficients for the k - ε model

| | (Launder and Spalding 1974) | (Yang et al. 2009) |
|----------------------|-----------------------------|--------------------|
| C_μ | 0.09 | 0.028 |
| σ_k | 1.0 | 1.67 |
| σ_ε | 1.3 | 2.51 |
| $C_{1\varepsilon}$ | 1.44 | 1.5 |
| $C_{2\varepsilon}$ | 1.92 | 1.92 |
| C_1 | -0.55 | -0.17 |
| C_2 | -5.21 | 1.62 |

Table A.2 Closure coefficients for the k - ω model

| | (Menter 1994) | (Yang et al. 2008) |
|---------------------|---------------|--------------------|
| a_1 | 0.31 | 0.31 |
| β^* | 0.09 | 0.04 |
| β_1 | 0.075 | 0.033 |
| σ_{k1} | 0.85 | 0.85 |
| $\sigma_{\omega 1}$ | 0.5 | 0.5 |
| β_2 | 0.0828 | 0.0368 |
| σ_{k2} | 1.0 | 1.0 |
| $\sigma_{\omega 2}$ | 0.856 | 0.856 |
| C_1 | -0.56 | -0.25 |
| C_2 | 5.22 | 2.32 |

B Model With Larger Origin Shift

In order to determine the influence of the origin shift on the velocity profile a model with the double value of the origin shift d is made. The exceedance of both the comfort and danger criteria is given for both models in Figure B.1 to B.4.

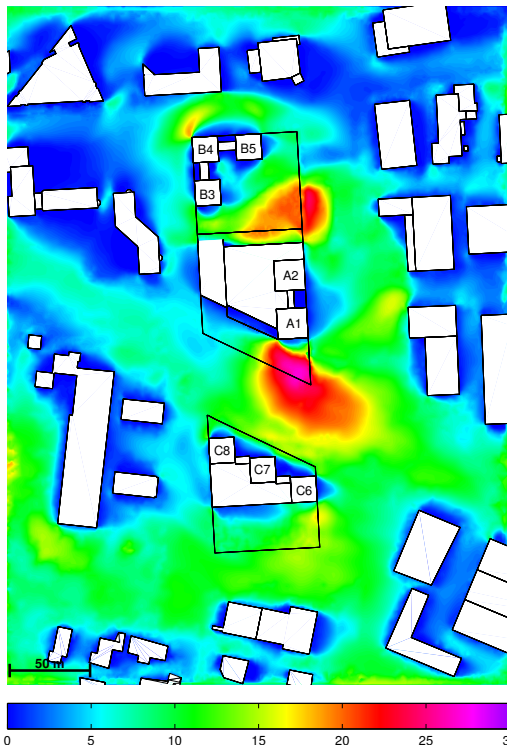


Figure B.1 Exceedance probability of the comfort criteria with $d = 3z_0$.

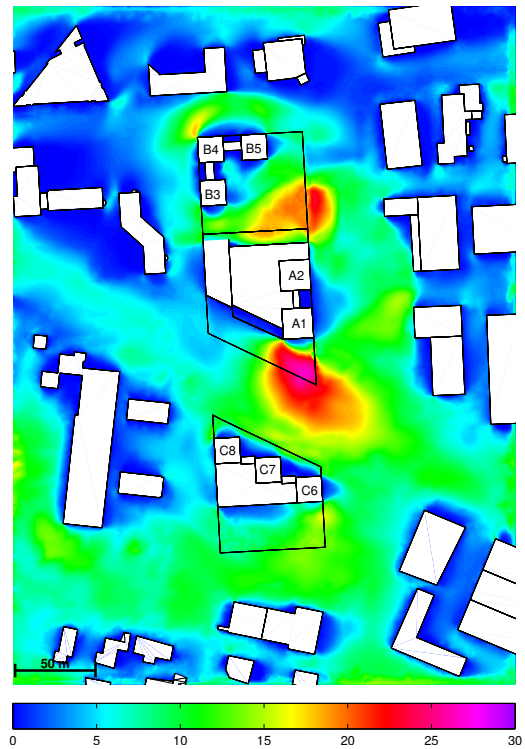


Figure B.2 Exceedance probability of the comfort criteria with $d = 6z_0$.

Around the area of interest no remarkable changes, which could change the conclusion, is seen. The flow is therefore independent of the boundary conditions which lead to the conclusion that the boundaries are an adequate distance away from the high-rise buildings.

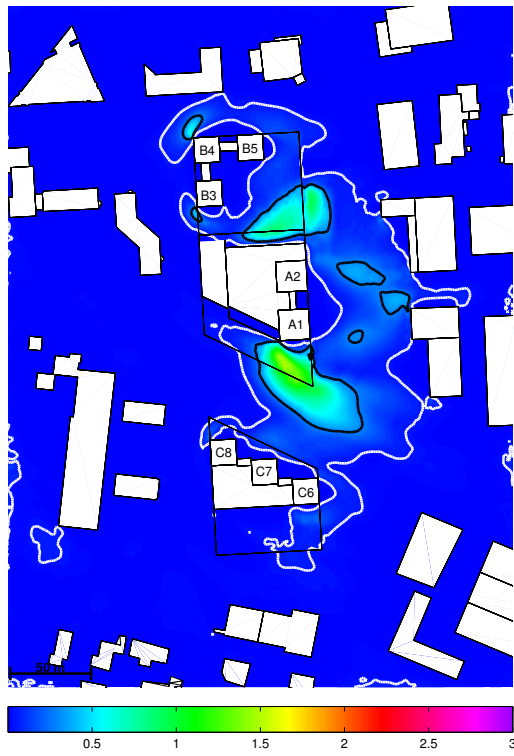


Figure B.3 Exceedance probability of the danger criterion with $d = 3z_0$.

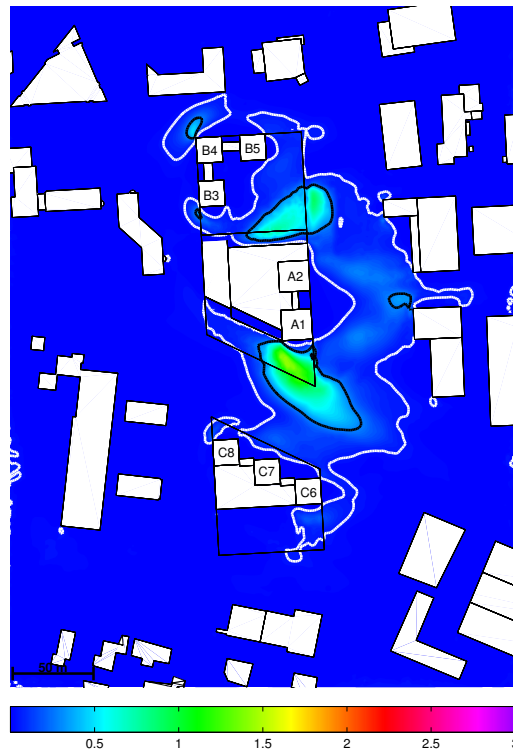


Figure B.4 Exceedance probability of the danger criterion with $d = 6z_0$.

C Measurements

For the measurements that are conducted at Høje Brygge in Nørresundby, some preparations are needed. First of all the equipments has to be calibrated. Also a list of equipment is made.

C.1 Calibration of 2D Anemometers

The 2D anemometers are connected to a HBM data logger that sends the information as a Voltage signal that is read in Catman 4.5. The anemometers are also connected to a power source, where approximately 10 V are needed, and from the power source the anemometers are earthed.

The three Anemometers have the names 359, 360 and 361. The experimental setup for the calibration of the 2D anemometers is as showed in [Figure C.1](#).



Figure C.1 Calibration setup for 2D anemometer seen from the side.

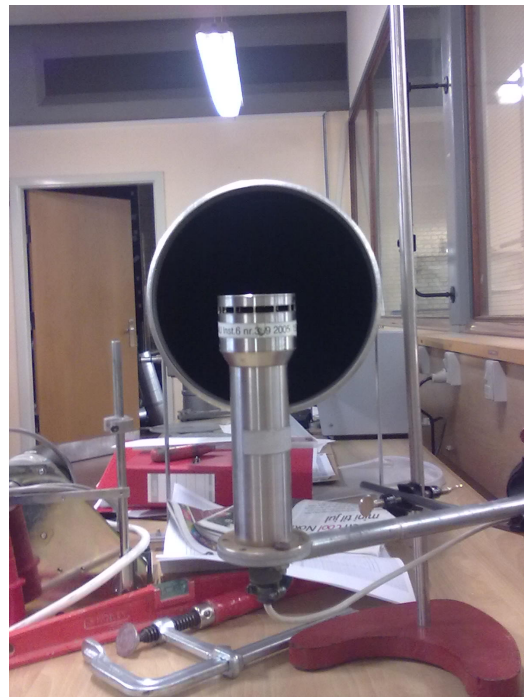


Figure C.2 Calibration setup for 2D anemometer seen from the front.

As seen in [Figure C.1](#) and [C.2](#) the anemometer is placed in the centre of the outlet of the wind tunnel and also placed just outside the outlet. This is because the calculated velocity is only valid in the centre until 15 cm from the outlet.

From the anemometers two Voltage signals are sent out. One that represents the magnitude of the wind, and one signal that represents the direction of the wind.

The three anemometers gives good results and from the Voltage signal, which is read in Catman, and the interrelated values measured in the wind tunnel, the calibration value for the magnitude of the wind can be found. The expressions from the calibrations can be seen in Equation C.1 to Equation C.3.

$$U_{359} = 8.91x + 0.22 \quad (C.1)$$

$$U_{360} = 7.69x + 0.10 \quad (C.2)$$

$$U_{361} = 7.62x + 0.22 \quad (C.3)$$

For the direction signal it is investigated how the signal fits the Voltage signal. Here the signal goes from 0 V to 3.59 V where 0 V is 0° from north and 3.59 V is 359° clockwise from north. Thereby anything in between is possible to find.

C.2 Calibration of 3D Anemometer

For the 3D anemometer, two different anemometers are used. An anemometer called R3 and another called Windmaster. For both anemometers three signals are displayed; direction, horizontal velocity, and vertical velocity.

Direction is like for the 2D anemometers measured from a zero in the north direction. R3 measures clockwise from north to south from 0 V to 2.5 V and counter clockwise from 0 V to -2.5 V. The Windmaster increases from 0 V in north to 2.5 V clockwise in south and further to 5 V in north again.

The two other Voltage signals give the horizontal and vertical velocity of the wind. First the anemometer is placed so the vertical velocity does not change when the velocity in the wind tunnel is increased, so it is possible to calibrate the horizontal velocity. To be sure that the vertical velocity does not change both horizontal and vertical velocity is computed.

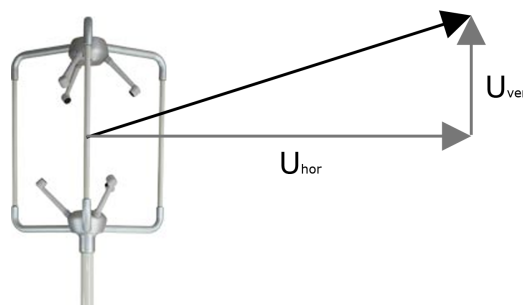


Figure C.3 Definition of horizontal and vertical velocity.

Afterwards the anemometer is placed in an angle of 45° from the outlet and thereby a component of the vertical velocity will appear as well. From this the component of the vertical velocity can be calibrated, when it is known that the horizontal and vertical velocity is given as seen in Figure C.3. The setup for the calibration of the vertical velocity is seen in Figure C.4

For the measurements a MATLAB program is written so the Voltage signals can be translated to information of the wind direction in a U, V coordinate system for 2D and a U, V, W coordinate system for the 3D anemometers.



Figure C.4 Setup for calibration of the 3D anemometer to determine the vertical velocity.

C.3 Sources of Error

During the calibration sources of errors were considered:

- Positioning the anemometers exactly at the centre of the wind tunnel. The formulas used for the calculated wind speeds from the wind tunnel are only valid in the centre of the outlet and until 15 cm from the outlet.
- For the 3D anemometers the size is a problem because the distance from one side of the anemometer to the other is bigger than 15 cm

C.4 List of Equipment for Measurements

For field measurements the following equipment were applied:

- 3 2D anemometers with an output frequency of 5 Hz .
- 2 3D anemometers with an output frequency of 10 Hz.
- Lift for the Windmaster to measure in 11 m.
- Stands for the 4 anemometers that is placed in 1.7 m.
- Power supply for the 2D anemometers - 10 V.
- Power supply for the Windmaster and the R3.
- Cables for the anemometers. For the 2D anemometers the cables are 35 m and for the 3D 50 m.
- HBM data logger.
- Computer where Catman 4.5, Wind and Rcom2 are installed.
- Map where the position for measurements are written down.
- Compass and GPS for positioning the anemometers in correct place and direction.
- Distance meter for positions of anemometers.
- Measuring tape to check the height of the Windmaster.
- Generator for power supply for the instruments.
- Different coloured stones for marking positions.
- Tools.

C.4.1 Least Square for Positioning of Anemometers

To calculate the position of the anemometers at the location of Høje Brygge, a least square method is used.

First positions of points that are easy to recognise in the area are found. The first point chosen is used as Origo and can be seen in Figure C.5.

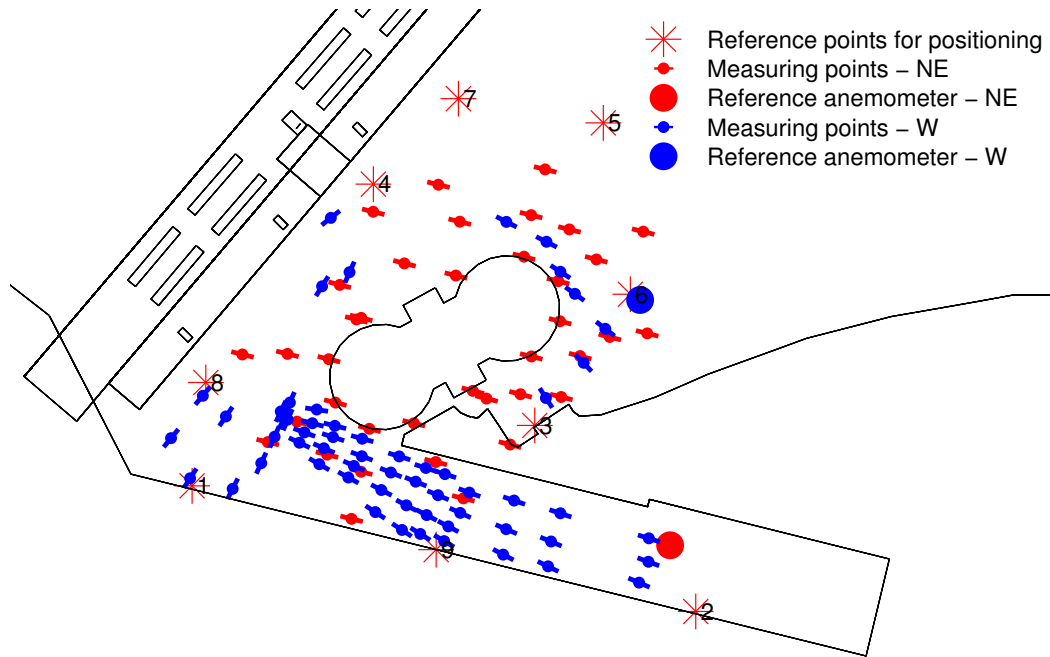


Figure C.5 Overview of the area and positions of reference points and anemometers.

The second point chosen is found by following the quay to another easy recognisable point which is a lamppost.

From the two points the abscissa of a coordinate system is made. From this line all the other reference points can be found. The third point is found by finding the length and angle between line 1 – 2.

The other points are found by finding the distance from the point of interest to three reference points. With centre in each of the reference points a circle is drawn with radius corresponding to the measured distance. The intersection of the three circles gives the coordinates to the point of interest.

In the calculation of the intersections an error can be found. This error can be minimised and the best guess on the point of interest can be found.

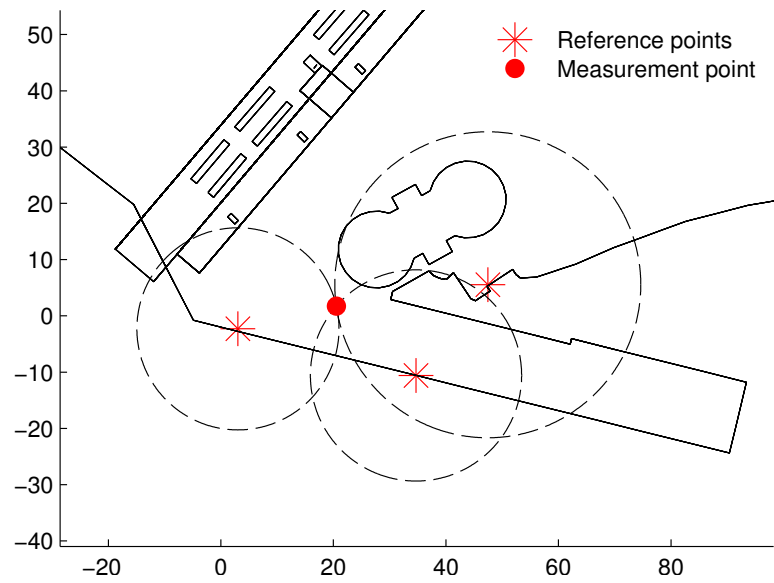


Figure C.6 Intersection in the point of interest of the three circles found from the measured distances.

This project is conducted in order to investigate the possibilities of analysing wind conditions at pedestrian level by use of Computational Fluid Dynamics (CFD). The purpose is to establish an operational procedure for evaluating wind conditions by coupling CFD, wind statistics, and evaluation criteria.

The project consists of three parts:

Part I deals with the problem of formulating evaluation criteria based on mean wind speed and turbulence. Based on the literature criteria are established for comfort and danger, along with limits of how often the criteria should be allowed to be exceeded.

Part II presents the mathematical model used to evaluate the flow field. This includes treatment of the wind statistics, modelling boundary conditions, selection of turbulence model, and comparison of the CFD model with field measurement in order to evaluate the proposed model.

It is shown that the SST $k-\omega$ model by Menter (1994) with parameters suggested by Yang et al. (2009) is best for modelling the turbulence. A method for transformation of wind statistics from meteorological sites to the location of interest is applied based on the work of Verkaik et al. (2005) and Wieringa (1986).

The overall procedure of evaluating wind conditions is presented, and in Part III two case studies are conducted. One from Høje Brygge, Nørresundby, where also the field measurements are conducted. Here the residents suffer under severe wind conditions. The other case study, from Viborgvej/Bredskiftevej in Århus, is for a proposed group of high-rise buildings.

In both cases the comfort and danger are evaluated and a number of solutions are suggested in order to reduce the wind speed at ground level. The directional discretisation is investigated and considerations on how to choose an adequate discretisation is presented.

